MANIPULATING THE BAND GAP OF DONOR-ACCEPTOR LOW BAND GAP POLYMERS

By

TIMOTHY THOMAS STECKLER

A DISSERTATION PRESENTED TO THE GRADUATE SCHOOL
OF THE UNIVERSITY OF FLORIDA IN PARTIAL FULFILLMENT
OF THE REQUIREMENTS FOR THE DEGREE OF
DOCTOR OF PHILOSOPHY

UNIVERSITY OF FLORIDA

2009

To my mom and dad

ACKNOWLEDGMENTS

I would like to thank my advisor, Dr. John Reynolds, for being the best teacher/mentor a graduate student could ever ask for. It was his sharing of knowledge and guidance that have molded me into the person I am today, both scientifically and personally, and for that I will never be able to give enough thanks.

I am very thankful to the numerous professors who have contributed to my education here at the University of Florida. I thank my committee: Dr. Ken Wagener, Dr. Ron Castellano, Dr. Randy Duran and Dr. Anthony Brennan. They have been a significant part of my educational development.

Many contributions from others at the university have been paramount to the work presented in this dissertation. I thank Dr. Khalil Abboud for his work on solving x-ray crystal structures; James Leonard for getting me in the door for x-ray analysis and his GPC work; Erik Berda, Jianguo Mei, Kate Opper for thermal analysis; Aburey Dyer, Merve Ertas, and Svetlana Vasilyeva for their wonderful insights into electrochemistry; Stefan Ellinger for his work on collaborative synthesis.

Numerous people in the Reynolds group have contributed to my development as a synthetic chemist, and for that I thank Stefan Ellinger, Ryan Walczak, Ben Reeves, Christophe Grenier, Emilie Galand, Barry Thompson, Genay Jones, Pierre Beaujuge, Jianguo Mei, Dan Patel, C.J. DuBois and David Whitker.

I also thank the many members of the George and Josephine Butler Polymer Research Laboratory who have had significant influences on me both professionally and personally; George and Josephine Butler; Travis Baughman, Tim Hopkins, Sophie Bernard, and Andrew Skolnik (SLS, Inc.).

I would like to give a special thanks to Bob Brookins, not only for many shared failures in collaborative work, but also for many successes in knowledge gained. He was a great friend to have around and I enjoyed the numerous "cookie dews." I also thank Stefan Ellinger for showing me not only how to work hard, but also how to enjoy a "small one." I bestow a special thanks to Merve Ertas for her friendship and support both in and outside of the lab.

Finally, I would like to thank my family for their support throughout my whole graduate school career. My parents, Tom and Lil Steckler, have always supported me and given me sound advice. My brother, Steve Steckler, has always been there for me and is a driving force for me to continue on in my career.

TABLE OF CONTENTS

page

LIST OF TABLES

LIST OF FIGURES

Abstract of Dissertation Presented to the Graduate School
of the University of Florida in Partial Fulfillment of the
Requirements for the Degree of Doctor of Philosophy

MANIPULATING THE BAND GAP OF DONOR-ACCEPTOR LOW BAND GAP POLYMERS

By

Timothy T. Steckler
May 2009

Chair: John R. Reynolds
Major: Chemistry

The work presented herein focuses on design of low band gap polymers via the donor-acceptor methodology. One of the advantages of low band gap polymers is their ability to reach multiple redox states in a small potential window. These different redox states are usually accompanied by color change. The use of stronger acceptors, with more positive reduction potentials, will ultimately lead to improved stability in the reduced state, for possible applications in charge storage and electrochromics. The goal of this study is to examine the structure-property relationships between the donor-acceptor connectivity and their control of the optical and electronic properties.

Initial investigation into the pyrido[3,4-*b*]pyrazine acceptors involved the electrochemical polymerization of 5,8-bis-(2,3-dihydrothieno[3,4-b][1,4]dioxin-5-yl)-2,3-dihexyl-pyrido[3,4-b]pyrazine (BEDOT-PyrPyr-$(C_6H_{13})_2$) and 5,8-bis-(2,3-dihydro-thieno[3,4-b][1,4]dioxin-5-yl)-2,3-didodecyl-pyrido[3,4-b]pyrazine (BEDOT-PyrPyr-$(C_{12}H_{25})_2$) to yield P(BEDOT-PyrPyr-$(C_6H_{13})_2$) and P(BEDOT-PyrPyr-$(C_{12}H_{25})_2$). Both polymers were dark blue and exhibited optical band gaps of 1.4 eV with a first reduction potential of E_p = ~ -1.6 V vs. SCE. The second reduction seen in the previously synthesized BEDOT-PyrPyr-Ph_2 polymer was either not observed or seen for only one to two cycles due to stability issues.

The next generation of DAD monomers developed for electrochemical polymerization involved 3,4-ethylenedioxythiophene (EDOT), 3,4-propylenedioxythiophene (ProDOT), and 2,2-dimethyl substituted ProDOT ($ProDOTMe_2$) donors. These donors were combined with either thiadiazolo[3,4-*g*]quinoxaline (TQ) or benzo[1,2-*c*;4,5-*c*′]bis[1,2,5]thiadiazole (BBT) acceptors. The lowest band gap in the family was ~0.5 to 0.7 eV for P(BEDOT-BBT) corresponding to a dark olive green neutral state while the highest optical band gap was ~ 1.5 eV for P($BProDOTMe_2$-$TQMe_2$) yielding a light grey/blue neutral state. Due to the low band gaps in this family, new spectroscopic materials were needed to replace ITO, which absorbs strongly beyond 1600 nm. This lead to the use of single walled carbon nanotube (SWCNTs) electrodes, which have a high degree of transparency in the NIR, for improved optical characterization at longer wavelengths. All BBT based polymers showed two reductions with onsets near -0.4 V and -1.2 V vs. SCE while TQ based polymers showed reductions onsets near -0.7 V and ~ -1.4 V vs. SCE. The onset of oxidation for the BBT based polymers could be controlled over a ~300 mV window from ~ 0.2 V for EDOT to ~ 0.5 V vs. SCE for $ProDOTMe_2$. Meanwhile the onset of oxidation in the TQ based polymers ranged from ~ 0.4 V to ~ 0.65 V vs. SCE.

A final project focused on the synthesis of soluble DA polymers via Stille polymerization using dibromo based acceptors; benzo[2,1,3]thiadiazole (BTD), TQ, and BBT based combined with N-(3,4,5-tri-*n*-dodecyloxyphenyl)-dithieno[3,2-*b*:2′,3′-*d*]pyrrole (DTP) based donor. The tri-alkoxyphenyl group allows for good solubility while the DTP core allows for planarity along the conjugated backbone, resulting in low band gap, soluble DA polymers. P(DTP-BThBBT) has an optical band gap of ~ 0.5 to 0.6 eV, which is the lowest reported band gap for a soluble spray-processable polymer to date. With this polymer showing both p- and n-type doping

characteristics at relatively low potentials, ambipolar charge-transport was investigated and confirmed.

CHAPTER 1
INTRODUCTION

History of Conjugated Polymers

The discovery that π-conjugated polymers (CP's) could be conducting in the late 1970's by Heeger, MacDiarmid, and Shirakawa when they found that polyacetylene (PA), when chemically doped, became highly conductive, stimulated immense interest and research efforts.[1,2] However, due to poor solubility, and stability issues in the doped state, other avenues were pursued to solve these problems. This lead to the investigation of other CP's such as polyaniline, polythiophene, poly(ρ-phenylene) and polypyrrole to name a few (Figure 1-1). Though none of these materials have the ideal properties for replacing metals such as copper (as related to conductivity), numerous other uses have surfaced. Based on a polymer's material advantages such as light weight, flexibility, and ease of processability, CP's are now used in polymer light emitting diodes (PLEDs),[3-6] electrochromic devices,[7-11] photovoltaic devices,[12-19] charge storage[20-25] and organic field-effect transistors (OFETs).[26-30] The inherent properties of the π-conjugated backbone in CP's play an important role in determining the material characteristics, and thus applications.

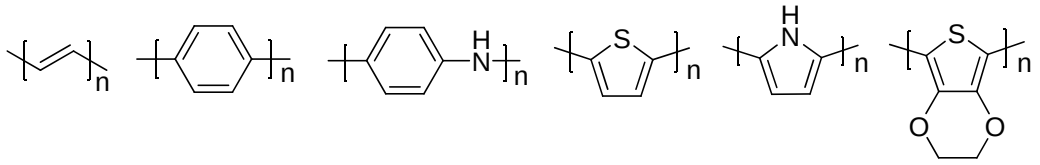

Figure 1-1. Common conjugated polymers: poly(acetylene) PA, poly(ρ-phenylene) PPP, poly(aniline) PANI, poly(thiophene) PTh, poly(pyrrole) PPy, and poly(3,4-ethylenedioxythiophene) PEDOT.

In order to optimize new conjugated polymers for the various applications mentioned previously, it is important to understand the structure-property relationships relative to the material's optical and electronic properties. By using more complex molecules such as donor-acceptors, it is possible to tailor these properties for multiple applications beginning from a

similar core structure. To develop such systems, it is important to understand how the individual fragments properties will morph together to yield a new set of final properties. The remainder of this chapter will deal with the electronic and optical properties of conjugated polymers along with the design and synthesis of low band gap polymers.

Electronic Properties

In a CP there is a delocalized π-electron system along the polymer backbone involving the overlap of p-orbitals. As more and more monomer units are connected, the orbitals of similar energy combine to form more levels until a saturation point is reached and they become bands. These bands can be divided into the highest occupied molecular orbital (HOMO) or valence band and the lowest unoccupied molecular orbital (LUMO) or conduction band. The difference in energy between the HOMO and LUMO levels is known as the band gap, E_g.[31,32] There are two different types of CP's relative to their conjugated backbones, degenerate and non-degenerate. PA is the exception for a degenerate polymer because it has two energetically equivalent forms in the ground state (Figure 1-2). All other conjugated polymers can be classified as non-degenerate polymers, since the different ground states are not energetically equivalent as can be seen for the aromatic form relative to the quinoid form for PTh (Figure 1-2).[33]

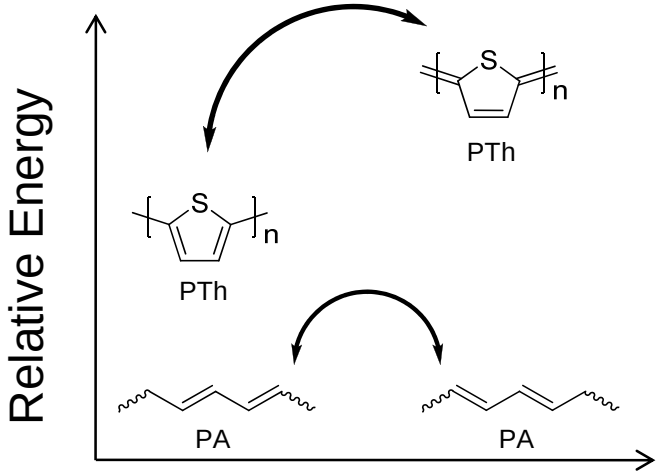

Figure 1-2. The different ground state energies for degenerate PA and non-degenerate PTh.

One can picture a CP, such as PA, as an infinite chain of alternating single and double bonds with each carbon being sp^2 hybridized, thus the chain would be a continuum of overlapping p orbitals each containing one electron. This type of structure should lead to a highly conductive material along the axis of the conjugated backbone since the valence band would be half filled and delocalized like that of a metal conductor. However, CP's suffer from Peierls distortion,[31] which is an electron-phonon coupling that leads to a symmetry lowering effect resulting in a less delocalized system. This results in an increase in stability for the bonding orbitals and a decrease in stability for the anti-bonding orbitals due to the lengthening of single bonds and the shortening of double bonds. The Peierls distortion in PA results in the opening up of a band gap, which is ~ 1.5 eV.[34,35] The band gap plays an important role in determining a polymer's optical and electronic properties.

Since most neutral CP's are usually considered semi-conductors (0.3 eV < E_g < 3-4 eV, E_g > 3-4 eV are considered insulators), they must be doped in order to see a change their optical or electronic properties.[36] The different ways to dope a polymer include chemical, electrochemical, metal-polymer interfacial, and photochemical. Detailed explanations of these processes and applications can be obtained from various Reynolds group dissertations and the literature.[33,37-40] Electrochemical doping will be discussed briefly since that is the foundation of characterization throughout this dissertation.

The doping of PA is unique compared to the rest of CP's, due to its degenerate ground state. In neutral *trans*-PA with an odd number of repeat units, there is a single π-electron (radical) that is delocalized over several repeat units known as a neutral soliton, which is located mid gap between the HOMO and LUMO levels with a spin of ½.[41,42] Upon oxidation (or reduction) an electron is removed (or added) leaving an empty (or doubly occupied) mid gap

state which is spinless and charged positively or negatively. Due to PAs degeneracy, these solitons can migrate along the backbone without an increase in the distortion energy, thus allowing for higher conductivity compared other CP's.

Oxidation (p-type doping) or reduction (n-type doping) of a non-degenerate CP causes the removal or addition of an electron to create a charged state known as a polaron (radical cation or anion), which has a spin of ½. Oxidative doping of PPy can be seen in Figure 1-3. Single oxidation of a polymer is usually accompanied by a change in the polymer backbone from the neutral aromatic structure to the polaronic quinoid like structure. Along with the change in the backbone there is the formation of intragap states known as the polaron bands.[43] The polaron is delocalized over ~ 4 rings for PPy.[43,44] If the procedure is repeated again an electron may be removed from somewhere else along the polymer backbone to produce another polaron, or an electron could be removed from the polaron to create a bipolaron (a spinless state). As a polymer becomes more heavily doped, usually the bipolaron state starts to become more dominant as was shown for PPy.[43] These energy states are located within the polymer band gap, with the polaron bands located closer to the original HOMO and LUMO levels compared to the bipolaron bands, which are compressed more. It is these bands that cause the optical changes associated with the different redox states in a CP (Figure 1-3).[33,45] It is through the synthetic chemist's ability to design and assemble new molecules and polymers that allows control over the desired electronic and optical properties.

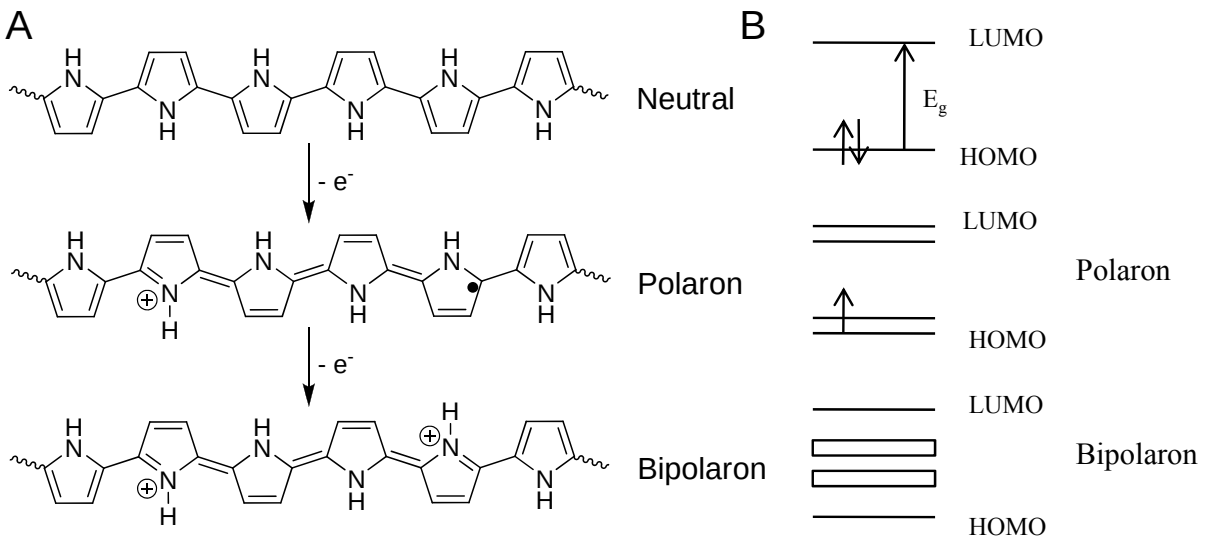

Figure 1-3. p-Doping of PPy. A) Successive one e^- oxidations of PPy. B) Polaron and bipolaron band formation.

Controlling the Band Gap Towards Low Gap Systems

Low band gap polymers are usually considered to be polymers that have a band gap below 1.5 eV (corresponding to an onset of the lowest energy absorption of the neutral polymer greater than or equal to ~800 nm) and have been the focus of many studies and reviews.[46-52] These polymers are colored in the neutral state due to the π-π^* transition located at low energies, and become more transparent upon doping with a decrease of the π-π^* transition and development of lower energy transitions. By having a low band gap, the conduction band can be reached easier, allowing for the possibility of n-type doping. Thus, low band gap polymers could lead to dual p-type and n-type devices with a single polymer such as ambipolar OFETs[27,30,53] and supercapacitors.[54-56] Through the careful choice and modification of various building blocks in different configurations allows for fine control over absorption (color), emission, oxidation/reduction potentials (for both tunability and stability in applications), and mobility/conductivity. Some of the methods used for the design and control of properties in low band gap polymers include, but are not limited to, minimizing bond-length alternation (BLA),

planarity, aromaticity (resonance), interchain effects and donor-acceptor (DA) effects.[47,48] It can be very hard to look at these methodologies individually because they often interrelate to each other.

As was discussed earlier, we found that PA along with other CP's suffer from a Peierls distortion, that results in BLA with the single bonds becoming longer and the double bonds becoming shorter, thus opening up a band gap. The classic example of minimizing BLA in heteroaromatic CP's is polyisothianaphthene (PITN) (Figure 1-4). This relates to both aromaticity (resonance) and BLA. As was discussed previously for non-degenerate CP's, the aromatic form is usually more stable in the ground state relative to the quinoid form (Figure 1-2). It is possible to minimize BLA by gaining a resonance contribution from the higher energy quinoid form in the ground state, since this would increase the double bond character between adjacent thiophene rings. Since PTh has a band gap of ~2.0 eV, it was thought that if one could force more quinoid character in the ground state of PTh, one could reduce BLA and the band gap. To demonstrate this, Wudl *et. al.*synthesized PITN, and they found that because the benzene ring has a higher energy of aromaticity than thiophene, the polymer in the ground state has a significant contribution from the quinoid resonance form. This produced a polymer with a band gap of ~1.0 eV, which is approximately half that of PTh.[57,58]

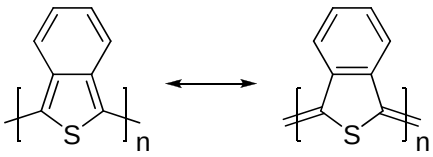

Figure 1-4. Resonance structures of the aromatic (left) and quinoid (right) forms of PITN.

Another way to control the band gap is through planarity. This involves the overlap of the p-orbitals along the conjugated polymer backbone. In a normal conjugated polymer, there is the ability for neighboring units to rotate out of planarity, thus diminishing the overlap of p-orbitals

and conjugation. This results in a higher band gap. By inducing the polymer backbone into a more planar structure, better overlap occurs amongst the p-orbitals so conjugation is increased and a smaller band gap can be obtained. One simple example is poly(pyrrole-benzothiadiazole) (Figure 1-5). When the soluble precursor polymer is in its non-planar Boc protected state, the λ_{max} is at 434 nm in chloroform, but when a spin coated film was deprotected, the polymer planarizes and we see a red shift in the λ_{max} to 704 nm.[59] With careful choice of where to add substituents to the monomers or the choice of certain monomers, the final planarity of the polymer can be controlled.

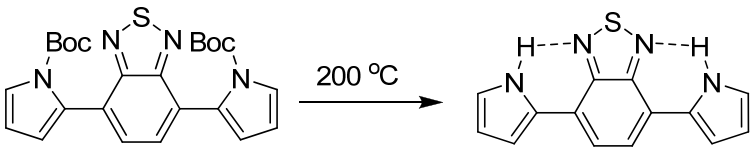

Figure 1-5. Increase in planarity for poly(pyrrole-benzothiadiazole) relative to the N-Boc protected precursor.

Interchain effects have best been shown with poly(3-alkylthiophenes). The 3-alkyl thiophenes in the polymer can be connected in a head-to-tail (HT), head-to-head (HH), or a tail-to-tail fashion (TT). Depending on the polymerization method, different amounts of HT, HH, and TT connections are observed. A HH connection leads to defects causing a severe twist along the backbone. This results in a higher band gap and diminished conductivity. Certain polymerization methods allow for the formation of 98-99 % HT poly(3-alkylthiophene). Regioregular HT poly(3-alkylthiophenes) (Figure 1-6) have improved electronic properties due to a more planar backbone and the ability to self assemble into highly ordered polymer films.[60-62]

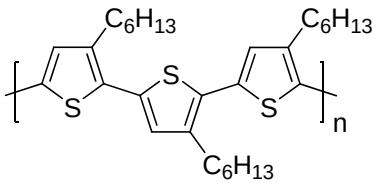

Figure 1-6. Demonstration of interchain effects in poly(3-hexylthiophene).

Low band gap DA polymers are of interest because of the accessibility to reach multiple redox states (p-type or n-type doping) in a small potential window. This is due to the placement of the valence band relative to the conduction band. The goal is to select a strong donor with a high HOMO level and a strong acceptor with a low LUMO level. When the donor and acceptor are coupled, the orbitals mix forming a new set of orbitals with a much smaller band gap compared to its individual parts (Figure 1-7), and upon polymerization can yield very small band gaps, as was demonstrated early on by Havinga *et. al*.[63] With the proper choice of donor and acceptor, the band gap can be modified and thus the final properties can be adjusted.[48]

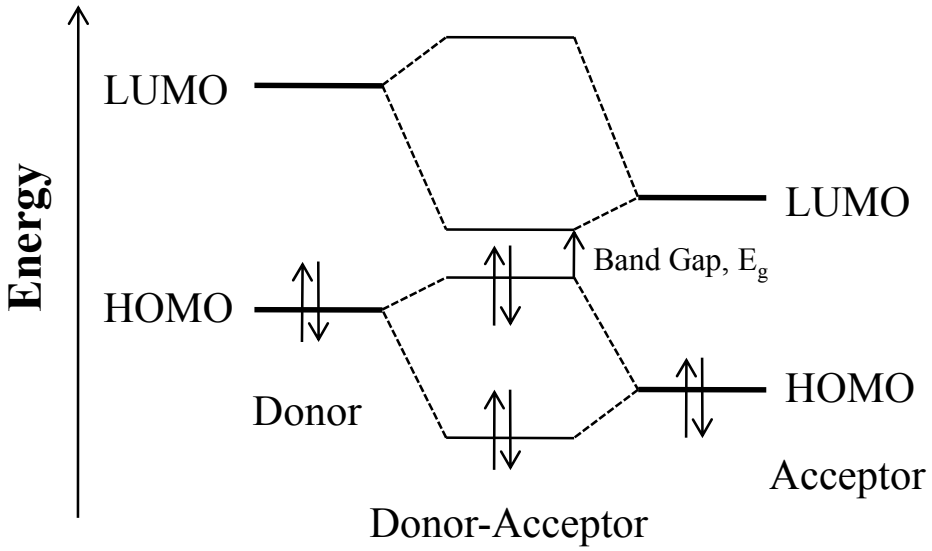

Figure 1-7. Donor-acceptor band gap compression. [Modified from van Mullekom, H. A. M.; Vekemans, J. A. J. M.; Havinga, E. E.; Meijer, E. W. *Mater. Sci. Eng.* **2001**, 32, 1-40].[48]

This idea for DA oligomers/polymers has been called into question over the last few years in theoretical work done by Salzner *et. al*.[64-66] The general assumption is that since the ionization potentials (IPs)/HOMO of the donor and the acceptor are closer in energy, they tend to mix better and result in an increase in the IP/HOMO of the polymer. However, the electron affinities (EAs)/LUMO of the donor and the acceptor are too energetically different to have significant mixing, thus you end up with a narrow LUMO band that is localized mostly on the

acceptor with an EA similar to that of the acceptor. The true conduction band is located at a higher energy. So, even though the band gap is low, one still does not observe a substantial increase in conductivity upon reduction. This was demonstrated by the study of PBEDOT-Pyr and PBEDOT-PyrPyr-Ph_2,[67,68] which measured in-situ conductivity associated with the different redox states. It was found that the conductivity in the n-doped state for PBEDOT-Pyr was 30 times less than when in the p-doped state, while the conductivity for PBEDOT-PyrPyr-Ph_2 was even less in the n-doped state relative to the p-doped state. No capacitive effects were seen in the n-type conductivity profile for either polymer, indicating a highly localized anionic state.

So while the famous orbital mixing diagram in Figure 1-7 has been questioned, that does not mean the DA approach does not work. It just means that getting a highly delocalized conduction band might be difficult. Perhaps a better way to think of the DA approach is to picture the mesomerism of $D–A \leftrightarrow D^{+}=A^{-}$. This can be thought of as the often used term intramolecular charge transfer (ICT). The stronger the donor and the acceptor are, the increased amount of ICT there is, thus resulting in increased quinoid character in the ground state, leading to a small band gap.[69] The stronger the DA interaction, the more red shifted the absorption becomes. This ICT band can be thought of as the gap between the HOMO and the low lying LUMO that is isolated more on the acceptor as explained above. It is these principles that become important factors for the design and application of new DA CP's, especially as it relates to electrochromic applications.[7,9,70,71]

Polymerization Methods for DA Conjugated Polymers

Though there are many different polymerization methods used to synthesize DA CP's, such as electrochemical, oxidative, and metal mediated couplings, this section will focus on the

methods used throughout the work done in this dissertation. The main focus will be on the design of donor-acceptor-donor (DAD) compounds for applications in oxidative polymerization.

Electrochemical Polymerization

Electropolymerization allows for the deposition of polymers onto different electrode surfaces (i.e. Pt button or ITO coated glass) for immediate characterization of optical or electronic properties. The mechanism for the electrochemical polymerization of heterocycles can be seen in Figure 1-8, which is thought to be very similar to the mechanism for chemical oxidative polymerization. For electrochemical polymerization, initially a monomer such as thiophene is dissolved in a monomer/supporting electrolyte solution. The solution is then subjected to an oxidizing potential for the given monomer, leading to radical cation formation (Figure 1-8). The radical cation can then couple to monomer, undergo oxidation again followed by the loss of two protons to yield the neutral dimer. This process can then be repeated multiple times to deposit polymer on the electrode surface. Another path is for the radical cation to couple with another radical cation, followed by the loss of two protons to yield the neutral dimer. Again, repetition of this procedure numerous times will yield polymer.[72]

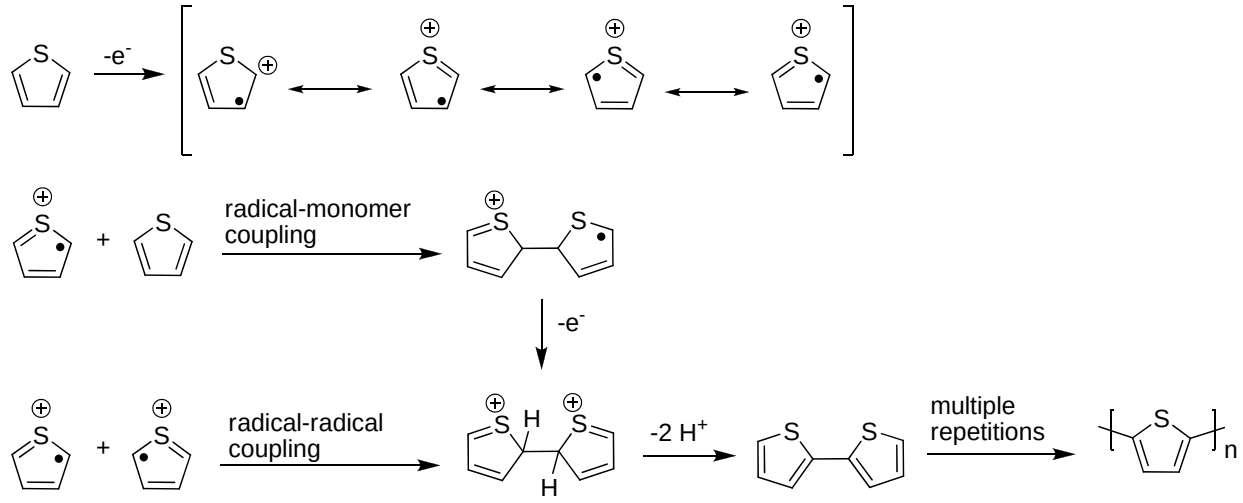

Figure 1-8. General mechanism for the oxidative (electrochemical & chemical) polymerization of thiophene.

One of the major drawbacks of electrochemical polymerization is the fact that it yields insoluble polymers which do not have the ability to be characterized by traditional methods such as NMR and GPC. An even more important drawback is the electrochemical polymerization of unsubstituted monomers like thiophene or pyrrole, which have the ability to couple at the 3- and 4-positons along with the 2- and 5-positions. These defective couplings lead to a decrease in conjugation, cross-linking, and diminished electronic properties.[73,74] This can be avoided through substitution of the 3- and 4- positions with blocking groups. 3,4-Dioxythiophene based monomers (XDOT) are a good example of this strategy.[11]

Not only does the dioxythiophene bridge on the XDOT monomers block the deleterious couplings during electropolymerization, but they also increase the electron density of the monomer. By using a donor that is more electron rich such as EDOT, the advantage of a low oxidation potential for ease of electrochemical synthesis is gained.[75,76] This avoids side reactions that can occur at higher potentials such as over oxidation of the resulting polymer film due to the high monomer oxidation potential. Dioxythiophene based donors are one of the few donor units that offer the chemical robustness for multi-step synthesis similar to that of thiophene and the advantage of being more electron rich for easier electrochemical polymerization.

Chemical Oxidative Polymerization

While chemical oxidative polymerizations are similar to electropolymerizations, this method allows for the synthesis of CP's on a large scale in a fairly inexpensive fashion along with high yields. The mechanism of polymerization follows the same principle as described in Figure 1-8, however a chemical oxidant such as $FeCl_3$ is used instead of an electrode.[77] An important note is that as the polymer chain forms, it stays in an oxidized state, so when complete, the polymer has to be isolated and dedoped with strong reducing agents such as ammonium hydroxide or hydrazine. Since the polymer is in an oxidized state as it is growing, it becomes

more rigid relative to the neutral form, and could precipitate out of solution. If the monomer is not properly substituted with flexible substituents to increase solubility, the molecular weight and thus the optical and electronic properties could suffer. Besides suffering from the same side reactions as mentioned for electrochemical polymerization, chemical oxidative polymerizations also suffer from the fact that they can leave residual oxidant trapped in the polymer, which can lead to poor device performance, and they are performed under very harsh conditions. During the polymerization, large amounts of HCl are produced and upon neutralization strong reducing agents are used. This can severely limit the types functional monomers used for polymerization, and thus alternative methods such as metal mediated couplings are desired.[78]

Metal Mediated Polymerizations

While there are numerous different ways to synthesize chemically polymerized polymers, the main methods used today are Grignard metathesis (GriM),[60,79] Yamamoto ($Ni(COD)_2$),[80-82] Suzuki[83-89] and Stille[90,91] coupling chemistries. While all have their advantages; GriM can produce highly regioregular poly(3-alkylthiophenes) along with high molecular weight polymers with narrow polydispersities,[92,93] Yamamoto polymerizations are good for the coupling of electron poor aryl halides,[80,94] Suzuki polymerizations are fairly tolerant of functional groups and can produce high molecular weight polymers along with AB monomers.[95-97] One of the set backs of the GriM polymerization method is that they are performed under strongly basic conditions, which can be problematic for strong acceptors that are base sensitive. There is also very few examples for multi-ring systems being polymerized successfully.[98,99] While the Yamamoto polymerization has been used successfully for the synthesis of DA CP's,[16,100,101] some of the draw backs are the use of stoichiometric amounts of expensive nickel catalyst along with the reaction being highly air and moisture sensitive. Suzuki polymerizations are also performed under basic conditions, but they are not nearly as strong and can tolerate some of the stronger acceptors,

however most of the reported cases involve copolymers with phenylene, fluorene, or carbazole.[12,102-105] For the DA polymers seen in the literature today that are thiophene or dioxythiophene based, the work horse polymerization methodology has been the Stille reaction.[17,26,53,69,106-109]

The Stille reaction/polymerization offers many benefits, as one of the most mild reactions that is very tolerant of many different functional groups such as amines, esters, aldehydes, ethers, and nitro groups.[110] It is its tolerance to many functionalities that make it useful not only in polymerization but also in the synthesis multi-ring systems for conjugated polymers/oligomers.[111-113] The stannyl compounds are stable to air and moisture, which allows for the easy purification and storage of the monomers. While palladium (0) is the active species in the catalytic cycle, this can be generated in-situ from palladium (II) catalysts by the homo-coupling of the stannyl reagent (Figure 1-9).[114] This allows for the use of inexpensive air stable catalysts such as $Pd(II)Cl_2(PPh_3)_2$. The palladium (0) species then reacts with an aryl halide or triflate and undergoes oxidative addition to the organopalladium halide . Then transmetalation of the stannyl compound occurs followed by reductive elimination to produce palladium (0) and the product. The most important part of this mechanistic cycle to the polymer chemist using a palladium (II) catalyst is the beginning. It is important to account for the loss of the appropriate amount of stannyl reagent required to make the palladium (0) active catalyst. While this is not as important for small molecule synthesis, if not accounted for, this would cause a stoichiometric imbalance and lead to lower molecular weights, as expected for a step growth polymerization modeled by the Carothers equation (Figure 1-9). The Stille reaction/polymerization is one of the easiest coupling reactions to set up due to the air stability of all the components. However, one major draw back is the toxicity of tin. While the trimethyl stannyl derivatives are more reactive than the tributyl version, the tributyl version is less toxic, however both are still very toxic.

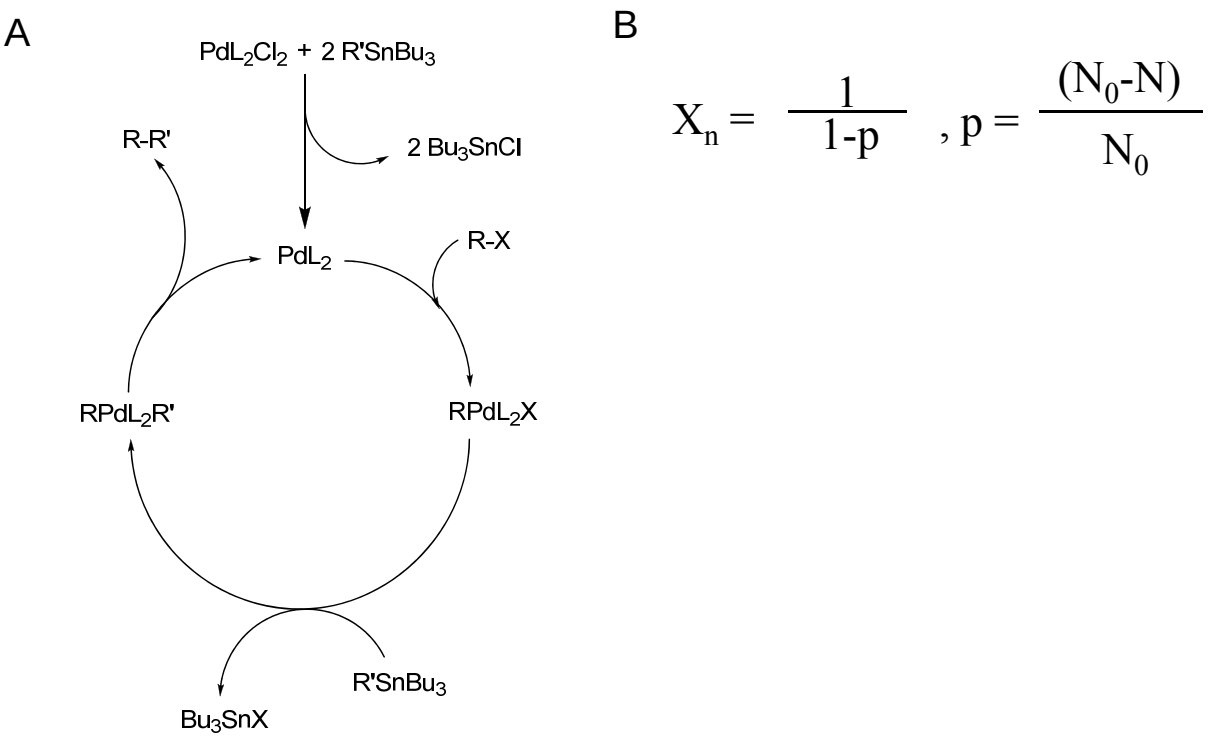

Figure 1-9. Outline of the Stille reaction and the Carothers equation. A) Mechanism of the Stille reaction. B) Carothers equation for step growth polymerization, X_n = degree of polymerization, p = reaction conversion, N_0 = number of monomers present initially, and N = number of monomers reacted.

Acceptors in DAD Oligomers/CP's

As was discussed earlier, the use of the DA methodology to control the band gap is a useful tool to the synthetic chemist. It has been demonstrated that by increasing the amount of imine nitrogens (C=N) in heterocycles, the reduction potential becomes more positive, thus making the system easier to reduce.[115] A simple example of this is shown in six-membered ring heterocycles. Going from pyridine (1 C=N)) to pyrazine (2 C=N) all the way up to s-tetrazine (4 C=N) there is an increase in reduction potential by ~ 1.85 V (Figure 1-10). The same trend is shown for fused-ring heterocycles, in going from quinoline (-1.59 V) to pteridine (-0.52 V), there is a ~ 1 V shift to more positive reduction potentials. We also see the arrangement of the imine nitrogens affect the reduction potential shifting it 200 mV more positive in going from pyrimidine (- 1.78 V) to pyrazine (- 1.57 V).

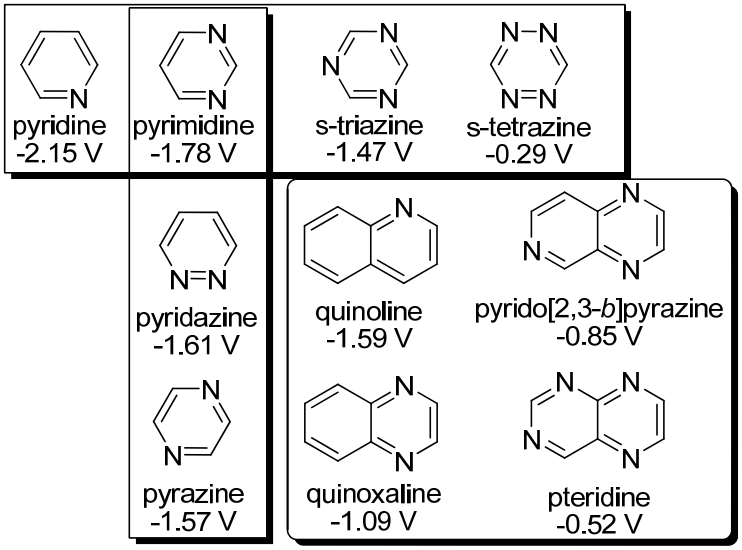

Figure 1-10. Reduction potentials of various nitrogen containing heterocycles measured in anhydrous DMF (V vs. Hg pool).[115]

These trends can be applied to a new set of acceptors known as o-quinoid type acceptors. These acceptors usually involve the incorporation of thiadiazole ring(s) and or imine nitrogens into the heterocycle. The advantage of the thiadiazole ring is that the hypervalent sulfur atom can help stabilize negative charge.[116] These are some of the strongest two or three-ring fused heterocycle acceptors known to date and dominate most of the research being done in DA oligomers/polymers (Figure 1-11).[7,12,16,17,26,49,71,101,102,105,107-109,117-119] The acceptors offer wide range of band gap control with peak ($E_{p,c}$) reduction potentials ranging from -1.51 V all the way down to -0.19 V for DAD oligomers and -1.74 V to ~ -0.4 V vs. SCE for the electrochemically polymerized polymers. It is important to note that the thiadiazole rings are much more electron withdrawing compared to their imine (C=N) counterpart. There is a +300 mV positive shift in going from quinoxaline to 2,1,3-benzothiadiazole. An important note is that while the thiadiazole rings increase the acceptor strength, they do not allow for synthetic flexibility towards solubility like the quinoxaline and pyrazine based acceptors do. Through various combinations of imine nitrogens and thiadiazole rings, one can control the reduction potential

and thus the band gap of a desired DAD oligomer/polymer. These acceptors have been incorporated into very low band gap polymers, with an electropolymerized BTh-TTP polymer having a band gap of 0.3 eV[120] and a soluble polymer, P(DTP-BThBBT), which has a band gap of ~0.5 eV will be discussed in chapter 5.[53]

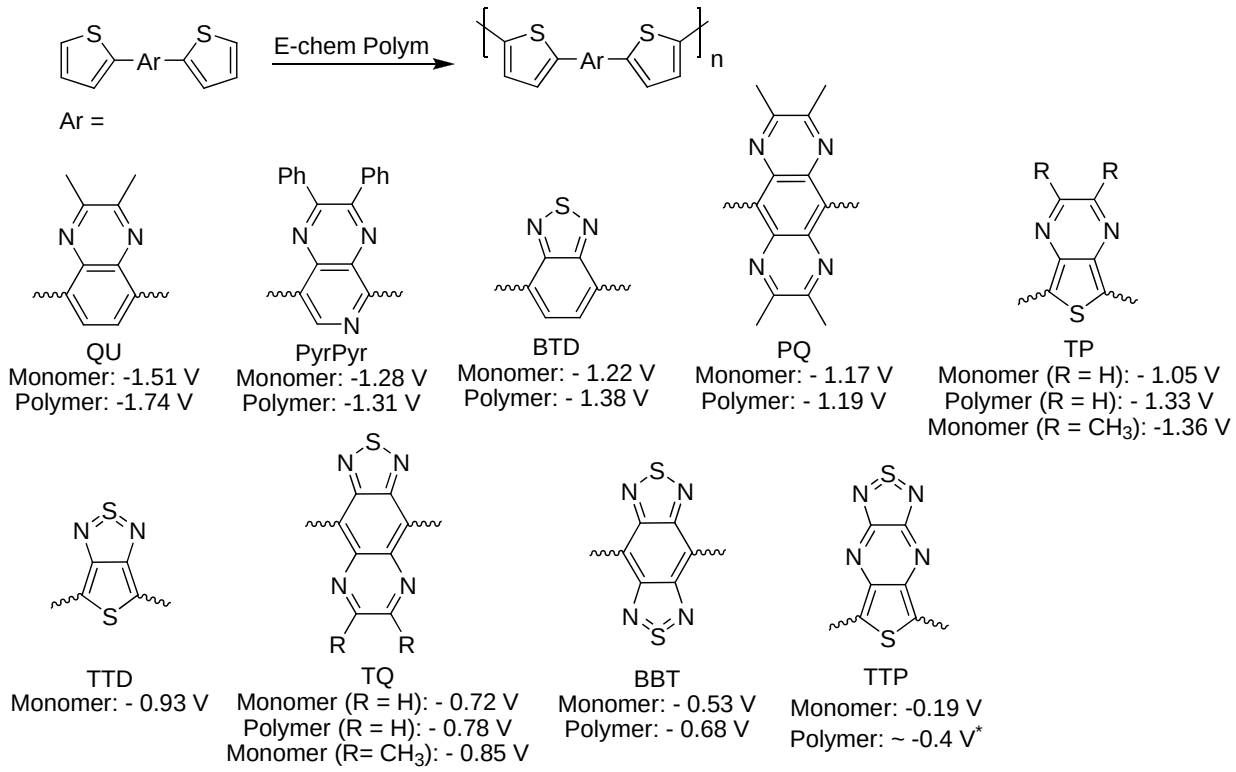

Figure 1-11. Reduction potentials of fused heterocyclic quinoid type acceptors incorporated into DAD oligomers/polymers with thiophene as the donor. The acceptors are quinoxaline (QU); pyrido[3,4-*b*]pyrazine (PyrPyr); 2,1,3-benzothiadiazole (BTD); pyrazino[2,3-*g*]quinoxaline (PQ); thieno[3,4-*b*]pyrazino (TP); thieno[3,4-*c*][1,2,5]thiadiazolo (TTD); [1,2,5]thiadiazolo[3,4-*g*]quinoxaline (TQ); benzo[1,2-c;3,4-c′]bis[1,2,5]thiadiazolo (BBT); [1,2,5]thiadiazolo[3,4-*b*]thieno[3,4-*e*]pyrazine (TTP). All potentials ($E_{p,c}$) are relative to SCE and taken from the literature.* polymer reduction potential was estimated from the CV shown.[111,112,120]

Design Principles of DAD Architectures for CP's

One of the major advantages of the DAD architecture is its ability to undergo electrochemical polymerization quite easily when designed properly. It is in the choice of the donors and acceptors that allows one to control the final properties of the polymers via the DAD monomer structure. While the structure property relationships between the DAD architecture

and the optoelectronic properties of the polymers will be examined throughout this dissertation, a few desirable properties will be highlighted.

The most important issue in the synthesis of DAD compounds is solubility. The nature of the DAD concept leads to at least a minimum of a three ring system, and usually many more. The more solublizing groups (i.e alkyl, branched alkyl, bulky substituents) there are on the compound, the easier it is to handle and purify during synthesis. If the DAD compound is to be used in a chemical polymerization (oxidative, metal mediated), then the more soluble it is, the better. Depending on the choice of donor and acceptor, one might be able to place the solublizing groups on the donor, the acceptor, both, or none. Usually stronger acceptors like, benzothiadiazole (BTD), benzobisthiadiazole (BBT), thienylthiadiazole (TTD), and thienylthiadiazolopyrazine (TTP) do not allow for incorporation of solublizing groups, so they must be incorporated onto the donor if required (depending on whether making a DAD homopolymer or copolymerizing with a different monomer). There are a myriad of acceptors that allow for incorporation of solubility such as quinoxaline (QU), pyridopyrazine (PyrPyr), thienylpyrazine (TP), and thiadiazoloquinoxaline (TQ). In these acceptors, the solublizing groups are located far enough away from the conjugated backbone not to cause steric interactions interfering with the planarity of the CP, but will influence the interchain interactions. If the acceptor chosen is a three ring acceptor system where the donors are attached to the middle ring, only small five-membered ring heterocyclic donors like thiophene, N-H pyrrole, and their fused analogs will be highly planar. Bulkier six-membered ring heterocyclic donors such as phenylenes, fluorenes, carbazoles, substituted pyrroles, and dioxythiophenes will be twisted out of plane, thus blue-shifting the band gap. An example of this is the comparison of BTh-BBT to BEDOT-BBT, and will be discussed in chapter 4. If the donor is attached to a multi-ring

acceptor at one end, then five-membered ring heterocyclic donors such as thiophene, N-H pyrrole, their fused analogs, and dioxythiophene donors can be nearly planar. BEDOT-PyrPyr-Ph_2 is a good example of this.[67] It is through these multiple interactions along with donor and acceptor strength that the chemist can design the DAD monomers for fine control over the polymers optical and electronic properties.

The remainder of this dissertation will deal with the structure-property relationships of various donor acceptor polymers starting from the DAD architecture. The DAD architecture lends itself to electropolymerization, which allows for easy and quick characterization of the optical and electronic properties. Chapter 3 explores the initial foray into the DAD polymer synthesis and characterization involving pyridopyrazine chemistry. Upon realizing the faults of the initial system, Chapter 4 explores increasing the acceptor strength to stronger TQ and BBT based acceptors. Multiple dioxythiophene based donors were also investigated, to come up with a family of polymers capable of fine control over the optical and electronic properties with hopes of improved stability. Finally, Chapter 5 will deal with incorporating these types of acceptors into new soluble, very low band gap polymers. The goal was to find a strong donor with the proper connectivity to these strong acceptors in order to create even lower band gap polymers that are solution processable. Through collaboration with Seth Marder at Georgia Tech, a strong dithienylpyrrole (DTP) based donor was coupled to the various thiadiazole based acceptors discussed previously, yielding the lowest band gap, soluble, conjugated polymers to date.

CHAPTER 2
EXPERIMENTAL

Overview

This chapter provides an overview of the experimental methods and analytical techniques used to prepare and characterize the monomers and polymers in this dissertation. These methods and techniques will only be highlighted since previous Reynolds group dissertations have exhaustively explained these techniques. The synthetic details for the specific compounds can be found in Chapters 3-5.

Molecular Characterization

Compounds were characterized by ^{1}H and ^{13}C NMR using a Mercury 300 FT-NMR, VXR-300 FT NMR, and a Gemini 300 FT-NMR. High resolution mass spectrometry was performed at the University of Florida, Department of Chemistry using either an Agilent 6210 time-of-flight mass spectrometer, a Bruker Apex II FTICR mass spectrometer, or a Finnigan MAT 96Q mass spectrometer. Elemental (CHN) analysis was performed at the University of Florida, Department of Chemistry, Atlantic Microlabs, and Robertson Microlit labaoratories.

X-Ray Crystallography

X-ray quality crystals were obtained from slow evaporation/diffusion of solutions in the following manner. The compounds were dissolved in good solvent, such as dichloromethane or chloroform, and placed inside a test-tube. Then heptane, a poor solvent for the compound, was added carefully to form a layer on top of the good solvent. The test-tube was then covered with aluminum foil and the solution was allowed to diffuse and evaporate slowly.

Data were collected at 173 K on a Siemens SMART PLATFORM equipped with A CCD area detector and a graphite monochromator utilizing MoK_{α} radiation ($\lambda = 0.71073$ Å). Cell parameters were refined using up to 8192 reflections. A full sphere of data (1850 frames) was

collected using the ω-scan method (0.3° frame width). The first 50 frames were re-measured at the end of data collection to monitor instrument and crystal stability (maximum correction on I was < 1 %). Absorption corrections by integration were applied based on measured indexed crystal faces.

The structure was solved by the Direct Methods in SHELXTL6, and refined using full-matrix least squares. The non-H atoms were treated anisotropically, whereas the hydrogen atoms were calculated in ideal positions and were riding on their respective carbon atoms.

For **6a** (Chapter 4), the asymmetric unit consists of two half molecules (each located on an inversion center). One of the molecules has a disorder in the C18-C19 unit and was refined in two parts (minor part is labeled C18'-C19'). Their site occupation factors were dependently refined. A total of 270 parameters were refined in the final cycle of refinement using 3205 reflections with $I > 2\sigma(I)$ to yield R1 and wR2 of 3.74% and 9.23%, respectively. Refinement was done using F2.

For **6b** (Chapter 4), the asymmetric unit consists of two chemically equivalent but crystallographically independent molecules. A total of 289 parameters were refined in the final cycle of refinement using 1990 reflections with $I > 2\sigma(I)$ to yield R1 and wR2 of 6.76% and 15.26%, respectively. Refinement was done using F2.

For **7a** (Chapter 4), a total of 298 parameters were refined in the final cycle of refinement using 3658 reflections with $I > 2\sigma(I)$ to yield R_1 and wR_2 of 4.07% and 9.74%, respectively. Refinement was done using F^2.

For **7c** (Chapter 4), a total of 352 parameters were refined in the final cycle of refinement using 4962 reflections with $I > 2\sigma(I)$ to yield R_1 and wR_2 of 4.00% and 10.48%, respectively. Refinement was done using F^2.

Polymer Characterization

Polymers were characterized by ^{1}H NMR using a Varian Mercury 300 MHz spectrometer. Elemental analyses were carried out by Atlantic Microlabs. Thermal gravimetric analysis (TGA) measurements were performed on NETZSCH thermogravimetric analyzer (model STA 449C) under a nitrogen flow at a heating rate of 10 °C/min or on a TA Instruments TGA Q5000 thermogravimetric analyzer under an air flow at a heating rate of 30 °C/min. Differential scanning calorimetry (DSC) was performed on a TA instruments DSC Q1000 equipped with liquid nitrogen cooling accessory calibrated with sapphire and indium standards. All samples (2-5 mg) were prepared in hermetically sealed pans and referenced to an empty pan. Gel permeation chromatography (GPC) was performed using a Waters Associates GPCV2000 liquid chromatography system with its internal differential refractive index detector (DRI) at 40 °C, using two Waters Styragel HR-5E columns (10 μm PD, 7.8 mm i.d., 300 mm length) with HPLC grade THF as the mobile phase at a flow rate of 1.0 mL / min. Injections were made at 0.05 - 0.07 % w/v sample concentration using a 220.5 μL injection volume. Retention times were calibrated against a minimum of nine narrow molecular weight polystyrene standards (Polymer Laboratories; Amherst, MA).

Electrochemical Methods

Electrochemistry allows one to probe the electronic redox properties of conjugated polymers in order to determine the band gap and position of the highest occupied molecular orbital (HOMO) and lowest unoccupied molecular orbital (LUMO) levels. The HOMO level is usually taken as the onset of oxidation, while the LUMO level is taken as the onset of reduction as determined by cyclic voltammetry (CV) or differential pulse volatmmetry (DPV).

All potentials reported in this dissertation were measured relative to the Fc/Fc^+ redox couple, and then converted to volts verses the saturated calomel electrode (SCE), since most of the literature reports potentials relative to SCE. In this work, $E_{(SCE)} = E_{(Fc)} + 0.38$ V.[121] To determine the HOMO/LUMO levels relative to vacuum, $E_{(VAC)} = E_{(SCE)} + 4.7$ V.[37]

General Set-Up

Electrochemical experiments were performed in a three electrode cell consisting of a platinum button (0.02 cm^2) working electrode, a platinum flag counter electrode and a Ag wire pseudo reference electrode or a Ag/Ag^+ reference electrode calibrated using a 5 mM Fc/Fc^+ in 0.1 M supporting electrolyte solution. Spectroelectrochemical experiments were performed on ITO-coated glass working electrodes (~ 1.5 cm^2) using a Ag wire pseudo reference electrode and a platinum wire counter electrode.

The supporting electrolyte used in all of the experiments was tetrabutylammonium perchlorate (TBAP) dissolved in freshly distilled methylene chloride (DCM), acetonitrile (ACN) or propylene carbonate (PC). All electrochemical and spectroelectrochemical measurements were made with an EG&G PAR model 273A potentiostat/ galvanostat, and optical data was measured with a Cary 500 UV-VIS-NIR spectrophotometer or a StellerNet Diode Array UV-VIS-NIR.

Preparation of DAD Monomer Solutions for Electrochemicalpolymerization

In general, monomer concentrations used in elecrochemcial polymerization are in the range of 5 to 10 mM. Sometimes it is possible to deposit polymer films from lower concentrations. The most common used solvents for polymer deposition are DCM, ACN and PC. The goal is to synthesize a DAD compound with just enough solubility to dissolve in one or a mixture of these solvents, but yet still be able to handle on the synthetic end.

The choice of solvents can be troublesome, and usually involve a lot of trial and error depending on the molecule you are trying to polymerize. Ideally, there should be enough solubility for the monomer (5-10 mM), but poor solubility for the polymer (to prevent dissolution and increase deposition). For DAD monomers without any solublizing groups, usually straight DCM works quite well. For DAD monomers with solublizing groups, usually straight PC or ACN will work depending on solubility. More often than not a mixture of DCM/PC or DCM/ACN will be needed. The best way to make up solutions of mixed solvents is to use a minimum amount of good solvent to dissolve the monomer, and then add the poor solvent until the desired volume is reached. If the DAD compound crashes out during addition of the poor solvent, it may be necessary to add a little more of the good solvent to re-dissolve the DAD monomer. This is analogous to the recrystallization of compounds from acetone/water, and works quite well.

Deposition of Polymers

For soluble polymers, films were deposited onto the working electrode by drop-casting or spray-casting from 2 to 5 mg/mL toluene or chloroform solutions. However, most of the polymers studied in this dissertation were prepared by electrochemical polymerization. Polymer deposition onto the working electrode was performed potentiostatically or by repetitive scan cyclic voltammetry. In both cases, 5 mM monomer in 0.1 M TBAP supporting electrolyte solution was used. For repetitive scan cyclic voltammetry, the monomer was scanned from a neutral potential to a point just past the monomer oxidation potential. Potentiostatic deposition was done by holding the potential constant, just beyond the monomer oxidation potential, until a certain amount of charge (~0.04 C) had passed. The films were then rinsed with DCM or ACN and characterized in monomer free electrolyte solution.

Cyclic Voltammetry/Differential Pulse Volatmmetry

The majority of the work in this dissertation centers around cyclic voltammetry (CV) and differential pulse voltammetry (DPV) characterization of polymer films drop cast or electrodeposited onto platinum button or ITO coated glass working electrodes. Detailed explanations of these techniques in various Reynolds' group dissertations have been quite extensive and serve as a good reference point.[39,78,122] In CV, usually the potential of the working electrode is scanned from a neutral potential (the polymer is in its insulating form), to a vertex potential (oxidizing or reducing potential of the polymer) back to the neutral potential at a constant rate while the current is monitored. As the potential approaches the polymers oxidation potential, electrons are removed from the polymer and the charge is counter balanced by the supporting electrolyte. This results in a current flow and is measured as a function of change in potential relative to time (scan rate). For polymer films adhered on an electrode surface which are not under diffusion control, the relationship between peak current and scan rate can be seen in equation 2-1.

$$I_p=(n^2F^2/4RT)\,\upsilon A\Gamma_O^* \quad \text{Equation (2-1)}$$

Here, n = the number of electrons, F = Faraday constant (96,485 C/mol), R = the universal gas constant, T= temperature, υ = scan rate (V/s), A = area of the electrode (cm^2, and Γ_O^* = concentration of adsorbed O (mol/cm^2). For well adhered films, the peak current varies linearly with scan rate, and the film is not under diffusion control. For reversible systems, the peaks on the forward and reverse scans should be symmetrical in shape and intensity, but with equal and opposite signs for the current. For polymers though, the forward and reverse scans are usually not symmetrical due to different adsorption strengths or O and R, double layer charging, different film morphologies, charge transport, and various changes in the film during the process (swelling & contracting).

The best way to minimize the factors that contribute to the asymmetry of the CV curve (especially charging currents) is through the use of DPV. Comparing CV to DPV, CV uses a saw tooth wave form while DPV utilizes a potential square wave form (Figure 2-1). In the CV waveform, the current is being measured constantly, so background currents (such as charging of the double layer) are included in the measurement along with the current associated with the oxidation or reduction. In DPV, the potential is held constant for certain amount of time while the background current is monitored, and then right before the pulse, the current is measured at i_o. Then a pulse is applied (amplitude is usually 10 -100 mV), and the current is measured again immediately after the pulse i. Then the potential comes back down to a slightly higher potential, depending on the step size (usually 1-2 mV). The advantage of DPV is by measuring the differential current (i-i_o), it allows for the background charging currents to reach equilibrium before the pulse is applied, and if the pulse is not close to the $E^{0'}$ of the system, no faradaic current is measured, thus yielding no real current response. Only when the pulse approaches the $E^{0'}$ of the system and oxidation or reduction begins to occur will a faradaic current be measured.[123] The longer the step time the better the sensitivity you will have since the charging currents will be minimized. The increased sensitivity of DPV allows for improved accuracy for measuring the onsets for oxidation and reduction, and thus determining the HOMO/LUMO values. This also can be a good indication of how reversible a system really is. For a reversible system, the peaks should be highly symmetrical and sharp with minimal peak to peak separation (less than 100 mV for conjugated polymers).

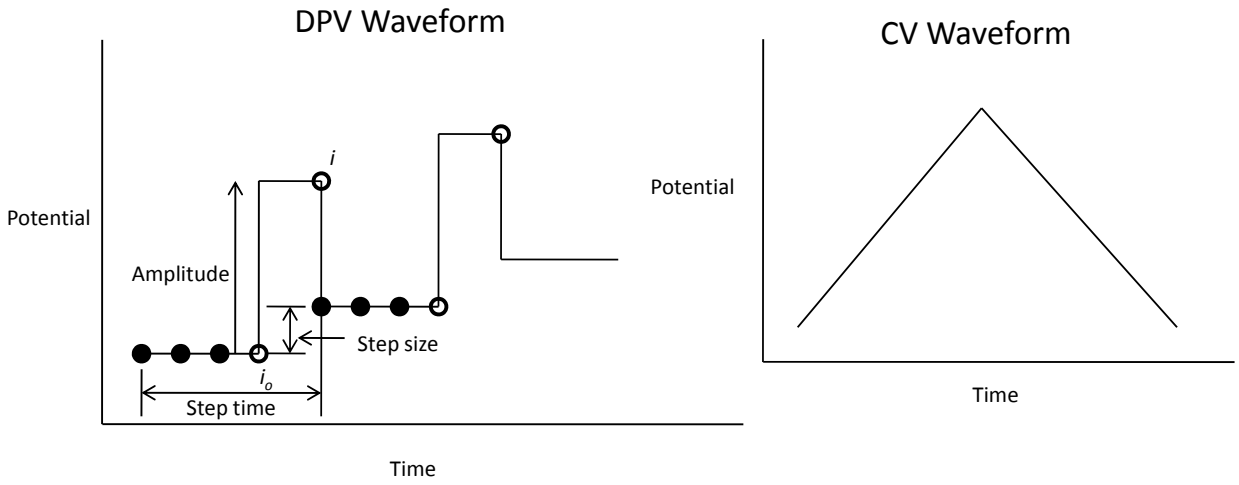

Figure 2-1. Example of DPV waveform relative to CV waveform.

Optical Characterization

Materials for Optical Characterization

Most often polymer optoelectronic properties are investigated using ITO coated glass working electrodes. These electrodes are highly transparent in the visible region of the spectrum, allowing for optimum characterization for the different colored states (redox states) of a conjugated polymer. This electrode is well suited for polymers with band gaps (defined as the onset of the lowest energy absorption) ≥1 eV. However, when working with donor-acceptor systems with low band gaps, ITO can be a problem due to a strong absorption beyond 1600 nm. This makes it hard to determine the optical band gap due to poor baseline resolution. Switching to single walled carbon nanotube electrodes (SWCNTs), which are highly transparent into the NIR, allow for increased accuracy in bad gap determination.[124] This electrode material has played an important role in the characterization of some of the low band gap polymers in this dissertation, and has proven to be a valuable commodity in the band gap determination for very low band gap polymers.

Spectroelectrochemistry

To develop a more complete understanding of the systems studied in this dissertation, spectroelectrochemistry was performed on these systems. Typically, the polymers were electrodeposited potentiostatically onto ITO coated glass working electrodes from 5 mM monomer 0.1 M TBAP solutions containing various amounts of DCM, ACN, or propylene depending on monomer solubility. For soluble polymers, films were spray cast from 3-5 mg/mL polymer solutions in chloroform or toluene. The films were then placed in a cuvette equipped with a platinum wire counter electrode and a silver wire pseudo reference electrode. The cuvette was then filled with degassed monomer free electrolyte solution (usually 0.1 M TBAP-PC for most of the work in this dissertation), and the films were then broken in by repetitive scanning in a potential window containing the desired redox couple until a reproducible trace was attained (*ca.* 20 times). Characterization of a polymer's neutral to oxidized state was performed on the bench top using a Carry 500 UV-VIS-NIR spectrophotometer. It is important to note that all bench top experiments were performed under an argon blanket. For characterization of a polymer's neutral state to the reduced state(s), the use of the glove box was required due to the high sensitivity of radical anions towards water and air. These measurements were recorded on a Stellarnet Photodiode Array spectrophotometer connected to the glove box via fiber optic cables. In certain cases, the reductive characterization was done on the bench top under stringent air and moisture free conditions. Spectroelectrochemistry allows one to monitor the change in the absorption profile of a polymer as it is switched between different redox states. This gives insight into the optical band gap, how to control the polymers colored states through structural modification, and the nature of charge carriers formed upon oxidation or reduction.

CHAPTER 3
P(BEDOT-PYRIDOPYRAZINE): PROBING THE PROPERTIES OF A MULTIPLE REDOX STATE POLYMER

Introduction

Low band gap polymers have been the focus of many studies, and were reviewed briefly in Chapter 1. These polymers are colored in the neutral state due to the π-π^* transition located at low energies, and become more transparent upon doping with a decrease of the π-π^* transition and development of lower energy transitions. By having a low band gap, the conduction band can be reached easier, allowing for the possibility of n-type doping. Thus, low band gap polymers could lead to dual p-type and n-type electrochromic devices with a single polymer. Some methods for obtaining these polymers were discussed earlier in Chapter 1, including, but not limited to, minimizing bond-length alternation, interchain effects, planarity, and donor-acceptor effects.

Donor-acceptor polymers are of interest because they possess multiple redox states (p-type or n-type doping) in a small potential window. This is due to the placement of the valence band (highest occupied molecular orbital, HOMO) relative to the conduction band (lowest unoccupied molecular orbital, LUMO). The goal is to select a strong donor with a high HOMO level and a strong acceptor with a low LUMO level. When the donor and acceptor are coupled, the orbitals mix forming a new set of orbitals, with the newly formed HOMO taking on a similar energy to the donor while the LUMO will be similar in energy to the acceptor. As was discussed in Chapter 1, the LUMO is thought to be isolated on the acceptor instead of being a true conduction band, and the small gap is attributed to intramolecular charge transfer (ICT). Nonetheless, the new donor-acceptor material now has a much smaller HOMO-LUMO gap compared to its

individual parts. With the proper choice of donor and acceptor, the band gap can be modified and thus the final properties can be adjusted.

Some previously investigated donor-acceptor systems involved cyano and nitro functionalized acceptors,[125-127] polysquaraines,[63,128] cyanovinylenes[10,38,129] and fused ring aryl acceptors such as pyridopyrazine and thiadiazole rings.[59,112,130] One of the more interesting systems involves the pyridopyrazine acceptor moiety. This structure allows access to multiple redox states, which can lead to more complex devices.[67,68,112,131] Instead of just having two colored states associated with the neutral and oxidized species of a polymer, there is the possibility of having three to four different colored states depending if the polymer has one or two reductions. One of the benefits of using this acceptor for an initial study is the synthetic ease by which these acceptors can be prepared. The pyridopyrazine acceptor is capable of stabilizing two negative charges. When this unit is coupled to a donor that is easily oxidized, there is now the possibility of four electronic states. A polymer of this structure can be cycled electrochemically (in a suitable solvent/electrolyte system) from the neutral state to reveal the two possible reduced states and the oxidized state. These states can lead to different colors associated with the electrochromic properties of the polymer system. It is also possible to add solublizing groups to the pyridopyrazine acceptor unit via the installation of the pyrazine ring.[132] Poly[5,8-bis-(3-dihydro-thieno[3,4-b][1,4]dioxin-5-yl)-2,3-diphenyl-pyrido[3,4-b]pyrazine (PBEDOT-PyrPyr-Ph_2) (Figure 3-1), which was synthesized previously in our group,[68] shows four distinct electronic states; the neutral form is lime green, the oxidized state it is light gray, the first reduced state is a burgundy red, and the second reduced state it is a dark gray.

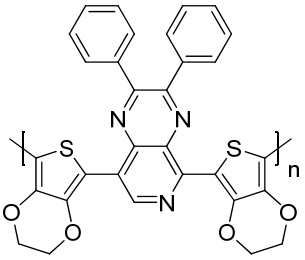

Figure 3-1. Structure of PBEDOT-PyrPyr-Ph_2.

Choosing the proper donor for the donor-acceptor-donor (DAD) monomer structure is important. By choosing EDOT as the donor, one can take advantage of its low oxidation potential for ease of electrochemical synthesis.[75,76] This allows for electrochemical deposition of polymers onto platinum button or ITO coated glass working electrodes for characterization of their electronic and optical properties. The DAD architecture can be accessed by different transition metal cross-coupling reactions. The Reynolds group and the Yamamoto group have demonstrated the effectiveness of the Stille and Negishi coupling reactions towards the DAD architecture.[112,133-135] Yamamoto *et. al.* have used the Stille method for the coupling of thiophene to various quinoxaline and pyridiopyrazine derivatives to make donor-acceptor polymers. Reynolds *et. al.* have used the Stille and Negishi couplings of EDOT to carbazole, pyridine, and pyridopyrazine.[67,68,136]

This work will investigate the differences in the optical and electronic properties relative to having solublizing alkyl groups verses phenyl groups located on a pyridopyrazine acceptor in the DAD architecture with 3,4-ethylenedioxythiophene as the donor. Functionalized acceptor targets of 5,8-dibromo-2,3-dihexyl-pyrido[3,4-b]pyrazine and 5,8-dibromo-2,3-didodecylpyrido[3,4-b]pyrazine were chosen since long alkyl chains have been shown to increase solubility, allowing for easier purification and handling of solutions. The polymers have been analyzed by cyclic voltammetry and spectroelectrochemistry to investigate their electronic and optical properties. A comparison of the electronic and optical data to that of the previously made phenyl derivative

will be used to establish structure-property relationships. These polymers might also be interesting for supercapacitor applications since previous investigations have shown PEDOT and its derivatives to have high stability, fast switching kinetics and high charge storage capacity.[137,138]

Monomer Synthesis and Characterization

The synthesis of 5,8-dibromo-2,3-dihexylpyrido[3,4-*b*]pyrazine (**5**) is outlined in Figure 3-2. First, 3,4-diamino pyridine was brominated at the 2 and 5 positions with bromine in 48 % HBr to yield 3,4-diamino-2,5-dibromopyridine (**2**).[112] This provides the base of the acceptor unit which can then be functionalized with α-diones. Second, tetradecane-7,8-dione (**4**) was prepared by the oxidation of 7-tetradecyne with $KMnO_4$ in acetone/H_2O.[139] Finally, (**5**) was obtained by the condensation between **2** and **4** in refluxing butanol.[112]

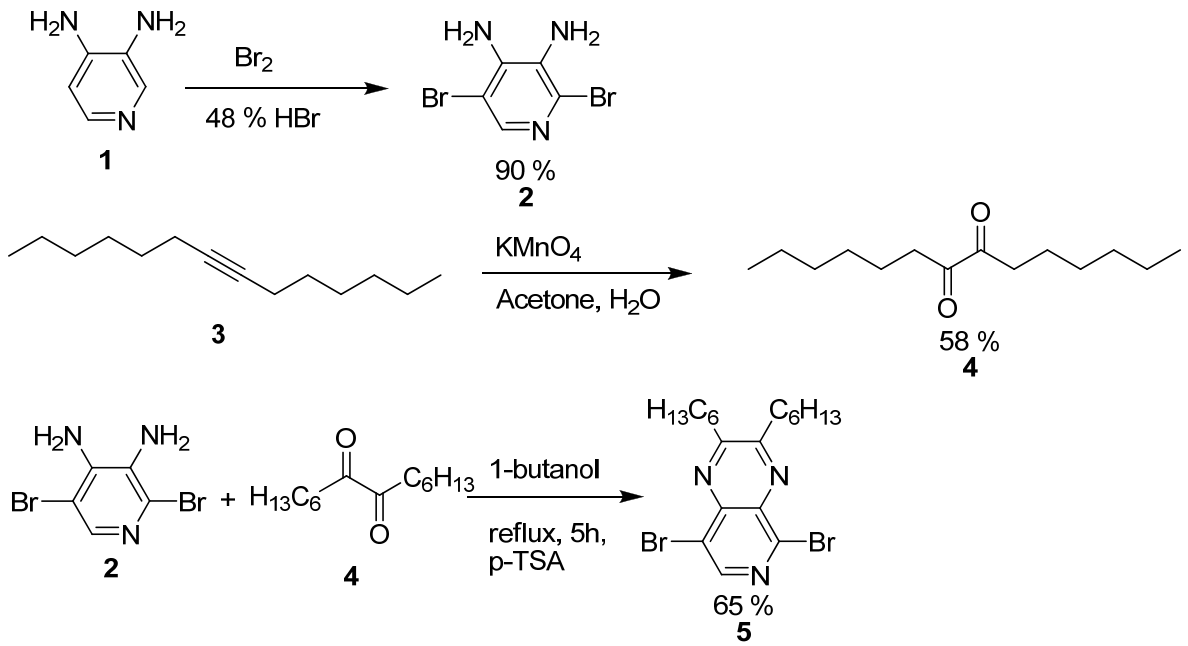

Figure 3-2. Synthesis of 5,8-dibromo-2,3-dihexyl-pyrido[3,4-b]pyrazine.

The synthesis of 5,8-dibromo-2,3-didodecylpyrido[3,4-*b*]pyrazine (**9**) (Figure 3-3), began with the formation of the internal alkyne. Lithiation of 1-tetradecyne (**6**), followed by the addition of 1-bromododecane, yielded hexacos-13-yne (**7**).[132] Subsequent $KMnO_4$ oxidation of **7**

yielded hexacosane-13,14-dione (**8**).[140,141] Finally, the condensation reaction between **2** and **8** in refluxing butanol yielded **9**.[112]

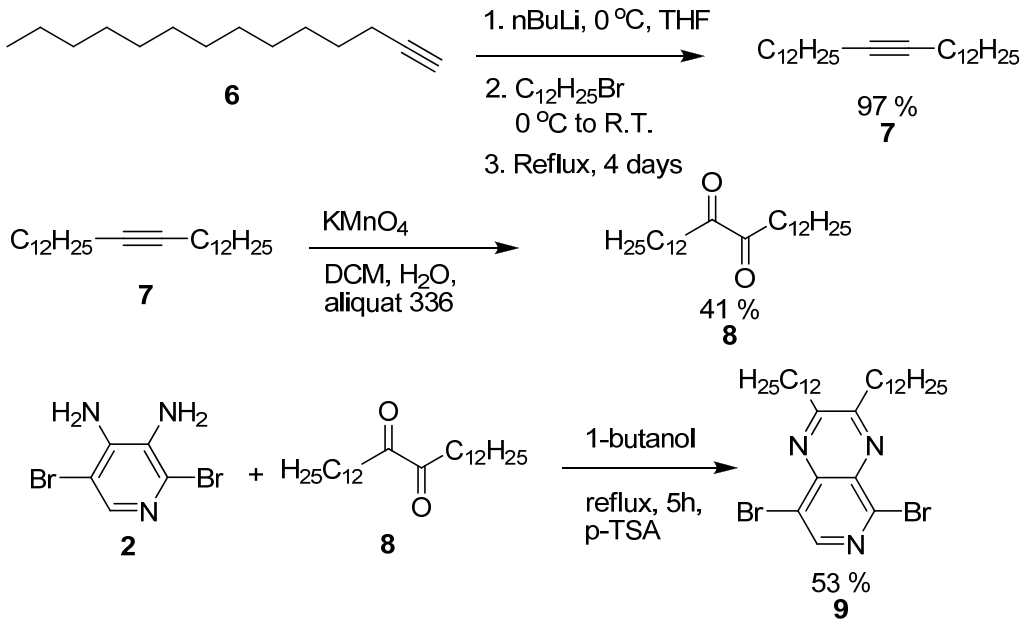

Figure 3-3. Synthesis of 5,8-dibromo-2,3-didodecylpyrido[3,4-b]pyrazine.

With the acceptor units in hand, the preparation of the DAD monomers and polymers were carried out (Figure 3-4). The DAD structure was chosen because it allows for the deposition of polymer directly onto working electrodes, such as platinum or ITO, for further electronic and optical characterization. (2,3-Dihydrothieno[3,4-b][1,4]dioxin-5-yl)trimethylstannane (**10**) was chosen as the donor due to the ability to isolate and purify it before coupling.[39,98,142] A Stille cross-coupling reaction between the donor (**10**) and the acceptors **5** and **9** yielded 5,8-Bis-(2,3-dihydrothieno[3,4-b][1,4]dioxin-5-yl)-2,3-dihexyl-pyrido[3,4-b]pyrazine (**11**) and 5,8-Bis-(2,3-dihydro-thieno[3,4-b][1,4]dioxin-5-yl)-2,3-didodecyl-pyrido[3,4-b]pyrazine (**12**) in moderate yields.

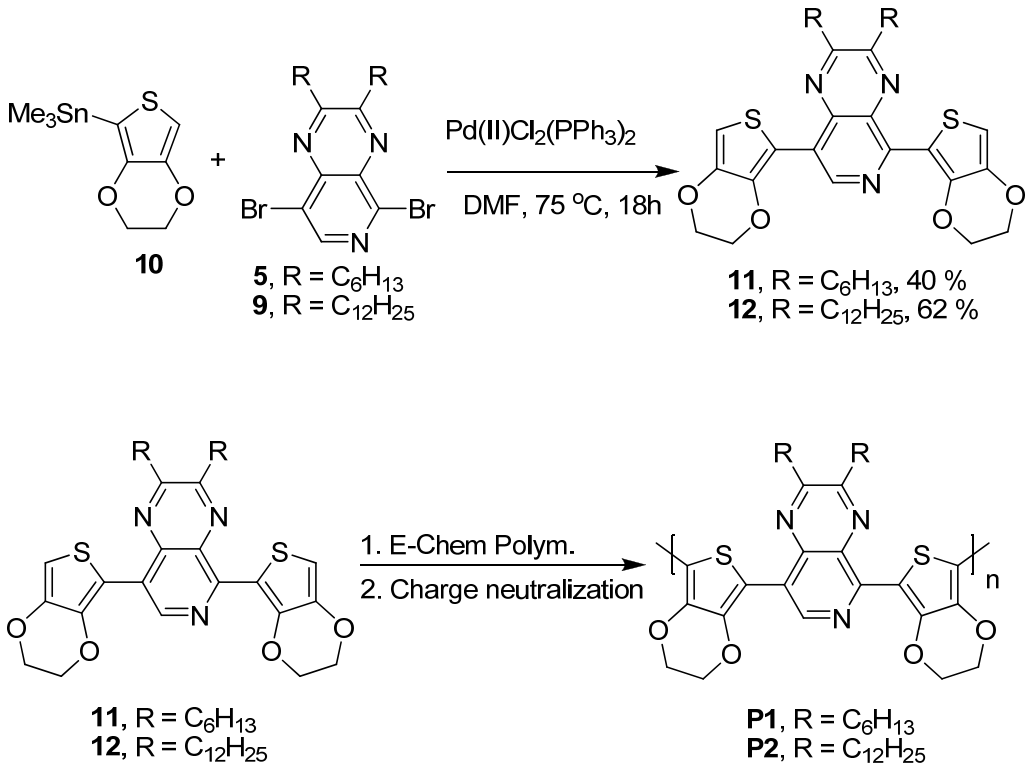

Figure 3-4. Synthesis of monomers **11** and **12** and their respective polymers **P1** and **P2**.

Electrochemical Polymerization/Characterization

Electropolymerization

One of the reasons for the monomers being functionalized with alkyl chains was to obtain continuous, optically clear films (due to the film forming properties of alkyl chains) relative to the previously studied phenyl derivative, which would sometimes crack. Electropolymerization of the monomers was carried out via repeated scan cyclic voltammetry in an electrochemical cell, consisting of a platinum button working electrode, a platinum (flag or wire) counter electrode, and a silver wire pseudo reference electrode. The pseudo reference electrode was calibrated with the ferrocene redox couple (Fc/Fc^{+}) from a solution containing 5 mM ferrocene and 0.1 M TBAP (tetrabutylammonium perchlorate) in acetonitrile. All of the potentials in this chapter are reported as V vs. SCE (as discussed in Chapter 2) for easy comparison throughout this dissertation and to literature values. The polymers were deposited from a 5 mM monomer,

0.1 M supporting electrolyte (TBAP) solution in 1:1 dichloromethane:acetonitrile (DCM:ACN). The formation of **P1** and **P2** from **11** and **12** can be seen in Figure 3-5.

During the first scan in Figure 3-5 A, there is a large peak at 0.88 V. This is due to the oxidation of monomer **11** at the electrode. On the reverse part of the first scan there is a slight reduction peak associated with the reduction of the deposited oligomers/polymer on the electrode. Subsequent cycling shows a broad oxidation and reduction that increases in intensity and develops at lower and lower potentials. This is due to the fact that as the monomer couples to form oligomers and polymer, the conjugation in these chains is extended and the oxidation of longer oligomers and polymer chains take place at lower potentials than the monomer. The increase in current density of these lower oxidation and reduction peaks is a good indication of polymer film formation on the electrode. This is similar to the electrochemical polymerization of monomer **12**, which has its monomer oxidation potential at 0.86 V (Figure 3-5 B). Both monomers gave smooth polymer films. The electrodes and attached polymer films were then rinsed with monomer free electrolyte to remove any residual monomer and the films were inspected before further characterization.

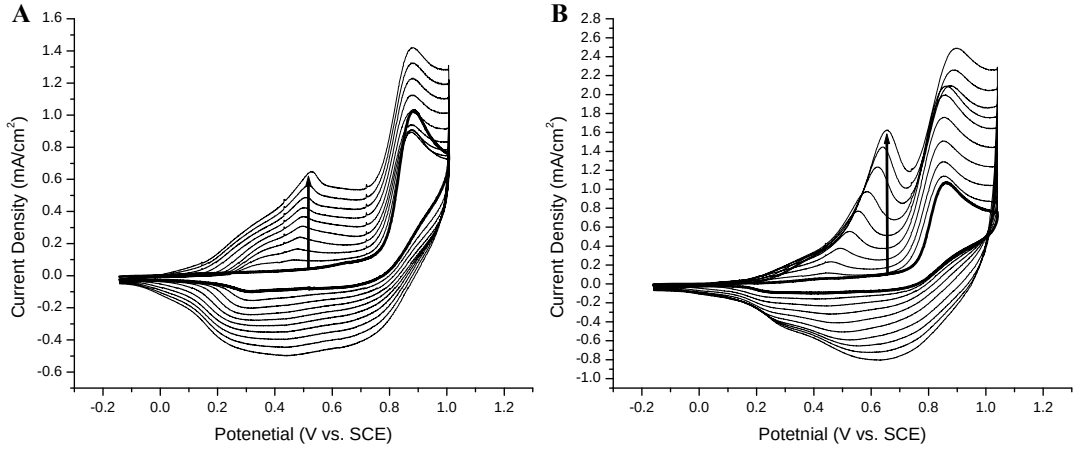

Figure 3-5. Repetitive scan electropolymerization (50 mV/s, 10 cycles) from a 5 mM monomer 0.1 M TBAP/1:1 DCM:ACN solution. A) Monomer **11** yielding **P1**. B) Monomer **12** yielding **P2**.

Cyclic Voltammetry

The electrodeposited polymer films were then transferred into an electrochemical cell set up as described previously, except a Ag/Ag^+ reference electrode was used, and characterized in monomer free electrolyte solution (0.1 M TBAP in ACN). The polymers were scanned using cyclic voltammetry (50 mV/s) until a reproducible CV was obtained (*ca.* 20 times) in order to investigate the electronic properties. **P1** (Figure 3-6 A) shows an onset of reduction at -1.38 V ($E_{1/2}$ = -1.49 V). The first reduction peak of the polymer is quite stable (over 50 to100 cycles) and quasi-reversible with adequate charge compensation on the reverse scan. However, the second reduction (not shown) is highly unstable and leads to film degradation and loss of electroactivity. The second reduction peak has been observed when a film of **P1** on ITO was switched, however the reduction is nearly irreversible and leads to film degradation. This could be due to the instability of the film at such a low potential and the high reactivity of the radical anions formed. The polymer shows a broad oxidation peak with the main onset of oxidation at ~ -0.03 V. The oxidation of the film is interesting because it shows both a faradaic (oxidation with charge transfer involving electroactive species from -0.03 V to 0.35 V) and non-faradaic response (no further oxidation or charge transfer reactions of electroactive species from ~ 0.35 V to 0.80 V) indicative of capacitive and pseudo capacitive behavior.[143-145] The polymer has an electrochemical band gap of 1.35 eV. The colors for **P1** (Figure 3-6 C) go from a neutral light navy-blue to an oxidized more transparent greenish grey. Upon reduction the film becomes a light greyish pink.

CV analysis of **P2** (Figure 3-6 B) shows an onset for reduction at -1.43 V ($E_{1/2}$ = -1.50 V) , establishing similar behavior to **P1**. While the first reduction has adequate charge compensation on the reverse scan, the peak to peak separation in **P2** is much larger than in **P1** indicating the reduction of **P2** is not as reversible as it is for **P1**. The long alkyl chains in **P2** may result in a

more compact film making it harder for the supporting electrolyte to move in and out of the film. The first reduction has good stability over the 50 to 100 cycles used for characterization. The second reduction for this polymer was highly unstable and could only be seen for a few cycles, as described for **P1**. The onset for oxidation of **P2** was observed at -0.04 V, and has both a faradaic and non-faradaic response similar to that of **P1**. The electrochemical band gap for **P2** is estimated at 1.39 eV.

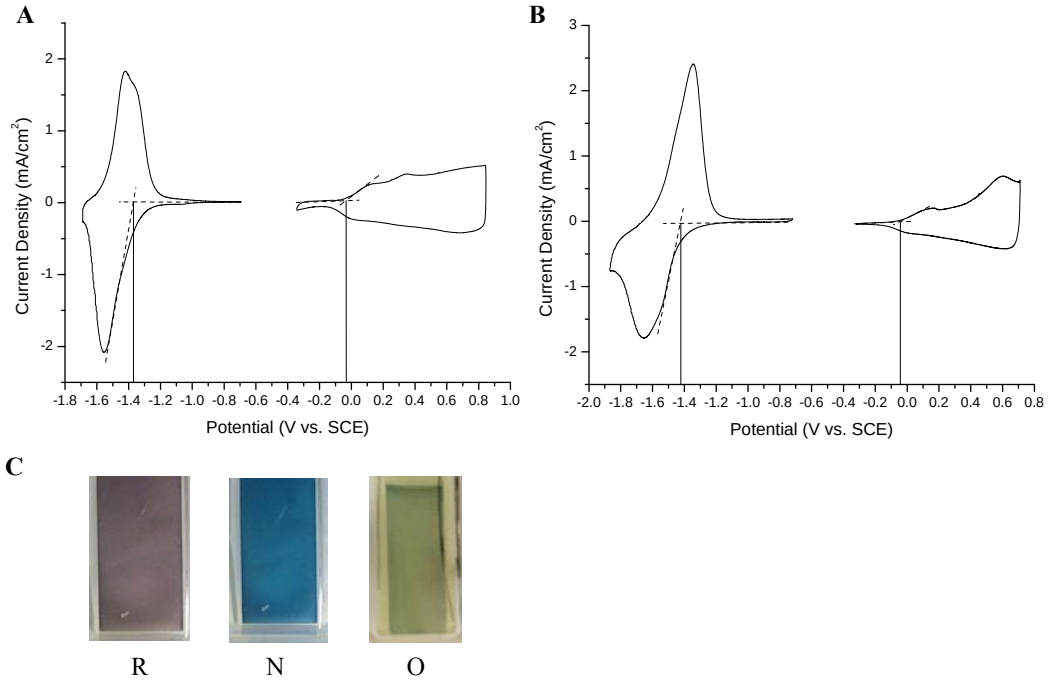

Figure 3-6. Cyclic voltammetry of polymers **P1** and **P2** and the associated colored states. Cyclic voltammetry was performed on a Pt button working electrode in 0.1 M TBAP/ACN at a scan rate of 50 mV/s. Individual films for oxidation and reduction were used. A) CV of **P1**. B) CV of **P2**. C) Pictures of the 1st reduction (R), neutral (N), and oxidized (O) states of **P1**.

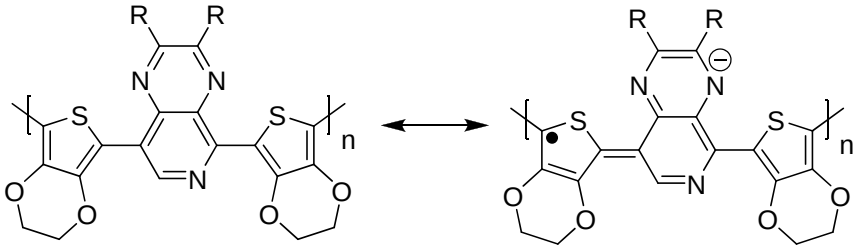

Figure 3-7. Proposed structure for the radical anion of the first reduction.

The key note here is that while both **P1** and **P2** have their first reductions at $E_{1/2}$ = ~ -1.5 V for the first reduction, these values are 400 mV more negative than the previously reported reduction value of $E_{1/2}$ = -1.1 V for P(BEDOT-PyrPyr-Ph_2. One possible reason for this is the electron donating nature of alkyl groups making it more difficult to reduce these polymers. Also, the phenyl groups could extend the conjugation in the solid state resulting in lower reduction poteentials.[146] When looking at the second reduction, the stability is greatly decreased compared to the phenyl derivative. So while we do gain better solubility of the monomers in terms of synthetic work, we lose the electrochemical advantages of having the phenyl groups. This demonstrates another possibility for controlling the band gap.

Spectroelectochemistry

Polymer films of **P1** and **P2** were deposited potentiostatically from 5 mM monomer 0.1 M TBAP/(DCM/ACN) solution onto ITO coated glass working electrodes in order to characterize their optical properties. The films were placed in a cuvette containing 0.1 M TBAP/ACN with a platinum wire counter electrode and a silver wire pseudo reference electrode calibrated to Fc/Fc^+. The films were then neutralized and cycled by CV until a reproducible CV was attained for oxidative spectroelectrochemistry.

Neutral **P1** has a λ_{max} at 689 nm and a high energy peak at 404 nm (Figure 3-8 A). The peak at 689 is attributed to intramolecular charge transfer interactions while the peak at 404 nm is associated with the π-π^* transition.[27,147] The λ_{max} covers most of the visible region tailing off to minimum around 470 nm before rising back up. Thus the polymer is a blue/navy blue in the neutral state. The onset of absorption is at ~850 nm corresponding to an optical band gap of about 1.45 eV. Almost identical absorptions are seen for **P2** (Figure 3-8 B), which has a λ_{max} at 691 nm and a high energy peak at 401 nm. The same tail of the λ_{max} is seen from the red down

to the blue resulting in a blue/navy blue neutral polymer. The onset of absorption is also at ~ 850 nm corresponding to the same optical band gap of 1.45 eV. These values are in good agreement with the electrochemical gap of 1.35 eV for **P1** and 1.39 eV for **P2**. In comparison to the optical band gap of the previously studied P(BEDOT-PyrPyr-Ph_2, (E_g = ~1.2 eV), there is a ~ 0.25 eV increase in the band gap in going from phenyl substituted PyrPyr to the alkyl substituted PyrPyr. Though the difference is not as large as was in the electrochemical data, the trend is observed.

Upon oxidation, there is a bleaching of the both neutral absorptions in **P1** and **P2**, with the decreases beginning around -0.1 to 0.0 V, which matches up well with the CV data for the onset of oxidation. As the oxidation potential is increased, there is the development of a peak around 900 nm along with a tail from the NIR, indicating the formation of polaron charge carriers. In the oxidized state, both polymers now have a shallow v-shape with the tail from the peak at 900 nm reaching a minimum around 500-550 nm with a slight increase in absorption in going to shorter wavelengths yielding a lighter more transparent greenish grey color in the oxidized state.

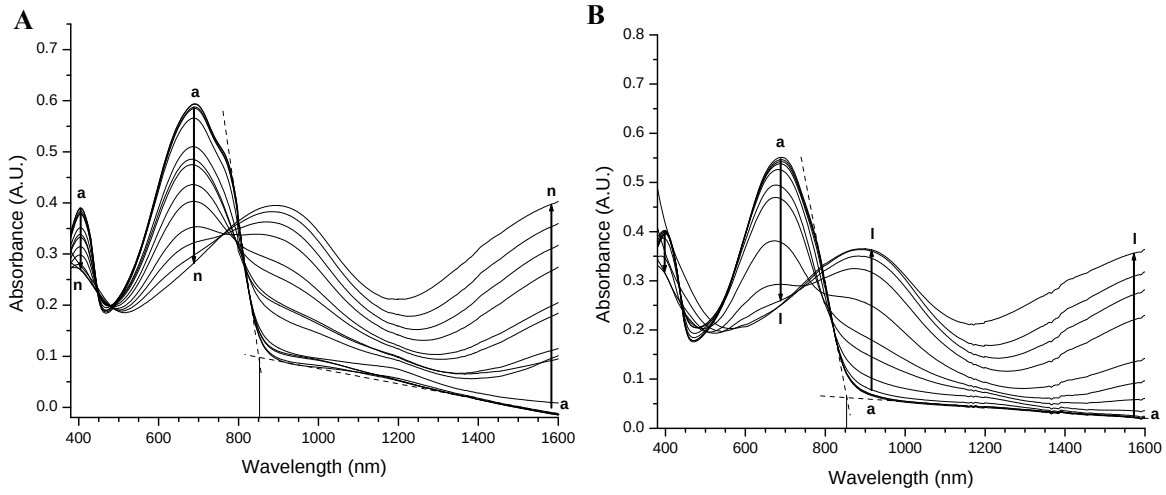

Figure 3-8. Oxidative spectroelectrochemistry of **P1** and **P2** on ITO in 0.1 M TBAP/ACN. (A) **P1** at potentials of (a) -0.49 V to (n) 0.81 V in 100 mV increments; (B) **P2** at potentials of (a) -0.49 V to (n) 0.61 V in 100 mV increments.

Due to the high reactivity of a polymer in the n-doped state to air and water, reductive spectroelectrochemistry was performed in the glove box.[148] This was done using a Stellarnet Diode Array VIS-NIR spectrophotometer which was connected via fiber optic cables into the glove box. This allows for characterization without the worries of water or oxygen contamination from the atmosphere.

Application of reducing potentials to neutral **P1** (the small peak in neutral spectrum around 970 nm is due to trapped charges, and disappears upon more negative potentials) (Figure 3-9) shows a bleaching of the ICT band and the high energy band up to the first reduction (-1.55 V). As these bands bleach, a band develops around 1200 nm tails into the visible region This band in the NIR is indicative of charge carrier formation involving a true n-doped state and matches up well with the first reduction seen by CV.[67] There is also a peak that evolves at ~470 nm during this reduction process that yields a polymer that is grayish pink in color. In going to more negative potentials, there is almost a complete loss of intensity for the charge carrier band at 1200 nm, along with an increase in intensity of the high energy peak at 470 nm with concurrent formation of a shoulder at 630 nm. This peak is probably due to film degradation, as can be seen for a typical film after reductive spectroelectrochemistry (Figure 3-11).

Upon reducing **P2** through the first reduced state, we see similar changes to the absorption spectrum as for **P1**. There is a bleaching of the ICT band and the high energy peak with the concurrent development of a fairly intense band peaking around 1400 nm tailing through the NIR into the visible region, indicative of the formation of an n-doped state. The intensity for this NIR band peaks at -1.75 V, which corresponds with the first reduced state for **P2** as seen by CV.

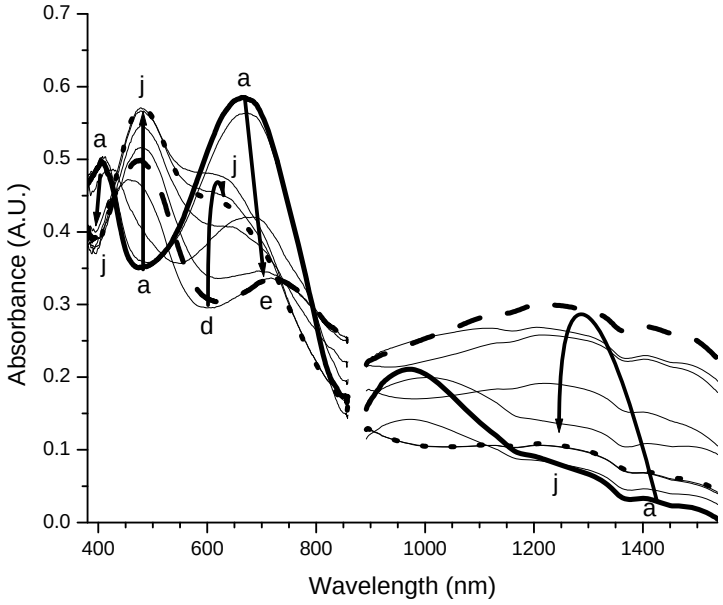

Figure 3-9. Reductive spectroelectrochemistry of **P1** on an ITO coated glass slide in monomer free electrolyte solution (0.1 M TBAP in ACN) at applied potentials of (a) -1.15 V to (j) -2.05 V in 100 mV increments. Bold black line = neutral (-1.15 V), dashed line = first reduction (-1.55 V), and bold dotted line = (-2.05 V)

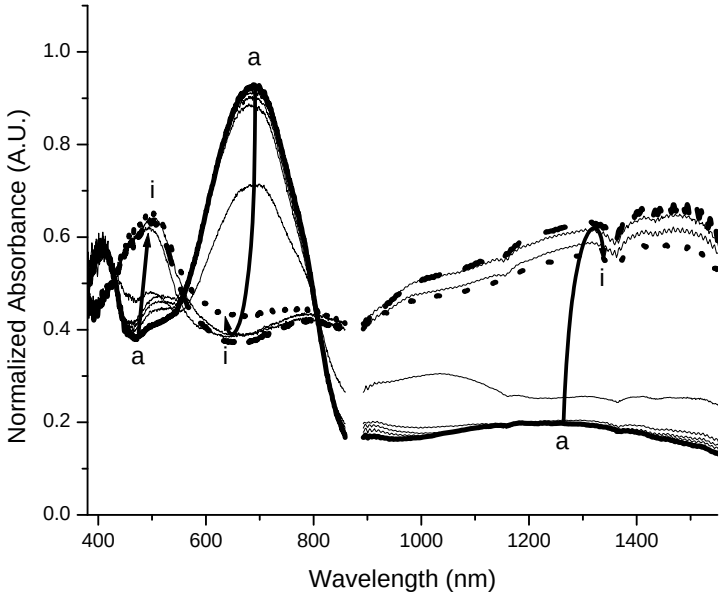

Figure 3-10. Reductive spectroelectrochemistry of **P2** on an ITO coated glass slide in monomer free electrolyte solution (0.1 M TBAP in ACN) at applied potentials of (a) -1.14 V to (i) -1.94 V in 100 mV increments. Bold black line = neutral (-1.14 V), bold yellow = first reduction (-1.75 V), and bold navy = (-1.94 V).

Figure 3-11. Photograph of a film of **P2** after reductive spectroelectrochemistry. The same observations were seen for **P1.**

Conclusions

In this chapter, DAD conjugated polymers with solublizing alkyl groups (C_6H_{13} and $C_{12}H_{25}$) were synthesized, electrochemically polymerized, and characterized. Electropolymerization allows for quick characterization and possible conclusions of structure property relationships. The neutral polymers are navy blue in color with a band gap of ~1.45 eV. The oxidation of these polymers by cyclic voltammetry shows the possibility for use in capacitors due to their faradaic and non-faradaic characteristics. Both polymers show access to multiple electronic and optical states via cyclic voltammetry and spectroelectrochemistry. Their optical properties change in accordance with the electronic states. It should be noted that the second reduction of these polymers were highly unstable upon repeated reductive cycling, where as the first reduction was quite stable. The stability issues seen with the second reduction thus only allows for three different colored states in these polymers compared to the diphenyl derivative, which had four colored states. It is not clear if the loss in stability of the second reduction for these alkyl derivatives is solely due to the more negative reduction potentials compared to the diphenyl derivative, or if it has to due with the nature of the alkyl groups, which have α-protons. These protons could be highly reactive to the radical anions formed during the second reduction. It is unclear right now what causes these stability issues, and further investigation is needed.

Another important aspect of this study shows the ability to fine tune the properties of these DA systems. We saw that in going from the previously reported diphenyl derivative to the alkyl derivatives, there is ~0.2 eV increase in the band gap. This corresponds to a neutral navy blue colored polymer for the alkyl derivative compared to a green color for the neutral phenyl derivative. We also saw a 200-300 mV negative shift in reduction potentials compared to the phenyl derivatives. These properties demonstrate another useful tool for the synthetic organic chemist to fine tune the voltage window of these polymers for possible applications in supercapacitors.

The ability to functionalize the acceptor, via the condensation reaction of the dicarbonyl moiety, is an important feature of these polymers. This could not only lead to solubility, but also to the tailoring of desired properties depending on the application. By synthesizing a dicarbonyl moiety containing different functionalities such as organic dyes instead of alkyl chains, one could access different colors for electrochromic devices.

Experimental

3,4-diamino-2,5-dibromopyridine (2).[112] 3,4-Diaminopyridine (4.99 g, 0.0457 mol) and 110 mL of 48 % HBr was placed into a 250 mL 3-neck round bottom flask equipped with a reflux condenser, addition funnel, and vented to a NaOH scrubber. The solution was then heated to reflux. Bromine (4.73 mL, 0.0293 mol) was added drop wise over ~1 h. The solution was then heated at reflux for 5 h. Upon cooling, a precipitate was collected by filtration and washed with an aqueous solution of saturated $Na_2S_2O_3$, K_2CO_3, and then distilled water. After drying under vacuum 9.37g (77 %) of a cream-colored solid was obtained. ^{1}H NMR (300 MHz, DMSO-d6) δ7.53 (s, 1H), 5.99 (s, 2H), 5.05 (s, 2H); ^{13}C NMR (75 MHz, DMSO-d6) δ104.47, 125.90, 128.80, 138.39, 139.17 HRMS calcd. For $C_5H_5N_3Br_2$ 264.8850 Found 264.8851.

Tetradecane-7,8-dione (4).[139] A 3 L Erlenmeyer flask equipped with a magnetic stir bar was charged with 7-tetradecyne (5.25g, 0.027 mol) and 1.05 L of reagent grade acetone. In a separate flask, 1.36 g of $NaHCO_3$, 13.6 g of $MgSO_4$, and 600 mL of H_2O were combined to form a buffer solution, which was added to the 3 L Erlenmeyer flask. $KMnO_4$ (16.6 g, 0.105 mol) was added and the solution was stirred for 4 h. The unreacted permanganate and precipitated MnO_2 were converted to soluble Mn^{2+} by adding ~ 21 g of $NaNO_2$ and ~140 mL of H_2SO_4. The solution was then saturated with sodium chloride and extracted (3 x 200 mL) with a 1:1 hexane:ether mixture. The organic solvent was removed under reduced pressure and the residue was dissolved in 50 mL of ether and extracted (4 x 50 mL) with 5 % NaOH. After washing the solution with brine, and drying over $MgSO_4$, the solvent was removed under reduced pressure to yield a yellow solid. After recrystallization from MeOH, 3.56 g (58 %) of yellow plates were obtained. mp 40 ^oC (lit. 38-39 ^oC).[27] ^1H NMR (300 MHz, $CDCl_3$) δ 0.88 (t, 6H), 1.29 (m, 12H), 1.57(p, 4H), 2.73 (t, 4H) HRMS calcd. For $C_{14}H_{26}O_2$ 226.1933 Found 226.1927.

Hexacos-13-yne (7).[132] Under an argon atmosphere, 125 mL of dry THF was transferred into a dry 500 mL 3-neck round bottom flask equipped with a stir bar, reflux condenser, and addition funnel. 1-Tetradecyne (10.0 mL, 0.041 mol) of was added via syringe and the solution was cooled to 0 ^oC. Then n-BuLi (16.2 mL, 2.5 M) was added drop wise. The solution was then allowed to warm up to room temperature and 1-bromododecane (9.82 mL, 0.041 mol) was added drop wise. The solution was then heated to reflux for 3 days. After cooling, the solution was extracted (3 x 65 mL) with Na_2SO_4 and (3 x 75 mL) H_2O. The solution was dried over $MgSO_4$ and the solvent was removed under reduced pressure to yield 14.33 g (97 %) of a white solid. mp 29-33 ^oC. ^1H NMR (300 MHz, $CDCl_3$) δ 0.88 (t, 6H), 1.2-1.5 (m, 40H), 2.14 (t, 4H); ^{13}C NMR (75 MHz, $CDCl_3$) δ 14.11, 18.76, 22.69, 28.87, 29.18, 29.36, 29.57, 29.64, 29.68, 31.93, 80.25.

Hexacosane-13,14-dione (8).[140,141] A 500 mL Erlenmeyer flask equipped with a reflux condenser and stir bar was charged with $KMnO_4$ (5.85 g, 0.037 mol) and 100 mL H_2O. In a separate flask, hexacos-13-yne (3.26 g, 0.009 mol) of, 100 mL of CH_2Cl_2, 1.5 mL aliquot 336 (Aldrich), and 1.5 mL of acetic acid were combined. This solution was then added to the $KMnO_4/H_2O$ solution and heated to reflux for 6 h. After cooling, 2 g of sodium bisulfite was added and the solution allowed to stir for 15 min. Next the solution was acidified with conc. HCl, and 4 g of sodium bisulfite was added in small portions. The aqueous layer was separated and saturated with NaCl, followed by extraction (3 x 75 mL) with CH_2Cl_2. The organic layers were combined and extracted (3 x 75 mL) with 5 % NaOH. After drying over $MgSO_4$, the solvent was removed under reduced pressure to yield a light yellow solid. Recrystallization from MeOH yielded 1.45 g (41 %) of light yellow plates. mp 73-75 ^oC (lit. 76-78 ^oC).[30] ^1H NMR (300 MHz, $CDCl_3$) δ 0.88 (t, 6H), 1.25 (m, 36H), 1.57 (p,4H) 2.72 (t, 4H); ^{13}C NMR (75 MHz, $CDCl_3$) δ 14.11, 22.68, 23.07, 29.14, 29.33, 29.43, 29.58, 29.62, 31.91, 36.09, 200.22. HRMS calcd for $C_{26}H_{50}O_2$ 394.3811 Found 394.3813.

5,8-dibromo-2,3-dihexyl-pyrido[3,4-b]pyrazine (5).[112,132] 3,4-Diamino-2,5-dibromopyridine (1.31 g, 0.0049 mol), tetradecane-7,8-dione (1.14 g, 0.0050 mol), *p*-toluenesulfonic acid monohydrate (0.02 g, 0.00010 mol) of, and 20 mL of 1-butanol were combined in a 100 mL 3-neck round bottom flask equipped with a reflux condenser and stir bar. The solution was then heated to reflux for 5 h. After cooling, a precipitate was collected by filtration. Recrystallization from EtOH yielded 1.46 g (65 %) of an off-white solid. mp 71.5-72.8 ^oC. ^1H NMR (300 MHz, $CDCl_3$), δ 0.92 (t, 6H), 1.3-1.5 (m, 12H), 1.92 (m, 4H), 3.10 (m, 4H), 8.68 (s, 1H); ^{13}C NMR (75 MHz, $CDCl_3$) δ 14.06, 22.56, 22.57, 27.43, 29.06, 29.10, 31.65, 31.69, 34.85, 35.12, 120.08, 135.97, 142.49, 145.70, 146.40, 160.51, 163.16. Elemental Anal.

Calcd. For $C_{19}H_{27}N_3Br_2$: C, 49.91; H, 5.95; N, 9.19; Br, 34.95. Found: C, 50.03; H, 5.99; N, 9.06. HRMS calcd. for $C_{19}H_{27}N_3Br_2$ 457.0551 Found 457.0556.

5,8-Dibromo-2,3-didodecyl-pyrido[3,4-b]pyrazine (9).[112,132] 3,4-Diamino-2,5-dibromopyridine (1.32 g, 0.0049 mol), hexacosane-13,14-dione (1.99 g, 0.0050 mol), *p*-toluenesulfonic acid monohydrate (0.02 g, 0.00010 mol), and 23 mL of 1-butanol were combined in a 100 mL 3-neck round bottom flask equipped with a reflux condenser and stir bar. The solution was heated to reflux for 5 h. Upon cooling, a light yellow solid was collected by filtration. Column chromatography (7:3 CH_2Cl_2:Hexane) yielded 1.63 g (53 %) of a white solid. mp 58-59.5 ^oC. ^1H NMR (300 MHz, $CDCl_3$) δ 0.88 (t, 6H), 1.22-1.54 (m, 36H), 1.86-1.98 (m 4H), 3.06-3.12 (m, 4H), 8.68 (s, 1H); ^{13}C NMR (75 MHz, $CDCl_3$) δ 14.10, 22.67, 27.50, 29.34, 29.39, 29,43, 29.46, 29.48, 29.54, 29.63, 31.91, 34.86, 35.13, 120.09, 135.98, 142.50, 145.72, 146.40, 160.54, 163.18. Elemental Anal. Calcd. for $C_{31}H_{51}N_3Br_2$: C, 59.52; H, 8.22; N, 6.72; Br, 25.55. Found: C, 60.15; H, 8.66; N, 6.61. HRMS calcd. for $C_{31}H_{51}N_3Br_2$ (M+H) 624.2528 Found 624.2547

5,8-bis(2,3-dihydrothieno[3,4-b][1,4]dioxin-5-yl)-2,3-dihexylpyrido[3,4-b]pyrazine (11).[142] Under an argon atmosphere, 5,8-dibromo-2,3-dihexyl-pyrido[3,4-b]pyrazine (0.42 g, 0.00092 mol), (2,3-dihydrothieno[3,4-b][1,4]dioxin-5-yl)trimethylstannane (0.66 g, 0.0020 mol), and 25 mL of anhydrous DMF were combined in a dry 100 mL 3-neck round bottom flask with a stir bar. The mixture was degassed under argon for 1 h. Then $Pd(II)Cl_2(PPh_3)_2$ (0.07 g, 11 mol %) was added, the solution was heated to 75 ^oC, and allowed to react for ~18 h. After cooling, the reaction mixture was poured into 200 mL of H_2O and extracted repeatedly with ether. The organic solution was then concentrated and extracted repeatedly with brine. After drying over $MgSO_4$, removal of ether under reduced pressure gave an orange-red solid. Column

chromatography (1:1 DCM:EtOAc) yielded 0.21 g (40 %) of an orange crystalline powder. mp 167-168 ^{o}C. ^{1}H NMR (300 MHz, $CDCl_3$) δ 0.91 (t, 6H), 1.3-1.55 (m, 12H), 1.95-2.1 (m, 4H), 3.00-3.15 (m, 4H), 4.25-4.50 (m, 8H), 6.55 (s, 1H), 6.63 (s, 1H), 9.72 (s, 1H); ^{13}C NMR (75 MHz, $CDCl_3$) δ 14.06, 22.59, 27.57, 27.72, 29.20, 31.75, 34.90, 35.18, 64.21, 64.29, 64.77, 65.29, 103.15, 105.21, 110.89, 114.05, 122.30, 132.52, 139.46, 140.38, 141.29, 141.73, 142.50, 144.30, 149.82, 156.10, 159.20. Elemental Anal. Calcd. for $C_{31}H_{37}N_3O_4S_2$: C 64.22, H 6.47, N 7.25. Found C 64.21, H 6.68, N 7.19; HRMS calcd. for $C_{31}H_{37}N_3O_4S_2$ 579.2225 Found 579.2210.

5,8-bis(2,3-dihydrothieno[3,4-b][1,4]dioxin-5-yl)-2,3-didodecylpyrido[3,4-b]pyrazine (12).[142] Under an argon atmosphere, 5,8-Dibromo-2,3-didodecyl-pyrido[3,4-b]pyrazine (0.77 g, 0.0012 mol), (2,3-dihydrothieno[3,4-b][1,4]dioxin-5-yl)trimethylstannane (0.79 g, 0.0026 mol), and 25 mL of anhydrous DMF were combined in a dry 100 mL 3-neck round bottom flask with a stir bar. The mixture was then degassed under argon for 1 h. Next, $Pd(II)Cl_2(PPh_3)_2$ (0.09 g, 10 mol %) was added, the solution was heated to 75 ^{o}C, and allowed to react for ~19 h. After cooling, the solution was poured into 250 mL of H_2O and then extracted repeatedly with ether. The organic phase was then extracted repeatedly with brine. The solution was dried over $MgSO_4$ and the solvent was removed under reduced pressure to yield a red solid. Column chromatography (4:1 CH_2Cl_2:EtOAc) and then (EtOAc) yielded 0.57 g (62 %) of an orange solid. mp 108.5-109 ^{o}C. ^{1}H NMR (300 MHz, $CDCl_3$) δ 0.88 (t, 6H), 1.2-1.5 (m, 36H), 1.95-2.1 (m, 4H), 3-3.15 (m, 4H), 4.25-4.5 (m, 8H), 6.54 (s, 1H), 6.62 (s, 1H), 9.71 (s, 1H); ^{13}C NMR (75 MHz, $CDCl_3$) δ 14.09, 22.67, 27.62, 27.78, 29.34, 29.54, 29.58, 29.64, 29.67, 29.70, 31.90, 34.93, 35.21, 64.24, 63.32, 64.79, 65.31, 103.17, 105.23, 110.92, 114.08, 122.32, 132.55, 139.48, 140.39, 141.30, 141.74, 142.52, 144.32, 149.84, 156.13, 159.23. Elemental Anal. Calcd. for

$C_{43}H_{61}N_3O_4S_2$: C 69.04, H 8.22, N 5.62. Found C 69.16, H 8.20, N 5.61; HRMS calcd. for $C_{43}H_{61}N_3O_4S_2$ 747.4103 Found 747.4122.

CHAPTER 4
BXDOT DONOR-ACCEPTOR-DONOR LOW BAND GAP POLYMERS

Background

As was discussed in the general introduction and Chapter3, by combining strong donors with strong acceptors, it is possible to compress the band gap and tune the HOMO/LUMO levels of the final polymer. Through the proper choice of the donor and acceptor, one can tailor the properties of the final polymer for applications such as electrochromics, OLEDs, OFETs and charge storage.

One of the major draw backs of n-type polymers is their stability in the reduced state. As we saw in Chapter 3, the second reduction of the pyridopyrazine DAD polymers was highly unstable and could only be seen for a few cycles. Stability issues have also been seen for some pyridopyrazine vinylene polymers.[132,146] By using stronger acceptors with more positive reduction potentials, it should be possible to improve the stability of n-type polymers to repetitive cycling in the reduced state.[148]

To circumvent the stability issues seen in Chapter 3, and still maintain the advantages of dioxythiophene based systems for ease of electrochemical polymerization and characterization, the goal was to synthesize DAD monomers and polymers incorporating the highly electron poor [1,2,5]thiadiazolo[3,4-*g*]quinoxaline (TQ) and benzo[1,2-c;3,4-c′]bis[1,2,5]thiadiazole (BBT) based acceptors. One of the advantages of using these acceptors is that both are synthesized from the same intermediate.[111] Also, by broadening our donor selection from EDOT to include ProDOTs, we should be able to induce fine control over the band gap by varying the degree of intramolecular charge transfer for a family of DAD polymers.

Monomer Synthesis and Characterization

The synthesis of a family of 9 different DAD monomers and polymers involving three different donors and two different acceptors were investigated. The donors range from the most electron rich 3,4-ethylenedioxythiophene (EDOT) to the less electron rich 3,4-propylenedioxythiophene (ProDOT) and 2,2-dimethyl substituted ProDOT ($ProDOTMe_2$) (Figure 4-1). The two acceptors studied include thiadiazoloquinoxaline (TQ) and the more electron poor benzobis(thiadiazole) (BBT) (Figure 4-1). Through the various combinations of the donors and acceptors, we should be able to exert fine control over the band gap and voltage window between polymer oxidation and reduction.

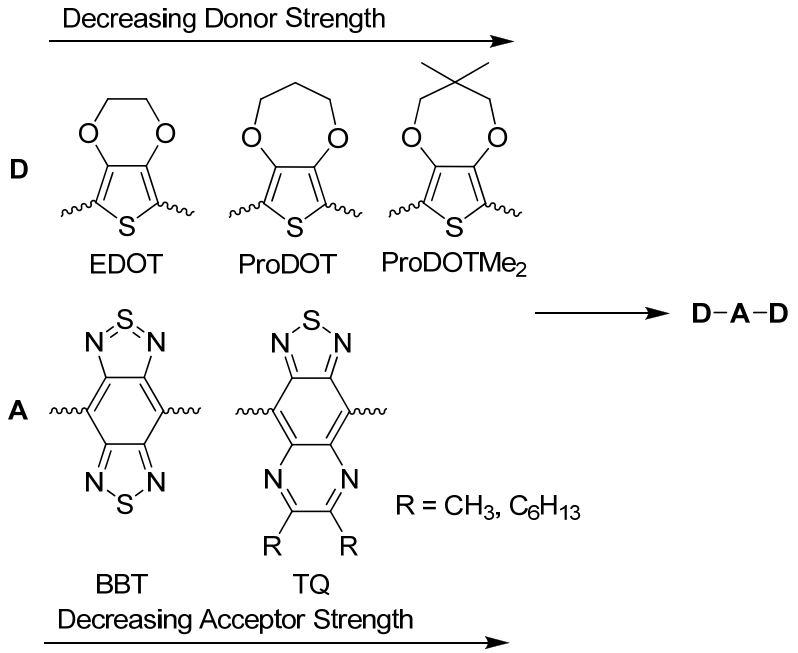

Figure 4-1. The different dioxythiophene based donors and thiadiazole based acceptors used to make a new family of DAD monomers and polymers.

The synthesis of the nine monomers starts with the bromination of 2,1,3-benzothiadiazole (**1**)[149] followed by nitration to yield 4,7-dibromo-5,6-dinitrobenzo[c][1,2,5]thiadiazole (**3**)[150] as illustrated in Figure 4-2. Although the yield of **3** is low, it is early on in the synthesis and can be scaled up. Next, a Stille coupling was performed between **3** and the stannyl compounds of

EDOT, ProDOT, and ProDOTMe$_2$ to yield **4a-c**.[98] This was followed by reduction with iron in acetic acid to yield compounds **5a-c**. Ring closing with N-thionylaniline in pyridine gave the BBT derivatives **6a-c**. Ring closing in acetic acid with 2,3-butanedione or 7-tetradecanedione gave the TQ derivatives **7a-c** and **8a-c** respectively.[111]

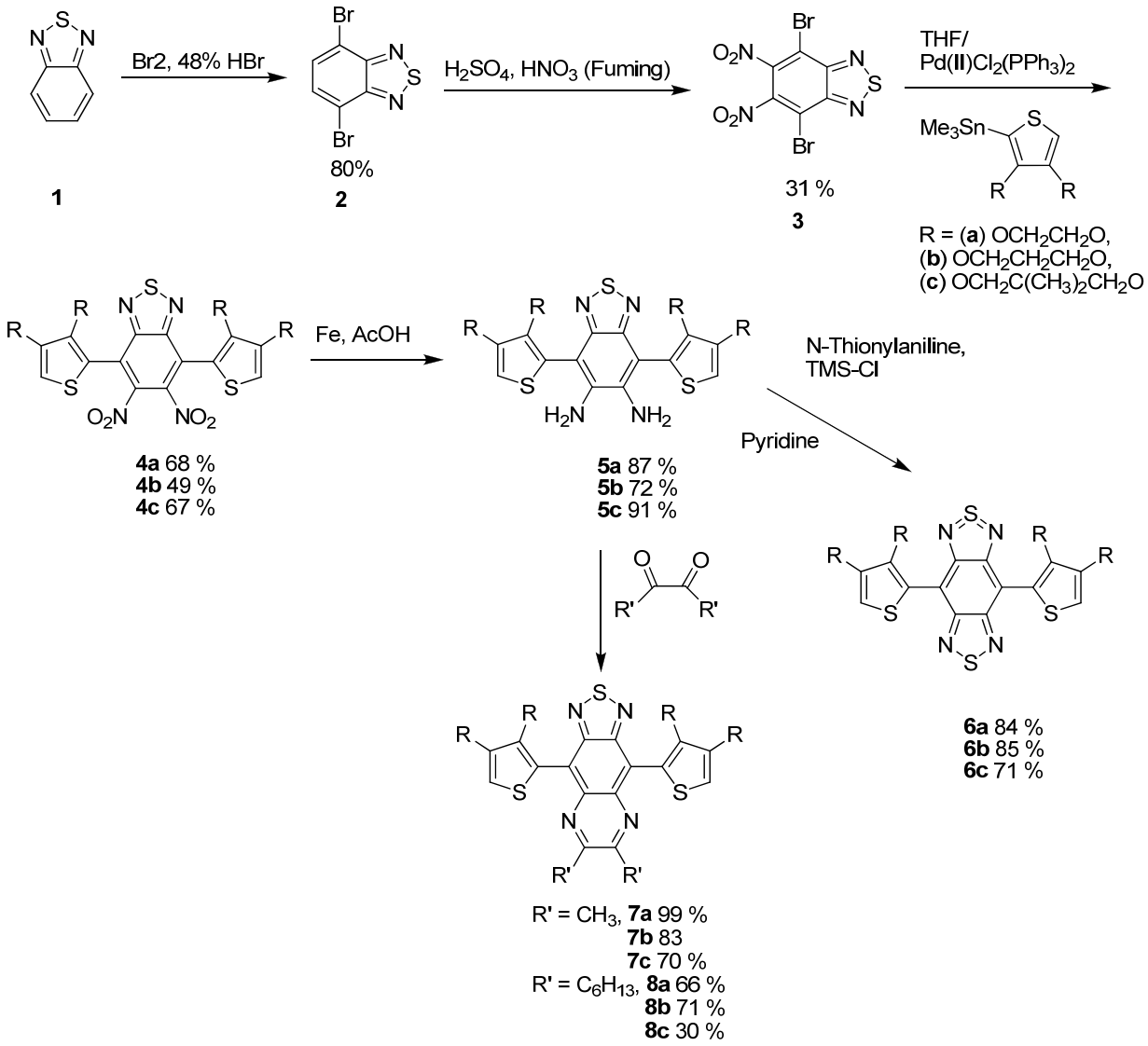

Figure 4-2. Synthesis of DAD monomers where (a) = EDOT, (b) = ProDOT, and (c) = ProDOTMe$_2$.

It was originally thought that by using a stronger donor like EDOT rather than thiophene, that **6a** would observe a red shift in absorbance relative to the bisthienylBBT derivative.

However, the λ_{max} for **6a** is 643 nm, which is significantly blue shifted relative to the bisthienyl-BBT derivative, which has a λ_{max} of 703 nm.[151] The cause of this was revealed by examining the crystal structure of **6a** (Figure 4-3) relative to that of the previously reported BTh-BBT derivative. The torsion angle between the EDOT donor and the BBT acceptor is 53 ° compared to 0 ° for the thiophene relative to the BBT acceptor.[151] The large dihedral angle in **6a** is caused by the steric interactions of the nitrogens on the BBT acceptor and the oxygens on the EDOT donors. This hinders the overlap of the p-orbitals and thus limits the amount of ICT and conjugation. Since **6a** has a large dihedral angle, it can be assumed that all of the other dioxythiophene derivatives are also highly twisted. Crystal structures of compounds **6b**, **7a**, and **7c** were obtained and also show large dihedral angles ranging from 47 ° to 56 ° (Appendix A). These large dihedral angles result in poor orbital overlap. However, we should still be able to exude fine control over the properties by varying the donor, the acceptor, or both.

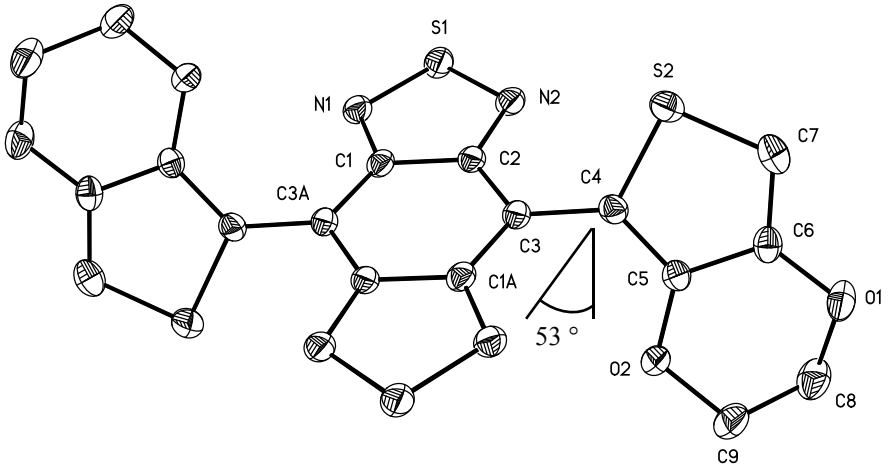

Figure 4-3. Crystal structure of Monomer **6a** showing a torsion angle of 53 ° between the EDOT donor and the benzobis(thiadiazole) acceptor. Selected bond lengths: C1-C3A, 1.405 Å; C1-C2, 1.447 Å; C2-C3, 1.412 Å; C3-C4, 1.463 Å; C4-C5, 1.372 Å; C5-C6, 1.420 Å; C6-C7, 1.356 Å; S1-N2, 1.603 Å; N2-C2, 1.365 Å.

A UV-VIS study of the monomers was performed to examine the effects of the donor and acceptor strengths on the intramolecular charge transfer (ICT) band absorbance. A summary of their properties can be seen in Table 4-1. Comparing monomers **7a-c** (Figure 4-4 A), **7a** has the greatest red shift with a λ_{max} at 538 nm, compared to **7c**, which is in the middle at 527 nm, while **7b** is the lowest at 522 nm. This suggests that EDOT > ProDOTMe$_2$ > ProDOT in donor strength. This trend is also seen for compounds **8a-c** (Figure 4-4 B). For compounds **6a-c** (Figure 4-4 C), the trend is similar, except that the ProDOT and ProDOTMe$_2$ derivatives are almost identical with λ_{max} at 626 nm and 627 nm respectively compared to **6a** with a λ_{max} at 643 nm, resulting in EDOT > ProDOTMe$_2$ ≈ ProDOT. Monomers **6a-c** have broad absorptions starting from 750 nm extending through the visible to 500 nm, while having minimal absorption from 500 to 400 nm. This results in blue colored solutions. Meanwhile monomers **7a-c** and **8a-c** have broad absorptions starting around 625 nm for **7a** & **8a** and 600 nm for **7b-c** & **8b-c** and ending around 450 nm to 430 nm respectively, resulting in dark pink solutions.

Table 4-1. UV-VIS absorption data for monomers **6a-c**, **7a-c**, and **8a-c**.

Monomer	λ_{max}/Molar Absorptivity, ε ($cm^{-1}M^{-1}$)	λ_{max}/Molar Absorptivity, ε ($cm^{-1}M^{-1}$)
6a	643 nm / 30,000	353 nm / 66,000
6b	626 nm / 10,000	354 nm / 21,000
6c	627 nm / 11,000	354 nm / 24,000
7a	538 nm / 16,000	371 nm / 23,000
7b	522 nm / 14,000	371 nm / 22,000
7c	527 nm / 13,000	371 nm / 19,000
8a	536 nm / 13,000	372 nm / 23,000
8b	523 nm / 8,000	373 nm / 14,000
8c	527 nm / 10,000	373 nm / 18,000

UV-VIS analysis has shown that monomer **6a** has a molar absorptivity of almost three times that of **6b-c** (Table 4-1). However, when looking at compounds **7a-c** and **8a-c**, compounds **7a** and **8a** have molar absorptivities that are only 2,000-5,000 $cm^{-1}M^{-1}$ higher than the other

derivatives. While this still suggests that the EDOT compounds absorb more strongly than the ProDOT or ProDOTMe$_2$ derivatives, this is much less pronounced for the TQ monomers.

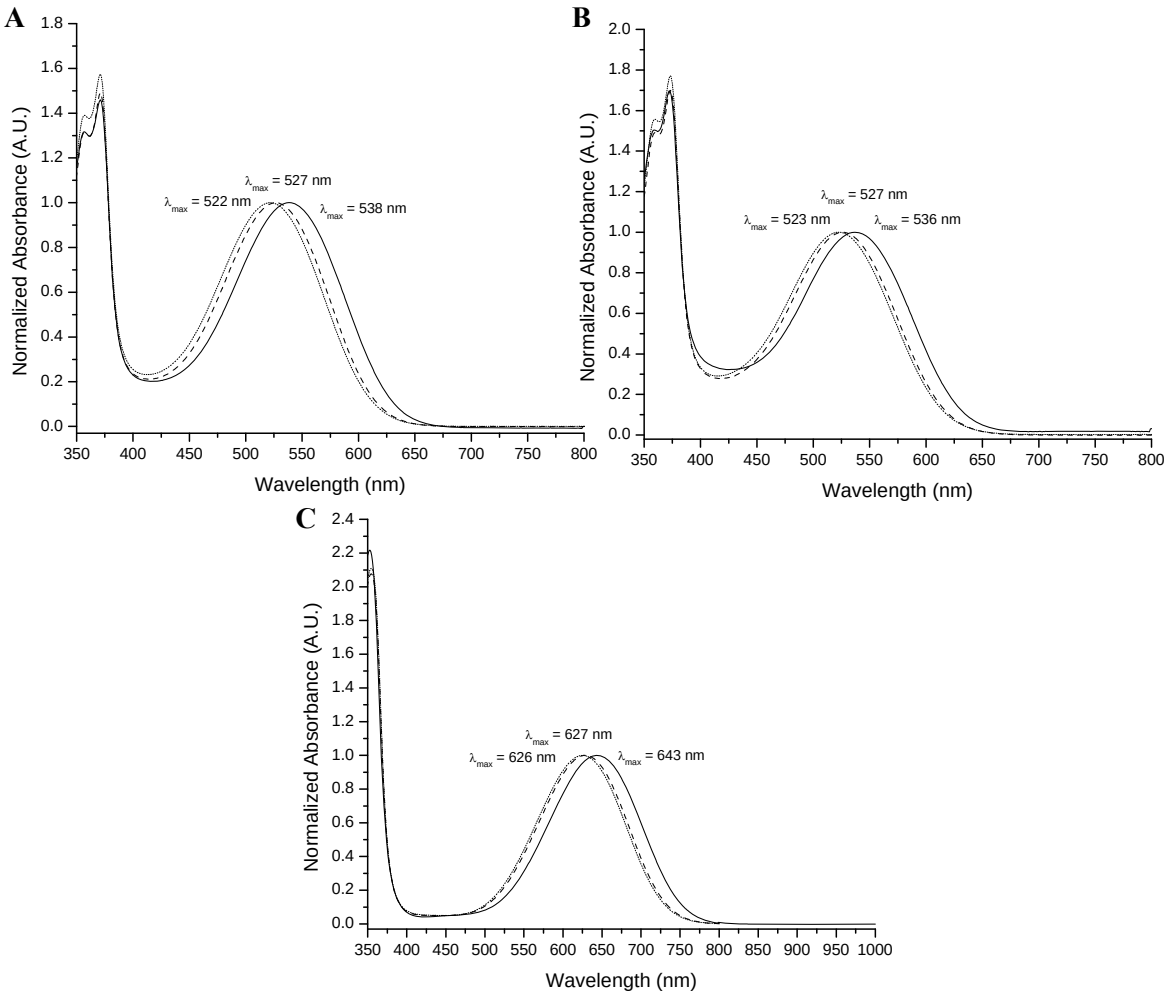

Figure 4-4. UV-VIS spectra of monomers. A) **7a** (solid: λ_{max} = 538 nm and 371 nm and 357 nm sh), **7b** (dotted: λ_{max} 522 nm and 371 nm and 357 nm sh) and **7c** (dashed: λ_{max} 527 nm and 371 nm and 357 nm sh). B) **8a** (solid: λ_{max} = 536 nm and 371 nm and 357 nm sh), **8b** (dotted: λ_{max} = 523 nm and 371 nm and 357 nm sh) and **8c** (dashed: λ_{max} = 527 nm and 371 nm and 357 nm sh). C) **6a** (solid: λ_{max} = 643 nm and 353 nm), **6b** (dotted: λ_{max} = 626 nm and 354 nm) and **6c** (dashed: λ_{max} 627 nm and 354 nm).

Electrochemical Polymerization and Characterization

Electrochemical Polymerization of Monomers

Electrochemical polymerization of monomers **6-8a-c** (Figure 4-5) were carried out from 5 mM monomer 0.1 M TBAP (supporting electrolyte) solutions in either pure dichloromethane

(DCM) for monomers **6a-c**, or in a mixture of propylene carbonate (PC):DCM (~9:1) for monomers **7-8a-c** (Figure 4-7). Pure DCM had to be used for monomers **6a-c** due to poor solubility. Even for monomers **7-8a-c**, ~ 10% DCM was needed to attain substantial solubility for electrochemical polymerization. Polymer films were deposited by repetitive scan cyclic voltammetry or potentiostatically in an electrochemical cell consisting of a platinum button or ITO working electrode, a platinum (flag or wire) counter electrode, and a silver wire pseudo reference electrode. The reference electrode was calibrated with the ferrocene redox couple (Fc/Fc^+) from a solution containing 5 mM ferrocene and 0.1 M TBAP (tetrabutylammonium perchlorate) in PC. All potential values were measured relative to Fc/Fc^+, and then converted to SCE ($E_{SCE} = E_{Fc/Fc+} + 0.38$ V)[121] to be consistent with the most frequently reported values in the literature.

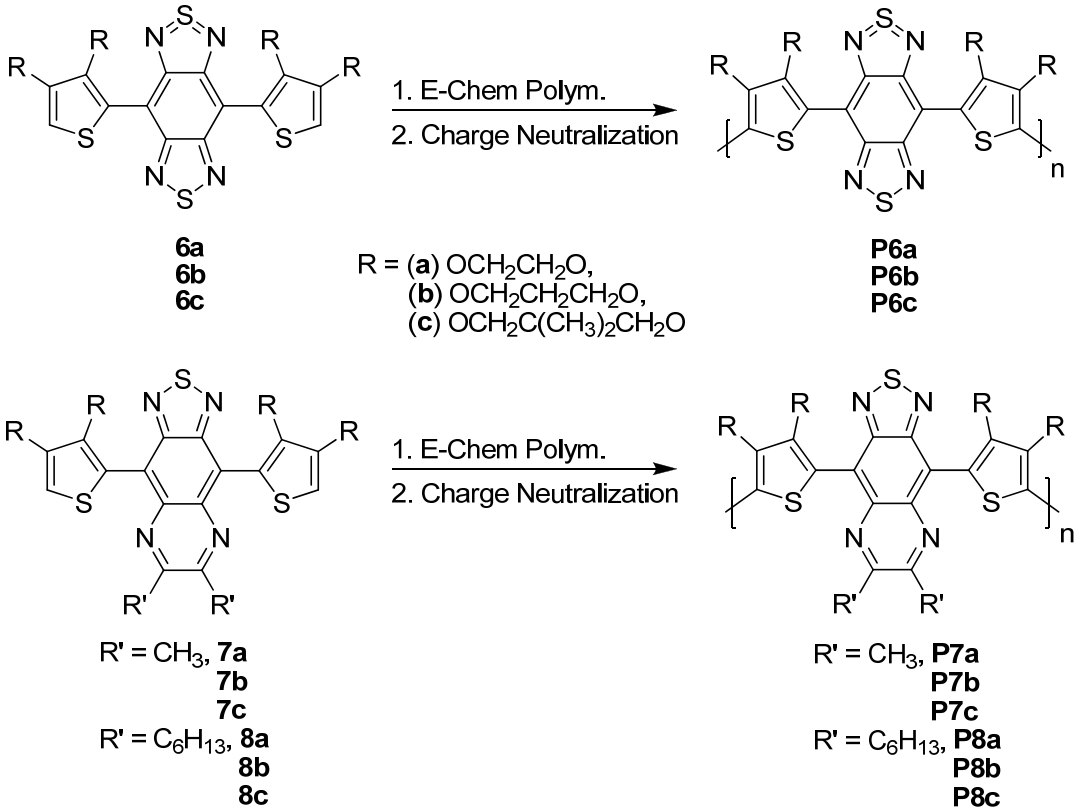

Figure 4-5. Electrochemical polymerization of monomers **6-8a-c** to yield polymers **P6-8a-c**.

A representative electrochemical polymerization of monomer **6b** is shown in Figure 4-6. Upon increasing the potential, monomer **6b** oxidizes at an E_p of 1.06 V vs. SCE. Upon the reverse of the first scan, there is a broad reduction peak due to the deposition of oligomers and polymers. Repetitive cycling shows broad oxidation and reduction peaks that evolve at lower potentials. This is due to the coupling of monomers to produce oligomers and polymers that oxidize at lower potentials due to the increase in conjugation. The increase in intensity of these peaks with repeated scans is associated with deposition of the polymer (**P6b**) on the electrode. The remaining electrochemical polymerizations of monomers **6-8a-c** can be seen in Appendix B. In general, all of the monomers oxidize near the same potential around 1.0 to 1.1 V. This is due to the experimental error associated with the use of the silver wire pseudo reference electrode.

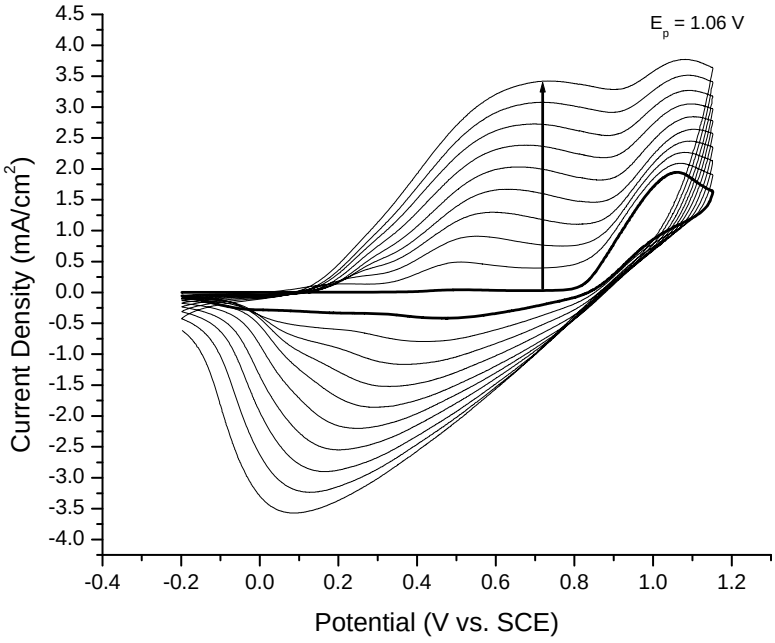

Figure 4-6. Repetitive scan electropolymerization (50 mV/s, 10 cycles) from a 5 mM monomer 0.1 M TBAP/DCM solution of **6b** yielding **P6b**.

Polymer Electrochemistry

In order to evaluate a polymers potential use in applications such as charge storage, electrochromics, and OFETs, it is important to understand the redox properties, magnitude of the band gap, and the position of the HOMO/LUMO levels. These properties were probed electrochemically by cyclic voltammetry (CV) and differential pulse voltammetry (DPV) as was discussed in Chapter 2. The difference between the onsets of oxidation and reduction correspond to the polymers electrochemical band gap with the values of the onsets relating to the position of the HOMO/LUMO levels. The electrodeposited polymers **P6-8a-c** were rinsed with monomer free electrolyte and characterized in 0.1 M TBAP-PC using the same set up as described earlier, except instead of a silver wire pseudo reference electrode used during growth, a Ag/Ag^+ reference electrode was used. This is a highly stable reference electrode which is not subjected to the extreme potential drifts that are sometimes seen with the silver wire pseudo reference electrode. The electrode was calibrated relative to Fc/Fc^+, and all measured potentials were then converted to SCE for consistency with the literature.[121] Polymer films were switched by repetitive potential scanning from the neutral state to either the oxidized or reduced state until a reproducible CV was obtained. DPV was also performed on the polymer films after they were conditioned to a reproducible redox response (*i.e.* broken in). Individual films were used for oxidation and reduction. This was done because upon full CV scans (oxidation and reduction), the evolution of prepeaks, attributed to trapped charges, made characterization of the onsets difficult.[152,153] Film stability was also an issue for full CV scans in some instances, as the film would degrade rapidly with a loss of electroactivity after only a few cycles. A summary of the electrochemical data as determined by CV can be seen in Table 4-2 and as determined by DPV can be seen in Table 4-3.

Table 4-2. Summary of electrochemical data (CV) for polymers **P6-8a-c**. All data is V vs. SCE. E_g is taken as $E_{onset\ ox} - E_{onset\ red}$.

Polymer	E_{ox} onset	$E_{p\ ox}$	$E_{1/2}$	HOMO (eV)	$E_{red\ 1}$ onset	E_p	$E_{1/2}$	LUMO (eV)	$E_{p\ red\ 2}$	$E_{1/2}$	E_g (eV)
P6a	0.23	0.63	0.53	4.93	-0.41	-0.68	-0.52	4.29	-1.37	-1.28	0.64
P6b	0.43	0.84	0.66	5.13	-0.36	-0.67	-0.55	4.34	-1.41	-1.30	0.79
P6c	0.5	0.76	0.68	5.20	-0.35	-0.66	-0.51	4.35	-1.37	-1.27	0.85
P7a	0.41	0.61	0.57	5.11	-0.72	-0.95	-0.89	3.98	-1.58	-1.54	1.13
P7b	0.55	0.76	0.69	5.25	-0.71	-0.93	-0.84	3.99	-1.53	-1.52	1.26
P7c	0.63	0.77	0.73	5.33	-0.71	-0.87	-0.82	4.00	-1.45	-1.46	1.33
P8a	0.43	0.64	0.57	5.13	-0.74	-0.95	-0.89	3.96	-1.58	-1.55	1.17
P8b	0.59	0.76	0.72	5.29	-0.72	-0.92	-0.84	3.98	-1.51	-1.50	1.31
P8c	0.63	0.78	0.74	5.33	-0.72	-0.90	-0.85	3.98	-1.50	-1.50	1.35

Table 4-3. Summary of the observed onsets for oxidation and reduction by DPV for polymers **P6-8a-c**. All data is V vs. SCE. E_g is taken as $E_{onset\ ox} - E_{onset\ red}$.

Polymer	E_{ox} onset	HOMO (eV)	$E_{red\ 1}$ onset	LUMO (eV)	E_g (eV)	E_g DPV-E_g CV
P6a	0.03	4.73	-0.23	4.47	0.26	-0.38
P6b	0.36	5.06	-0.25	4.45	0.61	-0.18
P6c	0.44	5.14	-0.23	4.47	0.67	-0.18
P7a	0.25	4.95	-0.63	4.07	0.98	-0.15
P7b	0.50	5.20	-0.63	4.07	1.13	-0.13
P7c	0.60	5.30	-0.65	4.05	1.25	-0.08
P8a	0.36	5.06	-0.65	4.05	1.01	-0.16
P8b	0.54	5.24	-0.64	4.06	1.18	-0.13
P8c	0.59	5.29	-0.66	4.04	1.25	-0.10

By switching to the stronger TQ based acceptors in **P7a-c** relative to the PyrPyr based acceptors studied in Chapter 3, there is an increase to more positive reduction potentials with an onset of reduction ~600 mV more positive. Application of reducing potentials to **P7a-b** (Figure 4-7) and **P7c** (Figure 4-8) shows two sharp quasi-reversible reductions by CV with onsets for the first reduction at -0.71 to -0.72 V. The onsets for reduction observed by DPV were ~70 mV more positive at -0.63 to -0.65 V. While the first reduction for polymers **P7a-c** was very stable over the 50 to 100 cycles required for break in and analysis, it should be noted that the stability of the second reduction for **P7a** was poor with almost complete loss of electroactivity of the second reduction over several cycles leading to film degradation, thus only the second CV scan

of the full reduction after break in for the first reduction is shown (Figure 4-7 A). The full DPV reduction of **P7a** was obtained after break in for the first reduction, and only the first set of DPV experiments are shown (Figure 4-7 C). Different films had to be used in order to obtain the CV and DPV results for both reductions in **P7a**.

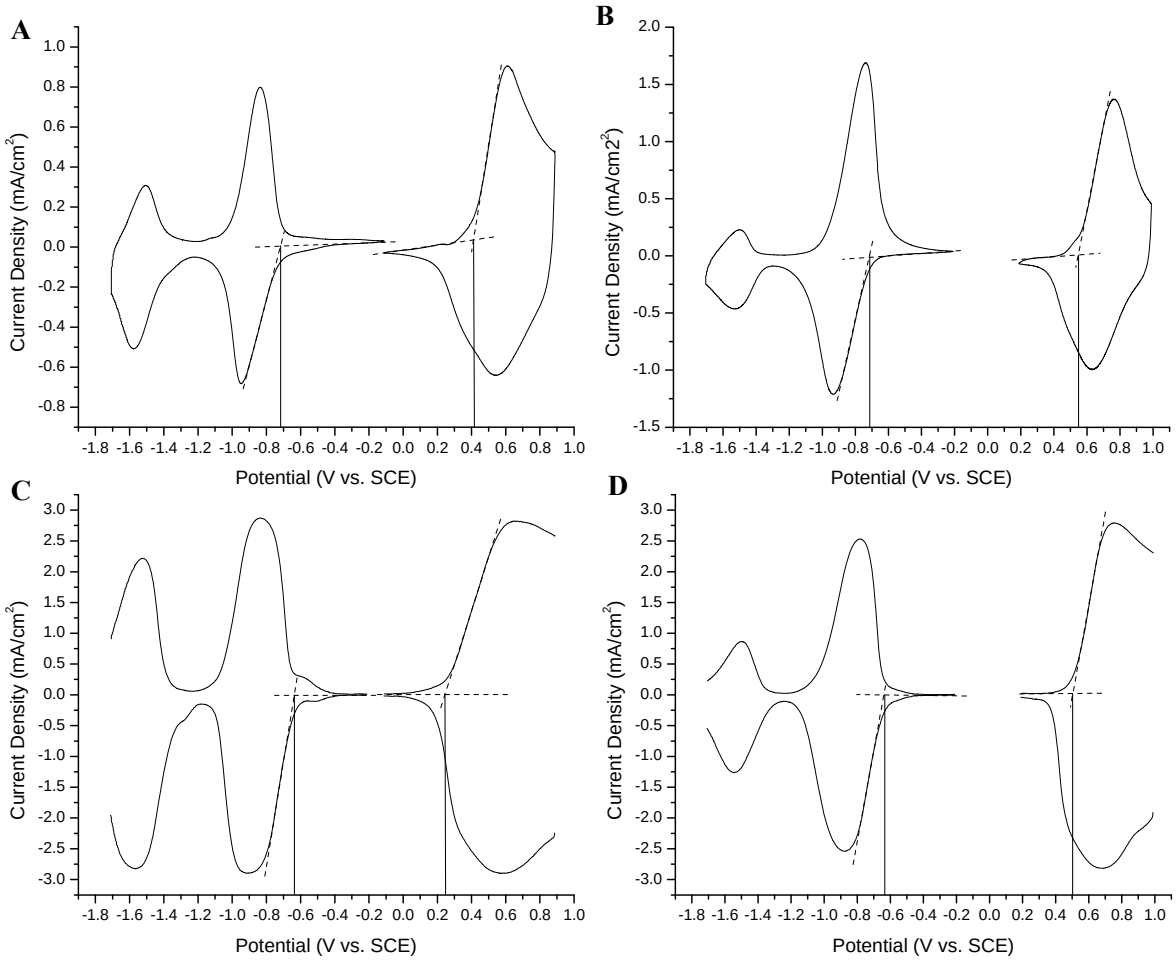

Figure 4-7. CV (scan rate = 50 mV/s) and DPV (step size of 2 mV and step time of 0.1 seconds) of polymers **P7a-b** on a Pt button working electrode in 0.1 M TBAP-PC electrolyte solution. A) CV of **P7a**. B) CV of **P7b**. C) DPV of **P7a**. D) DPV of **P7b**.

Upon application of anodic potentials to **P7a-b** (Figures 4-7) and **P7c** (Figure 4-8), fairly sharp oxidation peaks with a decrease in current after the E_p are observed, indicative of redox type conductivity. The onsets of oxidation for **P7a-c** range from 0.41 V, to 0.55 V, to 0.63 V as determined by CV (Table 4-2). This is in accord with EDOT (**P7a**) being a stronger donor than

ProDOT (**P7b**) and ProDOT being a slightly stronger donor than ProDOTMe$_2$ (**P7c**). DPV analysis of the onsets gives slightly lower values for oxidation (Table 4-3). This results in electrochemical band gaps of 1.13, 1.26, and 1.33 eV for **P7a-c** respectively as determined by CV and 0.98, 1.13, and 1.25 eV by DPV.

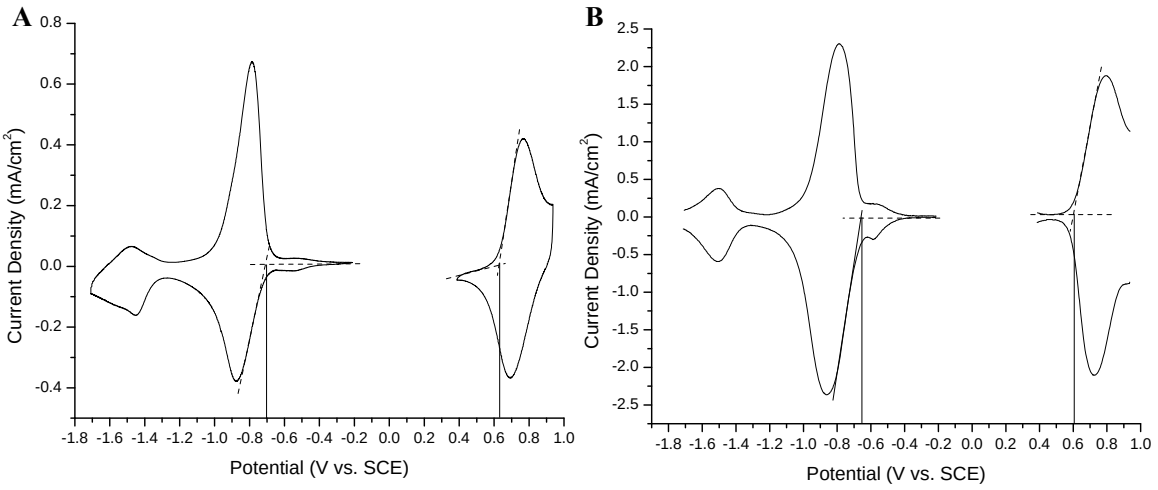

Figure 4-8. CV (scan rate = 50 mV/s) and DPV (step size of 2 mV and step time of 0.1 seconds) of polymer **P7c** on a Pt button working electrode in 0.1 M TBAP-PC electrolyte solution. A) CV of **P7c**. B) DPV of **P7c**.

Analysis of polymers **P8a-b** (Figure 4-9) and **P8c** (Figure 4-10) by CV and DPV were performed and show similar results to **P7a-c**. CV oxidation shows sharp peaks typical of site limited redox conductivity with onsets at 0.43 V, 0.59 V, and 0.63 V for **P8a-c** respectively. DPV estimation of the onsets for oxidation of **P8a-c** are 0.36 V, 0.54 V, and 0.59 V, which again is 40 to 80 mV less than estimated by CV. With the application of cathodic potentials to **P8a-c**, there are two sharp quasi-reversible reductions with onsets at -0.74 V, -0.72 V, and -0.72 V respectively. Reduction onsets estimated by DVP for **P8a-c** are at -0.65 V, -0.64 V, and -0.66 V accordingly. The first reductions for polymers **P8a-c** are very stable as described for **P7a-c**, but again it should be noted that the second reduction for **P8a** was highly unstable and a loss of electroactivity over a few cycles was observed, thus the first scan is shown for reduction. DPV

analysis of the second reduction of **P8a** (Figure 4-9 C) shows very little charge compensation on the reverse scan, and some film degradation is observed. Separate films were used to obtain the CV and DPV results as was done for **P7a**. The band gaps determined by CV for **P8a-c** were 1.17 eV, 1.31 eV, and 1.35 eV, while DPV gave 1.01 eV, 1.18 eV, and 1.25 eV respectively.

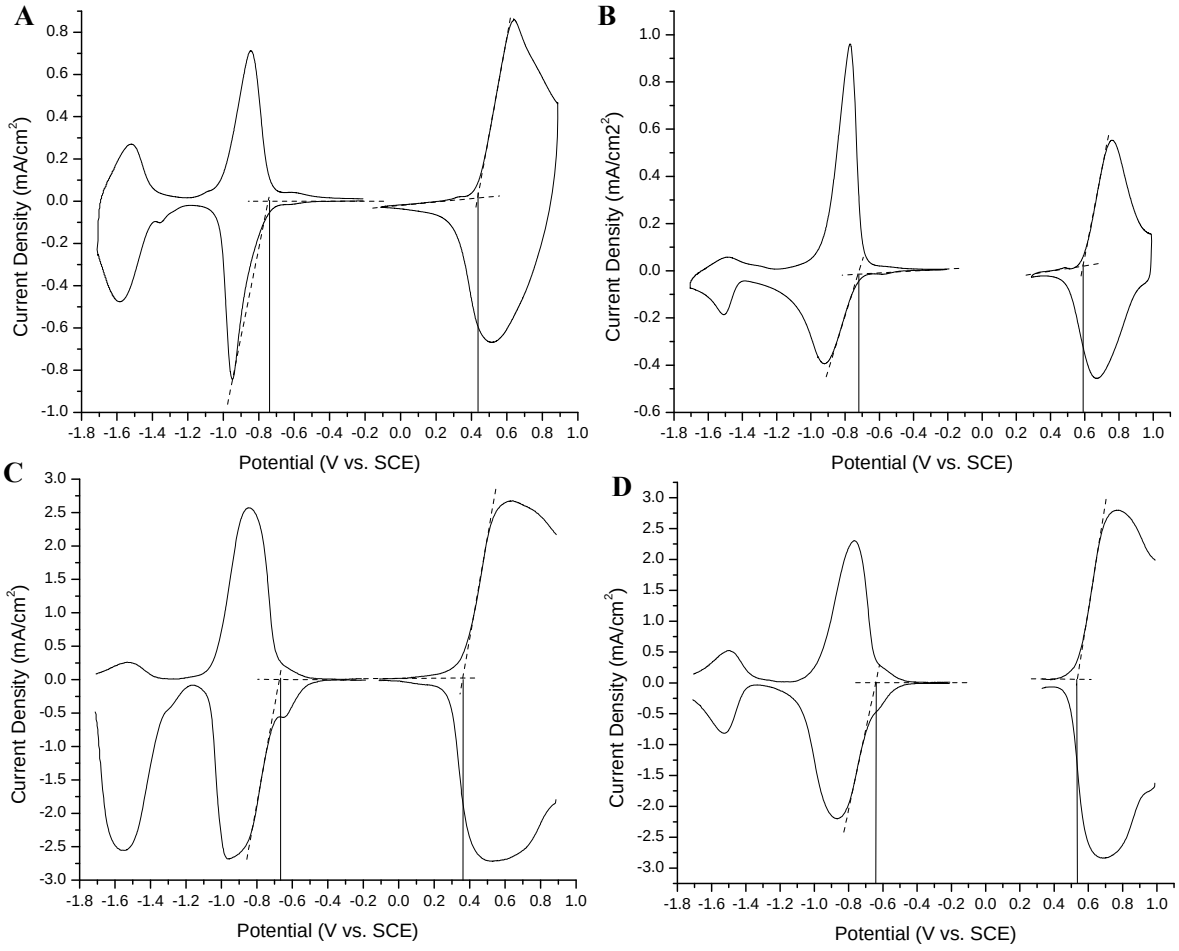

Figure 4-9. CV (scan rate = 50 mV/s) and DPV (step size of 2 mV and step time of 0.1 seconds) of polymers **P8a-b** on a Pt button working electrode in 0.1 M TBAP-PC electrolyte solution. A) CV of **P8a**. B) CV of **P8b**. C) DPV of **P8a**. D) DPV of **P8b**.

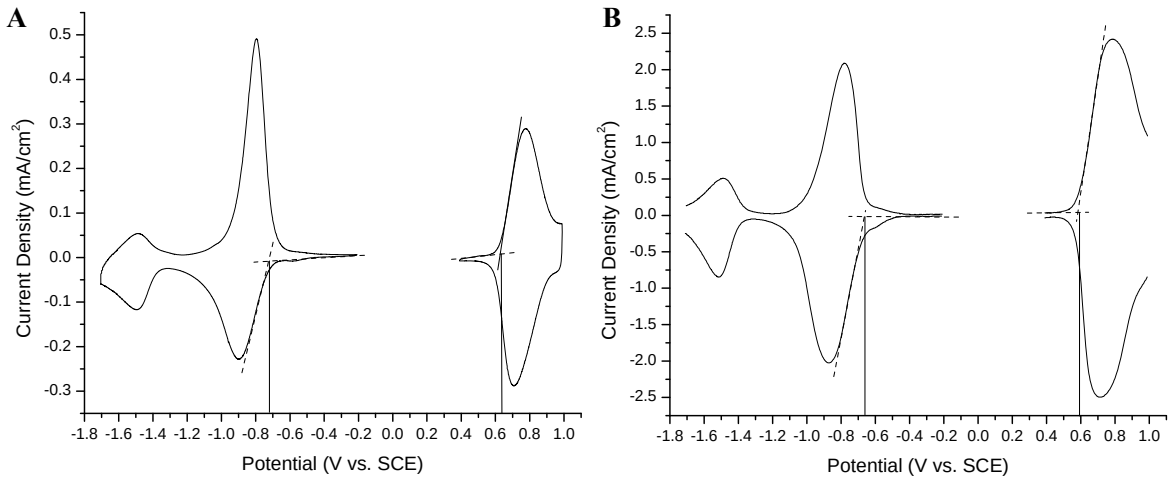

Figure 4-10. CV (scan rate = 50 mV/s) and DPV (step size of 2 mV and step time of 0.1 seconds) of polymer **P8c** on a Pt button working electrode in 0.1 M TBAP-PC electrolyte solution. A) CV of **P8c**. B) DPV of **P8c**.

Finally, CV and DPV analysis of **P6a-b** (Figure 4-11) and **P6c** (Figure 4-12) were performed. Applying an anodic potential to **P6a** (Figure 4-11 A) shows a normal faradaic response yielding a single oxidation at an $E_{1/2}$ of 0.53 V with an onset of oxidation at 0.23 V. However, the oxidation does not fall off sharply after reaching the peak oxidation potential as was observed for **P7-8a-c**, which is indicative of capacitive behavior.[143-145] This is demonstrated clearly in the DPV of **P6a** (Figure 4-11 C)**,** where after the peak oxidation potential from CV is reached (~0.63 V), the current stays relatively constant. Reduction of **P6a** (Figure 4-11 A) shows two reductions at an $E_{1/2}$ of -0.52 V and -1.28 V respectively, with an onset for the first reduction at -0.41 V. Both reductions are quasi-reversible with adequate charge compensation on the reverse scans. This demonstrates the high electron accepting ability of the polymer and that it can stabilize two negative charges due to having two thiadiazole rings on the acceptor. The electrochemical band gap is taken as the onset of oxidation minus the onset of reduction. Thus, **P6a** has an electrochemical band gap of 0.64 eV estimated by CV. One of the advantages of DPV is the increased sensitivity allowing for a more accurate estimation of the onsets of

oxidation and reduction. DPV was performed on **P6a** (Figure 4-11 C) and shows an onset for reduction at -0.23 V, and an onset for oxidation at 0.03 V. It is interesting to note that there is a slight shoulder peak around 0.2 V in the DPV oxidation. This peak makes it hard to draw an accurate tangent line and to determine the onset, but the change is not expected be that significant. While the band gap estimated by DPV was found to be 0.26 eV (~0.3 eV), it is unlikely that the band gap is 0.3 eV. Determination of the band gap for very low band gap polymers will be discussed in more detail later in this chapter, especially in reference to the optical data.

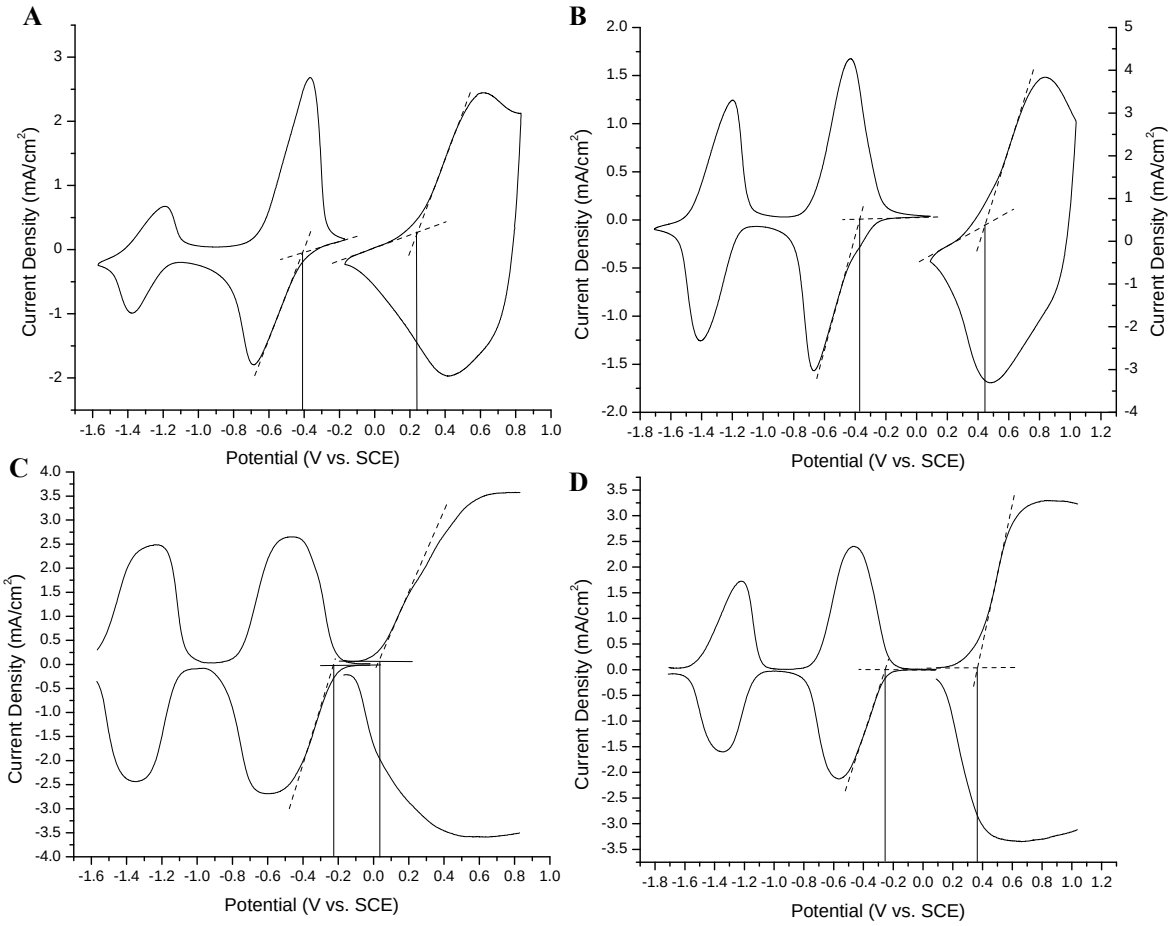

Figure 4-11. CV (scan rate = 50 mV/s) and DPV (step size of 2 mV and step time of 0.1 seconds) of polymers **P6a-b** on a Pt button working electrode in 0.1 M TBAP-PC electrolyte solution. A) CV of **P6a**. B) CV of **P6b**. C) DPV of **P6a**. D) DPV of **P6b**.

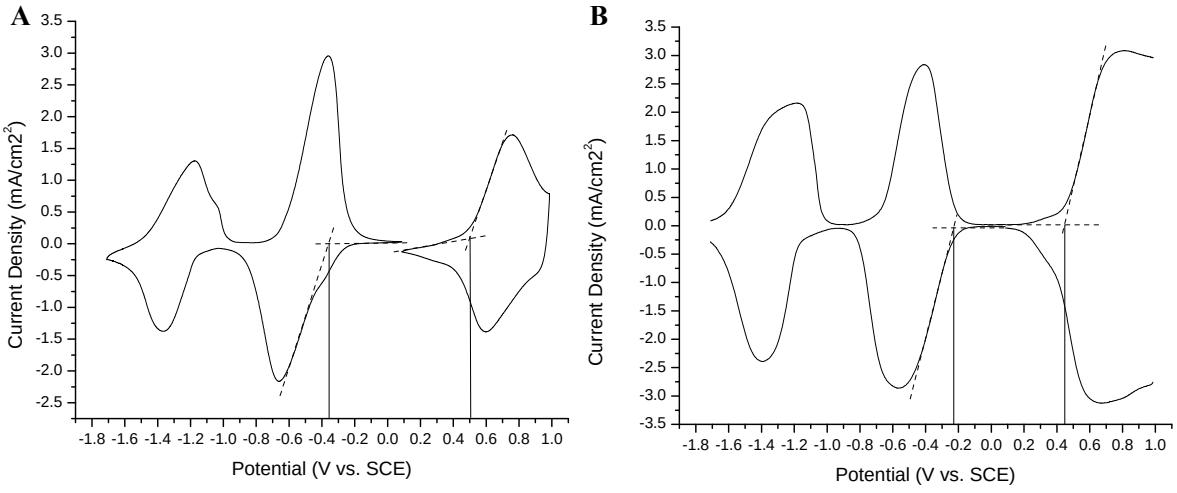

Figure 4-12. CV (scan rate = 50 mV/s) and DPV (step size of 2 mV and step time of 0.1 seconds) of polymer **P6c** on a Pt button working electrode in 0.1 M TBAP-PC electrolyte solution. A) CV of **P6c**. B) DPV of **P6c**.

CV analysis of **P6b** (Figure 4-11 B) shows a single oxidation with an $E_{1/2}$ of 0.66 V with an onset of oxidation at 0.43 V. Again the behavior is quite similar to **P6a**, with the capacitive nature of the oxidation around the $E_{p\ ox}$ (as determined by CV) as shown in the DPV (Figure 4-11 D). The onset for oxidation increased by 200 mV while the $E_{1/2}$ increased by 130 mV relative to **P6a**. This reflects the diminished electron donating ability of ProDOT relative to EDOT. **P6b** has an onset of reduction at -0.36 V and shows two reductions at $E_{1/2}$ of -0.55 V and -1.30 V. These values are quite similar to the reduction potentials for **P6a** and **P6c**. The electrochemical band gap determined by CV for **P6b** is 0.79 eV, which is 0.15 eV higher than **P6a**, due to the decreased donor strength. In looking at the DPV (Figure 4-13d), the onset for reduction is around -0.25 V while the onset for oxidation is near 0.35 V, corresponding to an electrochemical band gap of 0.6 eV.

CV analysis of **P6c** (Figure 4-12 A) shows very similar reductive behavior to **P6a-b** with two quasi-reversible reductions at $E_{1/2}$ of -0.51 V and -1.27 V and an onset of reduction at -0.35 V. Application of an oxidizing potential to **P6c** shows an onset of oxidation at 0.50 V ($E_{1/2\ ox}$ =

0.68 V), which is slightly higher (70 mV) than for **P6b**, yielding a band gap of 0.85 eV. This is due to a slight decrease in the donor strength in going from ProDOT to $ProDOTMe_2$. The oxidation of **P6c** is much sharper and shows an increase in loss of current after the E_p relative to **P6a-b**, which is indicative of a greater contribution of site limited redox conductivity to the overall current. The onsets for oxidation, reduction, and the electrochemical band gap, as determined by DPV (Figure 4-12 B) for **P6c** are 0.44 V, -0.23 V, and 0.67 eV respectively. This is consistent with CV data with an increase in the band gap by 0.06 eV.

The general trend so far is that the DPV determined band gap is about 0.1 to 0.2 eV smaller than what is estimated by CV for **P6-8a-c**. **P6a**, which has a DPV band gap almost 0.4 eV smaller than what was determined by CV, is an outlier from this trend probably due to trapped charges. It can be seen that within a sub-family of polymers (i.e. **P7a-c**) the LUMO remains relatively unchanged while the HOMO is changing with the different donors, demonstrating the donor control on the band gap. The difference in band gaps of EDOT donors (**P6-8a**) relative to ProDOT donors (**P6-8b**) is ~ 0.13 to 0.15 eV, while the difference between the ProDOT donors (**P6-8b**) relative to the $ProDOTMe_2$ (**P6-8c**) donors is only 0.04 to 0.07 eV. Comparison of the electrochemical band gaps to the optical band gaps will be discussed in the next section.

Optical Characterization

The electro-optical properties of this family of polymers was investigated via spectroelectrochemistry. Polymer films were electrodeposited potentiostatically onto ITO coated glass working electrodes. The polymer films were then placed in a cuvette with a platinum wire counter electrode and a silver wire pseudo reference electrode (calibrated to the Fc/Fc^+ redox couple) and switched by cyclic voltammetry in a 0.1 M TBAP/PC solution until a reproducible CV was attained before spectroelectrochemical measurements were performed. While oxidative

spectroelectrochemistry can usually be performed on the bench top, reductive spectroelectrochemistry is normally done in a glove box due to stability issues of the reduced polymers in regards to water and air. However, due to instrument problems, reductive spectroelectrochemistry was performed on the bench top using stringent conditions to prevent moisture and oxygen contamination. Due to stability issues of the films to repetitive reductive cycling on ITO, especially outside the glove box, the electrodeposited films were neutralized and then subjected to reductive spectroelectrochemistry. The optical band gaps for **P6-8a-c** were taken as the onset of absorption of the neutral polymer after break in for oxidative spectroelectrochemistry.

Oxidative Spectroelectrochemistry

Figure 4-13 shows the oxidative spectroelectrochemical series for **P6a-c**. **P6a-c** have λ_{max} at 985 nm (**P6a**), 874nm (**P6b**), and 858 nm (**P6c**) respectively. The higher energy peaks associated with these polymers can be attributed to π-π^* transitions (π-transition band) while the lower energy peak is attributed to intramolecular charge transfer (CT band), as has been seen in similar DA polymers and theoretical work.[30,64,105,112,135,154,155] The blue shift in the CT band for **P6a** to **P6c** correlates with the decreasing strength of the donors. **P6a** absorbs in both the red and the blue portions of the spectrum, while there is a very little absorption around 600 nm, corresponding to a neutral olive green color (Figure 4-13 D). **P6b** follows a similar absorption pattern as **P6a**, however, the gap around 600 nm is more flat and slightly wider, yielding a light green colored polymer. **P6c** is similar in absorption profile to **P6b**, with just a slight blue shift of the gap in the two band absorption leading to a more grey/green neutral polymer. The optical band gap for **P6c** was measured to be 1.09 eV while **P6b** was observed at 1.04 eV. These values are about 0.25 eV higher than the electrochemical band gap determined by CV (0.85 eV and 0.79

eV) and 0.4 eV higher by DPV (0.67 eV and 0.61 eV). The band gap for **P6a** is too low for the scope of traditional characterization on ITO. This is because ITO absorbs strongly beyond 1600 nm (Figure 4-14 A), making baseline absorption hard to quantify. By switching to the more transparent single walled carbon nanotube (SWCNT) electrodes, which have a high degree of transparency into the IR (Figure 4-14 A), allows for a more accurate optical band gap to be measured.[124] **P6a** was deposited electrochemically on a SWCNT electrode, broken in, neutralized, and analyzed by UV-VIS-NIR under solvent free conditions as described previously.[156] Figure 4-14 B shows neutral **P6a** on a SWCNT electrode. The optical band gap was observed to be between 0.53 and 0.68 eV depending upon which method is used to determine the onset of absorption. This value is in good agreement with the electrochemical band gap of 0.64 eV determined by CV.

Upon application of oxidizing potentials to **P6a**, a bleaching of both the CT band (985 nm) and the π-transition band (359 nm) start around +0.2 V (comparable to CV onset for oxidation), with formation of polaron charge carriers (Figure 4-13 A). Upon reaching higher potentials, bipolaron charge carriers are formed as seen by the peak at ~1300 nm. The intense absorptions in the NIR are indicative of the polymer being in a more conducting p-doped state. The absorption band of **P6a** in the fully p-doped state extends back through the visible region (decreasing in intensity down to 430 nm) with slightly increased intensity relative to the neutral state. This results in a grey colored film in the oxidized state. The same transitions seen in **P6a** are also seen in **P6b-c** (Figure 4-13 B and C) upon application of oxidizing potentials. The only difference is that in **P6b** the bleaching of the CT band (874 nm) and the π-transition band (359 nm) starts around +0.3 to +0.4 V, while in **P6c** the CT band (858 nm) and the π-transition band (358 nm) start to bleach around +0.4 to +0.5 V. These values are in good agreement with onsets

for oxidation in the CV data. When **P6b** is in the fully oxidized state, there is a noticeable shoulder peak around 560 nm on the tail from the NIR, followed by a sharper decrease down to 460 nm where the change in **P6a** is more gradual. This results in a darker grey/blue film. **P6c** shows an even larger shoulder peak at ~ 570 nm decreasing sharply down to 450 nm, resulting in a lighter grey/blue oxidized film.

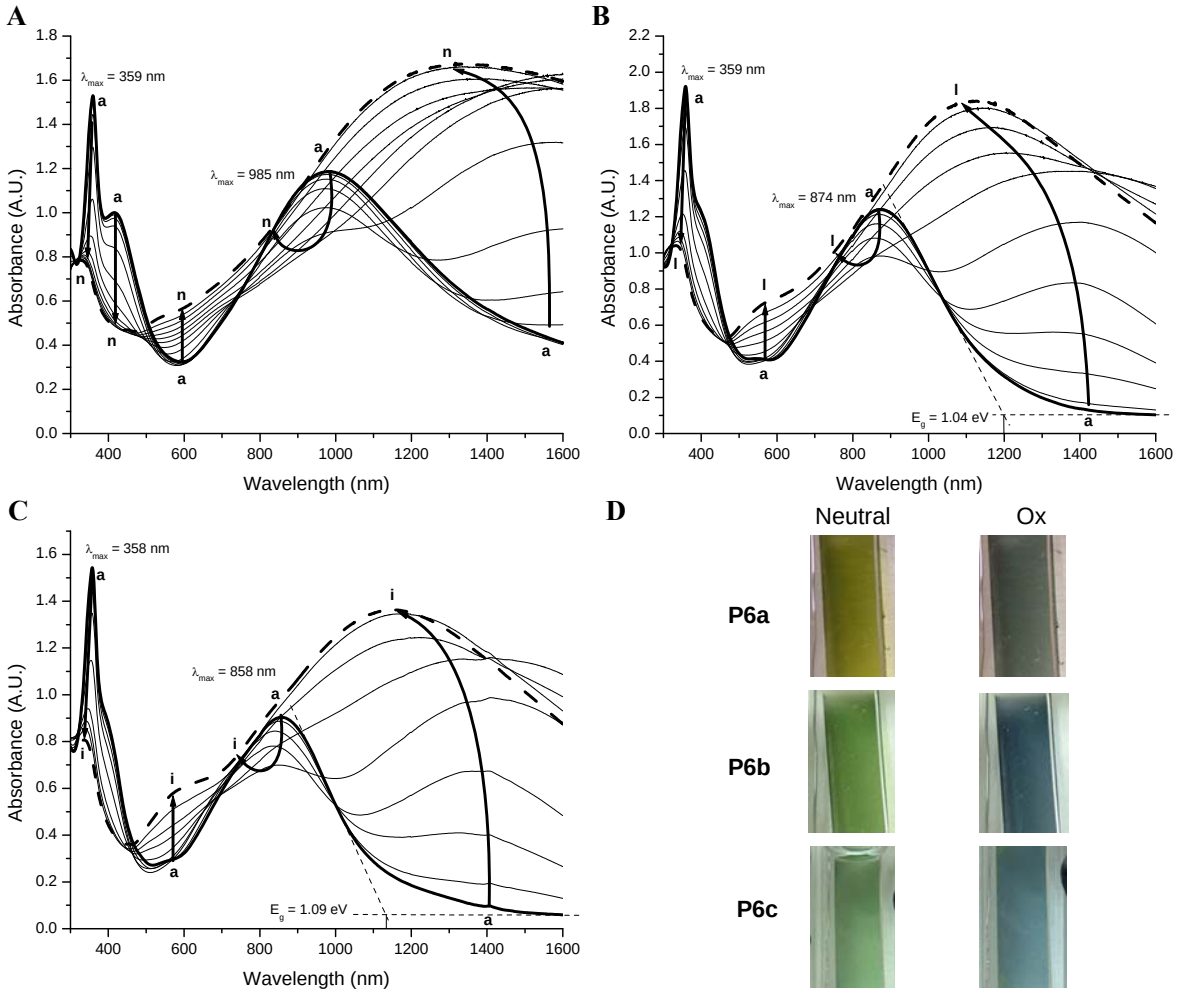

Figure 4-13. Oxidative spectroelectrochemistry of **P6a-c** on ITO in 0.2 M TBAP-PC. All potentials reported vs. SCE. A) **P6a** at potentials of (a) -0.24 V to (n) +1.06 V in 100 mV increments. B) **P6b** at potentials of (a) 0.0 V to (l) 1.0 V in 100 mV increments. C) **P6c** at potentials of (a) 0.06 V, (b) 0.26 V to (i) 0.96 V in 100 mV increments. D) Pictures of **P6a-c** in their neutral and oxidized states.

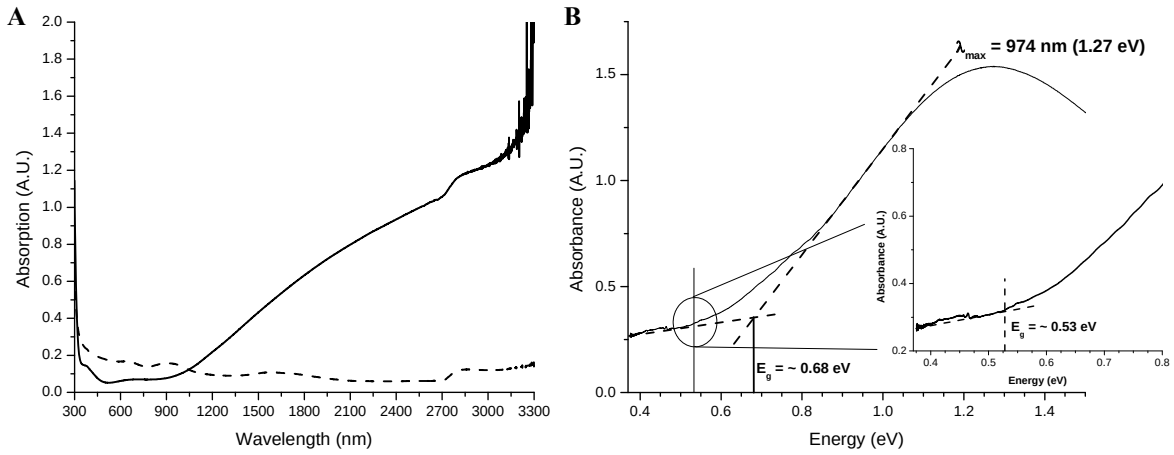

Figure 4-14. UV-VIS-NIR absorption of the electrodes used and **P6a** on a SWCNT electrode. A) UV-VIS-NIR absorption of ITO (solid) and SWCNT (dashed) relative to air. B) UV-VIS-NIR of neutral **P6a** on SWCNT electrode under solvent free conditions.

The oxidative spectroelectrochemistry for **P7a-c** can be seen in Figure 4-15. **P7a-c** have CT bands and the π-transition bands at 738 nm and 374 nm (**P7a**), 673nm and 371 nm (**P7b**) and 657 nm and 369 nm (**P7c**) respectively. It can be seen that by going from the strong BBT based acceptor in **P6a-c**, there is a blue shift of the CT bands of **P7a-c** due to the weaker TQ acceptor. The CT band of **P7a** is blue sifted about 250 nm relative to **P6a**, while the CT band for **P7b-c** are blue shifted about 200 nm each. The CT band for **P7a** at 738 nm tails off sharply through the visible region to a minimum at about 500 nm, upon which there is a sharp increase in absorbance up to 374 nm. This sharp two band absorption of the red and blue regions results in an emerald green neutral polymer (Figure 4-15 A). When looking at into the NIR of neutral **P7a**, there is a slight shoulder around 900 nm, which depending on what tangent is used for determining the onset, gives a band gap of 1.18 eV to 1.26 eV. This shoulder seems to have come from continued cycling from the neutral state to the oxidized state during break in. This can be seen relative to the neutral polymer film used for reduction (Figure 4-18 A), which after electropolymerization, was held at a neutralizing potential with no cycling before doing reductive spectroelectrochemistry, and the shoulder peak is almost completely gone. It is unclear

whether this shoulder is a result of trapped charges or if it could be the result of some change in morphology from repetitive cycling (which could be solvent/electrolyte dependent), possibly some kind of induced aggregation. Film neutralization with hydrazine would be the first experiment to do to make sure it is not due to trapped charges. If this does not prove to be the case, future studies could include switching the solvent/electrolyte system used for polymer deposition and break in, or performing temperature dependent spectroelectrochemistry. These experiments could provide insight into what is causing this shoulder. If 1.26 eV is taken as the optical band gap, the value is 0.13 eV higher than the electrochemical band gap determined by CV, or 0.05 eV higher if the shoulder peak is used. Based upon the results for the neutral polymer used for reductive spectroelectrochemistry, the optical band gap for **P7a** will be assumed to be 1.26 eV for future discussion.

P7b, with a weaker donor, has a CT band that is blue shifted ~75 nm relative to **P7a** (Figure 4-15 B). The CT band tails through the visible region down to 460 nm, with not nearly as sharp of an increase going up to the high energy peak at 371 nm, resulting in a light grey/blue film in the neutral state. The optical band gap was determined to be 1.5 eV. These results are quite similar to **P7c** (Figure 4-15 C), with a slight blue shift in the CT band of about 16 nm relative to **P7b**, resulting in a slightly darker grey/blue neutral film. The optical band gap for **P7c** was 1.48 eV, which is almost identical to the 1.5 eV of **P7b**. The optical band gaps range from 0.13 eV above the electrochemical band gap for **P7a** to 0.24 eV for **P7b** and 0.15 eV for **P7c**.

Application of an oxidizing potential to **P7a** results in the bleaching of the π-transition band along with a slight bleaching of the CT band starting around +0.4 to +0.5 V. Only a slight bleaching of the CT band occurs compared to the π-transition band when fully oxidized. This is

due to the tail from the NIR absorbing through the visible region as a result of the formation of polaron and bipolaron charge carriers (Figure 4-15). This results in a darker greenish grey film in the oxidized state. The same effect of the partial bleaching of the CT band due to the tail from the formation of polaron and bipolaron charge carrier bands is also seen in **P7b-c**. These transitions start to occur at +0.6 to +0.7 V in **P7b-c** respectively. The absorption tail from the NIR through the visible portion for **P7b** is not quite as intense as in **P7a**, resulting in a light grey color in the oxidized state. The tail from the charge carrier band in **P7c** has a slight increase in relative intensity to **P7b** and a sharper absorption well at 480 nm resulting in a darker grey oxidized film (Figure 4-15 C).

When comparing **P7a-c** and **P8a-c,** the only structural change is of the methyl group on the TQ acceptor to the longer hexyl group. Examining the neutral polymers (Figure 4-16), there is little change in the π-transition bands (4 nm red shift for **P8a** vs. **P7a** and 2 nm red shift for **P8b-c** vs. **P7b-c**), however the CT bands shift by 50 nm (**P8a**), 28 nm (**P8b**), and 33 nm (**P8c**) respectively. The general profiles of the neutral absorptions are quite similar to their analogous counter parts. The red shift in the CT band for **P8a** to 778 nm results in a slight change in color to lighter more pastel green. For **P8b**, the red shift of the CT band to 701 nm gives more of a navy blue color in the neutral state. **P8c** has a CT band at 690 nm and is very similar in color to **P7c**, with a small change to more of a pastel grey/blue. The optical band gaps for **P8a-c** were measured to be 1.27 eV (**P8a**) and 1.42 eV (**P8b-c**). While the band gap for **P8a** is almost identical to **P7a** (unless the shoulder of **P7a** is taken into account), the optical band gaps for **P8b-c** are about 0.08 to 0.06 eV lower relative to **P7b-c**, possibly due to interchain interactions.

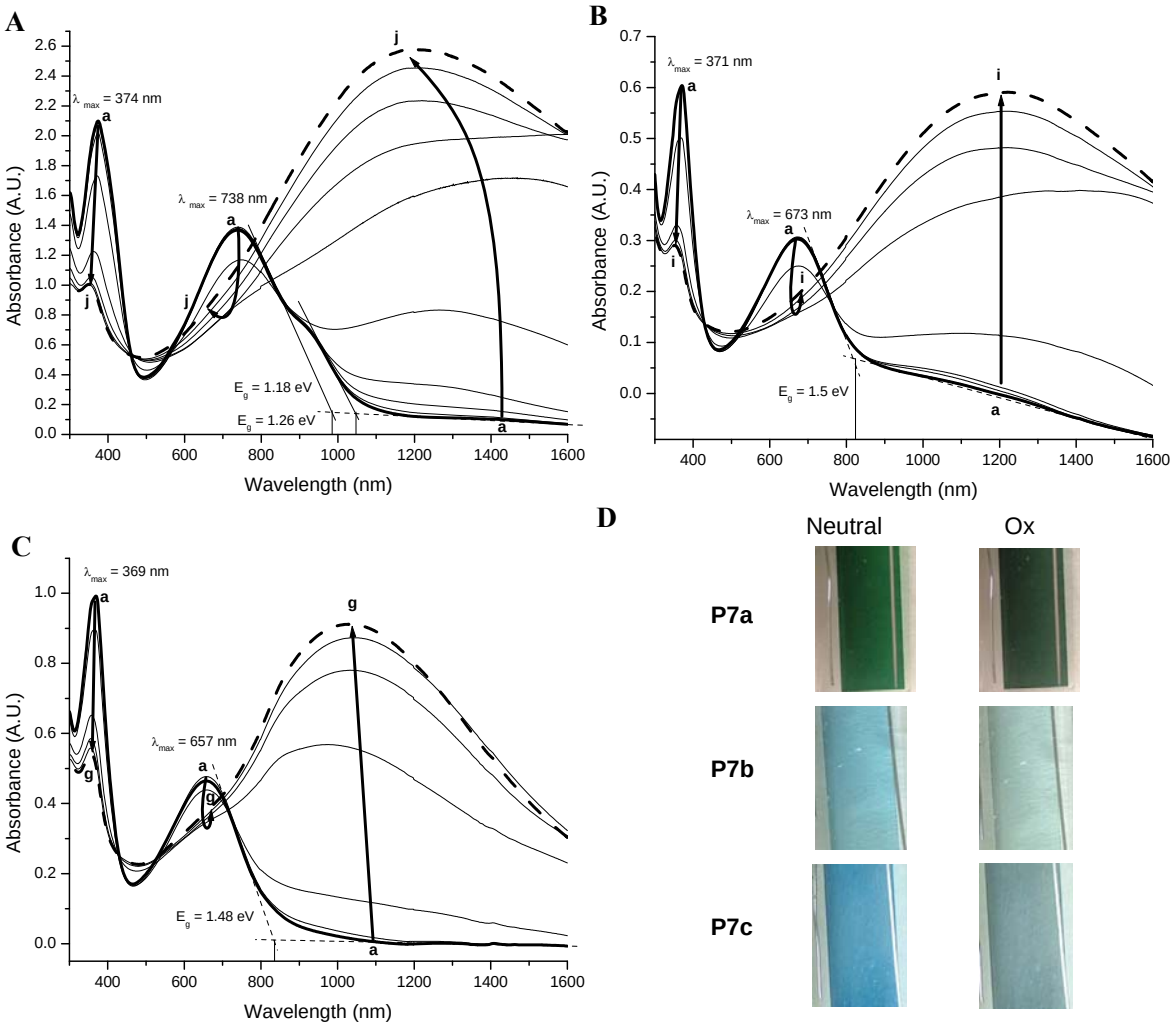

Figure 4-15. Oxidative spectroelectrochemistry of **P7a-c** on ITO in 0.2 M TBAP-PC. All potentials reported vs. SCE. A) **P7a** at potentials of (a) 0.04 V, (b) 0.24 V to (j) 1.04 V in 100 mV increments. B) **P7b** at potentials of (a) 0.1 V, (b) 0.3 V to (i) 1.0 V in 100 mV increments. C) **P7c** at potentials of (a) 0.4 V to (g) 1.0 V in 100 mV increments. D) Pictures of **P7a-c** in their neutral and oxidized states.

When a potential of about +0.45 V is applied to **P8a** (Figure 4-16 A), a bleaching of both absorptions begin (correlates well with CV data), and by +0.65 V, the film is quite bleached with the formation of polaron charge carriers. Upon application of higher potentials, there is a shift in the low energy transition to ~1250 nm, indicative of bipolaron formation. This peak tails down through the visible region bottoming out around 500 nm with little increase in intensity in moving past 400 nm, resulting in a pastel grey colored film with a hint of green.

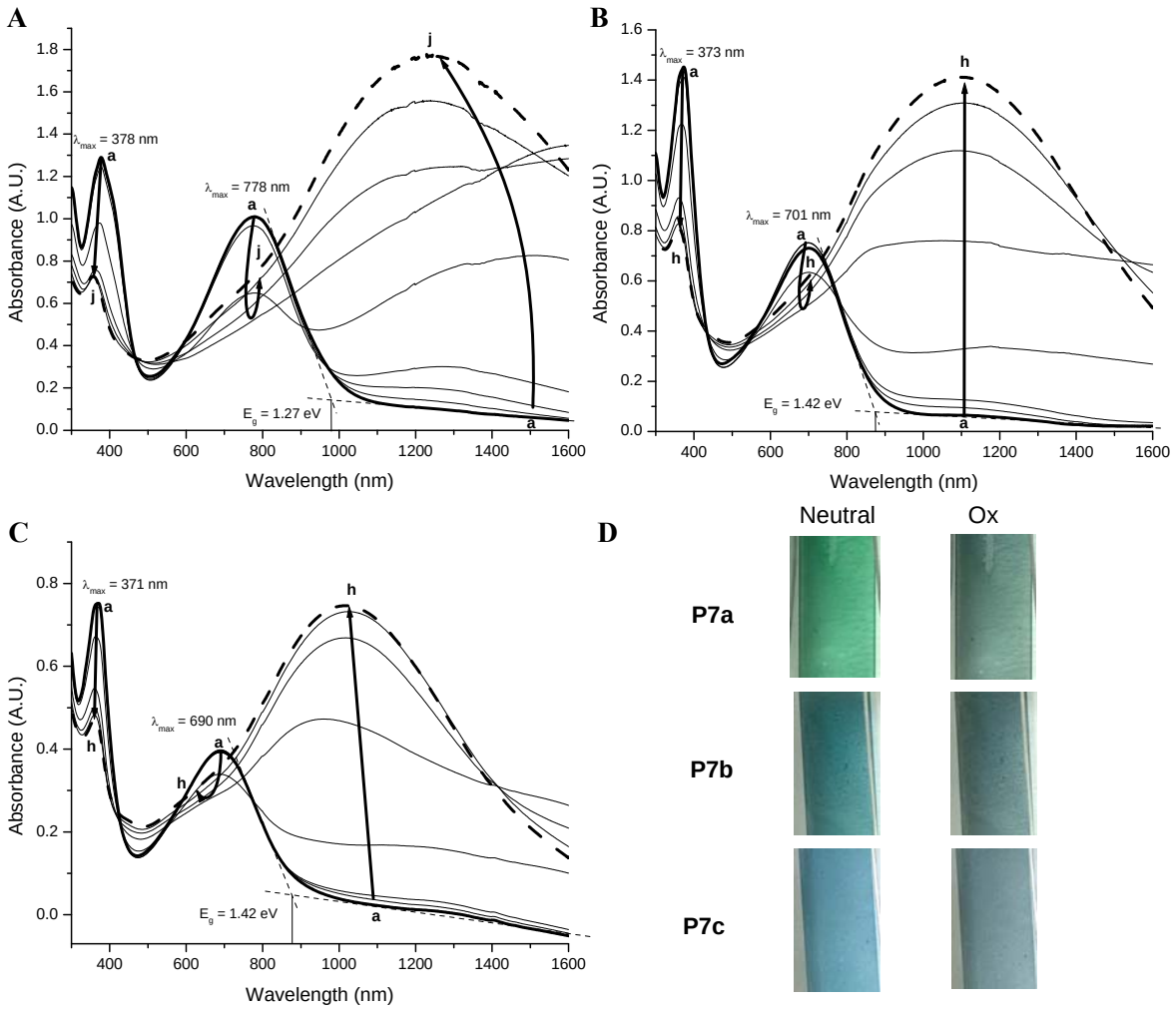

Figure 4-16. Oxidative spectroelectrochemistry of **P8a-c** on ITO in 0.2 M TBAP-PC. All potentials reported vs. SCE. A) **P8a** at potentials of (a) -0.15 V, (b) 0.05 V, (c) 0.25 V to (j) 0.95 V in 100 mV increments. B) **P8b** at potentials of (a) 0.26 V, (b) 0.46 V to (h) 1.06 V in 100 mV increments. C) **P8c** at potentials of (a) 0.4 V to (h) 1.1 V in 100 mV increments. D) Pictures of **P8a-c** in their neutral and oxidized states.

P8b shows a similar trend, with bleaching of the neutral absorptions beginning at a slightly higher potential, comparable to the CV data, around +0.66 V (Figure 4-16 B). The bleaching occurs over a small potential range, and by +0.76 V both absorptions are highly bleached with a strong absorption throughout the NIR. Upon higher potentials, a peak attenuates at ~ 1100 nm that tails through the visible reaching a minimum around 490 nm with little increase in absorption moving to 400 nm. This results in a grey colored film.

The bleaching of the neutral absorptions in **P8c** starts at +0.7 V (good CV correlation), and by +0.8 V the film is highly bleached (Figure 4-16 C). Applying higher potentials results in charge carrier peak attenuation just beyond 1000 nm, which tails through visible very similar to **P8b**, reaching a minimum around 490 nm. This results in a similar colored, but slightly lighter grey film.

Reductive Spectroelectrochemistry

To gain a better understanding of how these polymers behave optically and electronically when they are reduced, reductive spectroelectrochemistry was performed on **P6-8a-c**. Previous work done in our group on PBEDOT-PyrPyr-Ph_2 has demonstrated that even though a polymer may show an electrochemical reduction, that does not mean it can be attributed to true n-type doping.[67,68,142] It was demonstrated that charge carrier band formation should be seen optically via spectroelectrochemistry and there should be an increase in conductivity associated with the reduction as measured by in-situ conductivity.[67] The nature of the whether the conductivity measured is truly electronic or redox based was debatable. When looking at the n- and p-type conductance profiles for PBEDOT-PyrPyr-Ph_2, they were quite different. In the p-type doping, the conductivity remained high and showed capacitive behavior upon increasingly applied potentials past the $E_{1/2}$ (indicative of a highly conductive material), and also had a very intense absorption in the NIR. However, the n-type doping showed a drop off in conductivity (no capacitive behavior) mirroring the electrochemical reductions seen by CV/DPV. Also, the absorptions seen in the NIR upon reduction were not as intense as there were for p-doping, suggesting more of a redox type conductivity instead of a highly delocalized state. While definitions may vary from person to person, I think in order to be truly n-type doped, you must have the formation of intense absorption bands in the NIR upon reduction equivalent to p-type doping, along with a conductivity profile that is capacitive in nature. None the less, reductive

spectroelectrochemistry can give us insight into the n-doping process, while conductivity experiments would need to be performed to gain a complete understanding.

Examining spectral changes upon reduction for **P6a-c** (Figure 4-17) the general trend is for a steady decrease in the intensity of the CT band throughout the whole reduction process. Comparing **P6a** and **P6c**, there is the concurrent development of a small peak that grows in just beyond 1000 nm during the first reduction process, which heavily overlaps with the CT band, but with much lower intensity, making it hard to characterize. **P6b** does not show this slightly red shifted peak at 1000 nm, but does show a small flat increase in the NIR which then disappears upon full reduction. There is also the development of some small sharp peaks between 600-800 nm during the first reduction process for **P6a-c** which remain throughout the second reduction process. Examining the higher energy portion of the spectrum during the first reduction process reveals a decrease in the π-transition band at 359 nm is along with the formation of a new high energy band at 393 nm (**P6a,c**) and 396 nm (**P6b**). This is followed by a decrease in intensity of these newly formed bands during the second reduction process. The important thing to note here is that unlike oxidation, where there was a large increase in absorbance in the NIR associated with polaron and bipolaron charge carrier formation, very little change is occurring in the NIR for **P6a-c**. This is indicative of an isolated reduction that is not delocalized along the conjugated backbone, but highly localized on the acceptor. All of the films showed signs of degradation after the measurements were performed, especially **P6a** and **P6b**, as is evident by the sharp peaks around 500 nm developing during the second reduction process which would not go away upon returning to the neutral state. This is not surprising considering how negative the applied potentials were at the end of the experiment (-1.5 to -1.7 V) along with this being performed on the bench top with caution taken to prevent air and moisture exposure.

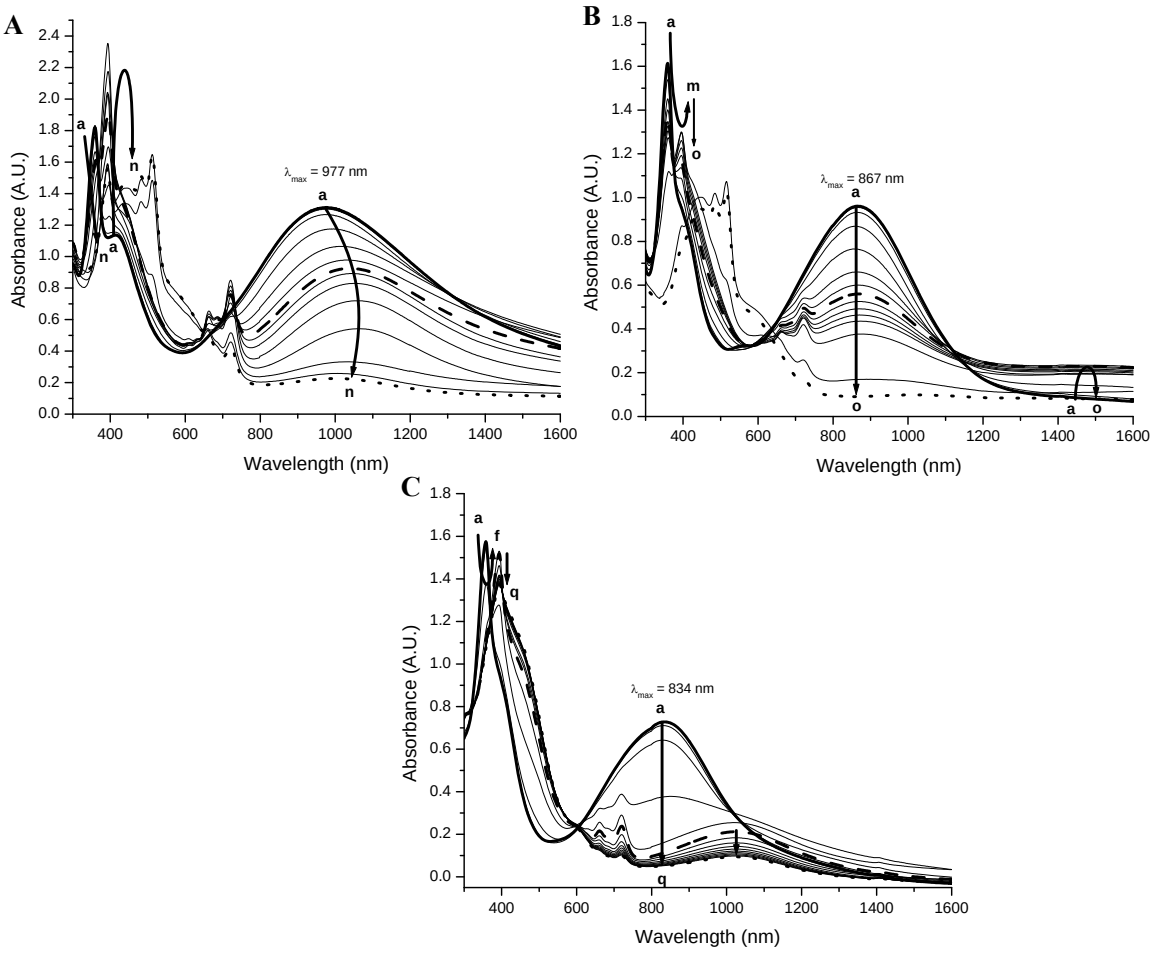

Figure 4-17. Reductive spectroelectrochemistry of **P6a-c** on ITO in 0.2 M TBAP-PC. Solid lines = neutral polymer, dashed lines = 1st red., and dotted lines = 2nd red. All potentials reported vs. SCE. A) **P6a** at potentials of (a) -0.2 V to (n) -1.5 V in 100 mV increments. B) **P6b** at potentials of (a) -0.1 V to (o) -1.5 V in 100 mV increments. C) **P8c** at potentials of (a) -0.07 V to (q) -1.67 V in 100 mV increments.

Analysis of **P7a-c** (Figure 4-18) shows similar results to **P6a-c**. There is a steady decrease in the CT band through out the reduction process. The π-transition band in the neutral polymers at 373 nm (**P7a**) and 370 nm (**P7b-c**) decrease during the first reduction process while new high energy bands forms at 399 nm (**P7a**, -1.1 V), 399 nm (**P7b**, -1.44 V), and 400 nm (**P7c**, -1.1 V) respectively. There is also the formation of a sharp peak where the CT band is decreasing during the first reduction process at 754 nm (**P7a**, -1.1 V) and 759 nm (**P7b**, -1.44 V, **P7c**, -1.1 V). It is unclear what these sharp peaks are from, but it is probably related to the change in the acceptor

structure upon stabilization of an added electron during the reduction process. Upon application of increased reducing potentials, all of the aforementioned peaks decrease in intensity. Again, the key is that there is no formation of any charge carrier bands in the NIR, indicating an isolated reduction of the polymer.

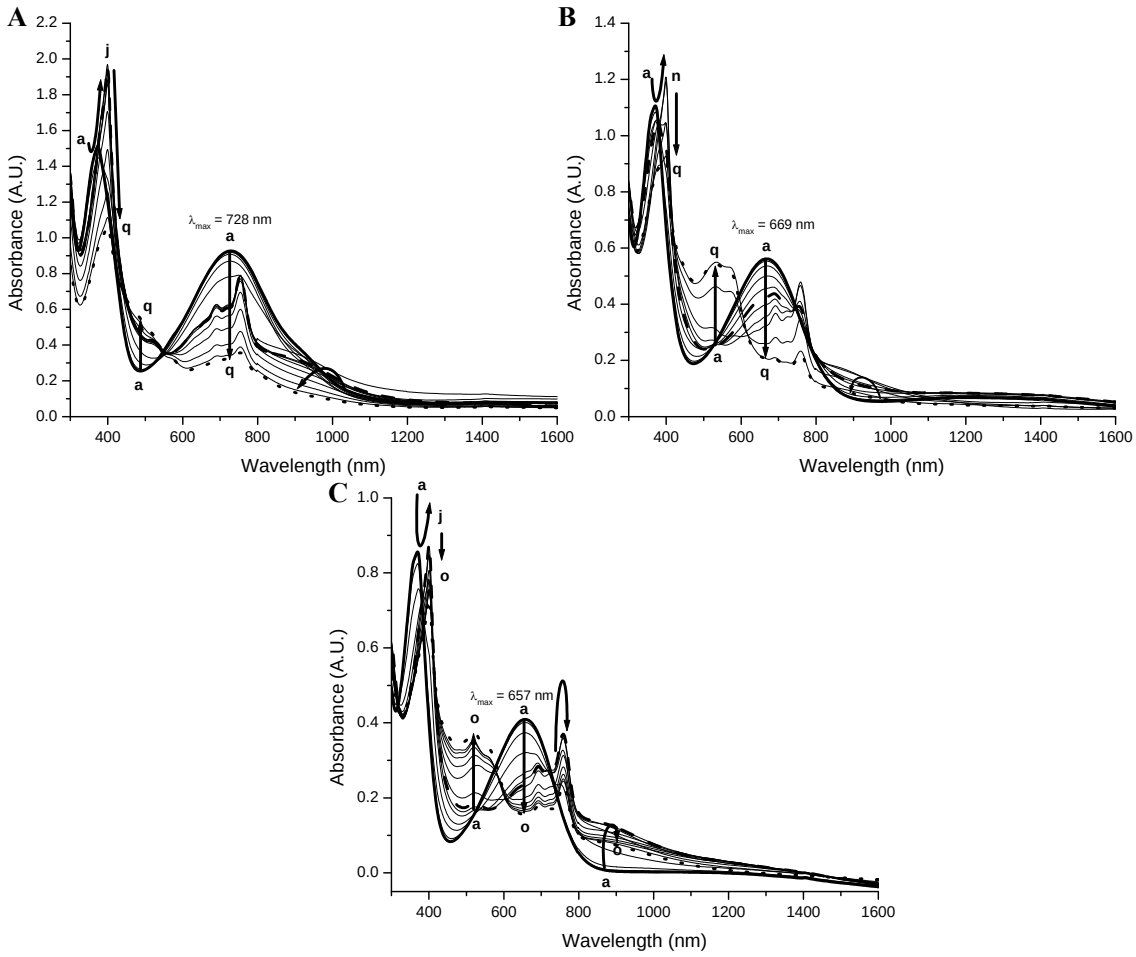

Figure 4-18. Reductive spectroelectrochemistry of **P7a-c** on ITO in 0.2 M TBAP-PC. Solid lines = neutral polymer, dashed lines = 1st red., and dotted lines = 2nd red. All potentials reported vs. SCE. A) **P7a** at potentials of (a) -0.2 V to (q) -1.8 V in 100 mV increments. B) **P7b** at potentials of (a) -0.34 V to (o) -1.74 V in 100 mV increments. C) **P8c** at potentials of (a) -0.4 V to (o) -1.8 V in 100 mV increments.

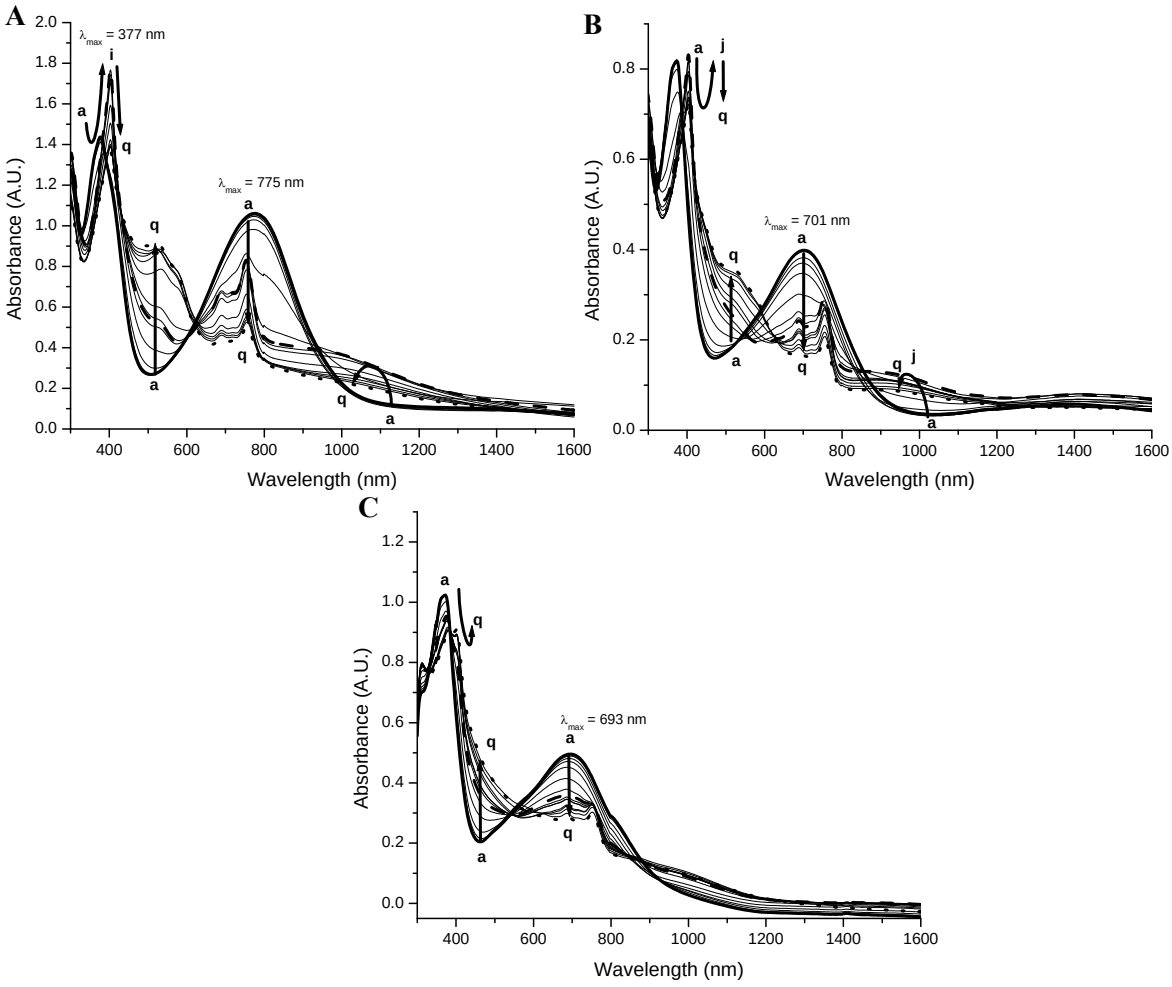

Figure 4-19. Reductive spectroelectrochemistry of **P8a-c** on ITO in 0.2 M TBAP-PC. Solid lines = neutral polymer, dashed lines = 1st red., and dotted lines = 2nd red. All potentials reported vs. SCE. A) **P8a** at potentials of (a) -0.25 V to (q) -1.85 V in 100 mV increments. B) **P8b** at potentials of (a) 0.0 V, (b) -0.20 V, (c) -0.40 V to (q) -1.80 V in 100 mV increments. C) **P8c** at potentials of (a) 0.0 V, (b) -0.20 V, (c) -0.40 V to (q) -1.80 V in 100 mV increments.

Reductive spectroelectrochemistry is shown for **P8a-c** in Figure 4-19. The low energy CT band decreases in intensity throughout the reduction process comparable to the previous polymers. During the first reduction process, there is the same sharp peak that develops on the decreasing CT band at 753 nm (**P8a**, -1.05 V), 754 nm (**P8b**, -1.10 V), and 748 nm (**P8c**, -1.10 V) as was seen for **P7a-c**. This can be attributed to the TQ acceptor. Meanwhile, the neutral π-transition bands at 377 nm (**P8a**), 373 nm (**P8b**), and 372 nm (**P8c**) start to bleach out with the

formation of a new high energy peak at 403 nm (**P8a-b**, -1.05 V and -1.10 V respectively) and 402 nm (**P8c**, -1.1 V, very small shoulder). In moving on to the second reduction, all the peaks decrease in intensity for **P8a-b**, while in **P8c**, the shoulder at 402 nm develops into a tiny peak during the second reduction up to -1.8 V, but all the other peaks continue to lose intensity. Again, no charge carrier band formation was seen, indicating an isolated reduction process is going on.

Conclusions

The data presented in this chapter has brought a few things to light relative to characterization methods needed for low band gap polymers and their stability issues. In relation to reductive stability, it was noted that for the TQ derivatives **P7a** and **P8a**, the second reduction was not that stable in the solvent/electrolyte system used for this study. While the other polymers were fairly stable, this stability issue with the second reduction has put up a red flag. The structure of the TQ derivatives in this chapter is similar to the PyrPyr acceptor used in Chapter 3, in that both polymers have alkyl chains attached to a pyrazine ring in the acceptor, and both have stability issues with the second reduction. It is possible that the anion radicals created during reduction in the presence of benzylic protons could lead to degradation. Perhaps by changing the alkyl groups on the acceptor to phenyl or phenoxy groups, one could see improved stability. While stability issues were seen for some of the TQ derivatives, the BBT systems proved to be quite stable, and reduced at even more positive potentials than the TQ derivatives, thus enhancing the stability in the reduced state. Both systems have shown the ability to stabilize multiple reductions, however optical characterization of the reduced states in these systems indicate a highly localized state with no delocalized charge carrier formation. While the systems studied here are not truly n-type doping systems, they can serve as redox active materials for applications in electrochromics or charge storage.

Another point is that for very low band gap polymers such as **P6a**, it was shown that determination of the optical band gap using traditional ITO electrodes for optical characterization is not necessarily the best method. The usefulness of SWCNTs has been shown, estimating a band gap of 0.53 to 0.68 eV, which was in good agreement with the CV data. This supports the use of SWCNTs for characterization of very low band gap polymers.

Experimental

Compounds **2**,[149] **3**,[150] 7,8-tetradecanedione,[139] ProDOT[157] and ProDOTMe$_2$[158] were made according to literature procedure. 2,3-butanedione, TMS-Cl, anhydrous pyridine, and N-thionylaniline was purchased from Aldrich and used as received. Glacial acetic acid was purchased from Fisher and used as received. (2,3-dihydrothieno[3,4-b][1,4]dioxin-5-yl)trimethylstannane,[98] (3,4-dihydro-2H-thieno[3,4-b][1,4]dioxepin-6-yl)trimethylstannane,[98] and (3,3-dimethyl-3,4-dihydro-2H-thieno[3,4-b][1,4]dioxepin-6-yl)trimethylstannane[98] were made according to literature procedure and used with out purification.

General procedure for the Stille coupling of stannylated dioxythiophenes with compound 3 to synthesize 4a-c: To a flame dried 100 mL 3-neck round bottom flask was added 6.7 mmol of **3** and 14 mmol trimethyltin-XDOT. Then 25 mL of dry THF was added and the solution was degassed for 30 minutes. Then 0.33mmol of Pd(II)Cl$_2$(PPh$_3$)$_2$ was added and the solution was refluxed for 3-4 hours. The solution was cooled and the solvent was removed under reduced pressure followed by column chromatography.

4,7-bis(2,3-dihydrothieno[3,4-b][1,4]dioxin-5-yl)-5,6-dinitrobenzo[c][1,2,5]thiadiazole (4a). Column chromatography ($CHCl_3$, SiO_2) yield 68 % of a red solid. mp 255-257 $^{\circ}$C. ^{1}H NMR (300 MHz, DMSO) δ 4.17-4.23 (m, 8H), 7.15 (s, 2H); ^{13}C NMR (75 MHz, DMSO) δ 64.15, 64.64, 104.02, 105.94, 119.97, 140.72, 141.67, 142.28, 152.09. Elemental Anal. Calcd. for

$C_{18}H_{10}N_4O_8S_3$: C, 42.68; H, 1.99; N, 11.06; O, 25.27; S, 18.99. Found: C, 42.89; H, 1.88; N, 10.84. HRMS Calcd. for $C_{18}H_{11}N_4O_8S_3$ (M+H) 506.97335 Found 506.97328.

4,7-bis(3,4-dihydro-2H-thieno[3,4-b][1,4]dioxepin-6-yl)-5,6-dinitrobenzo[c][1,2,5]thiadiazole (4b). Column chromatography ($CHCl_3$, SiO_2) yield 49 % of a red solid. ^{1}H NMR (300 MHz, $CHCl_3$) δ 2.22 (p, 4H), 4.08 (t, 4 H), 4.16 (t, 4H), 6.94 (s, 2H). Elemental Anal. Calcd. for $C_{20}H_{14}N_4O_8S_3$: C, 44.94; H, 2.64; N, 10.48; O, 23.94; S, 18.00. Found: C, 44.96; H, 2.67; N, 10.16. HRMS Calcd. for $C_{20}H_{15}N_4O_8S_3$ (M+H) 535.0047 Found 535.0017.

4,7-bis(3,3-dimethyl-3,4-dihydro-2H-thieno[3,4-b][1,4]dioxepin-6-yl)-5,6-dinitrobenzo[c][1,2,5]thiadiazole (4c). Column chromatography ($CHCl_3$/Hex 4:1, SiO_2) yield 67 % of a red/orange solid. ^{1}H NMR (300 MHz, $CHCl_3$) δ 1.01 (s, 12H), 3.74 (s, 4 H), 3.82 (s, 4H), 6.88 (s, 2H). Elemental Anal. Calcd. for $C_{24}H_{22}N_4O_8S_3$: C, 48..80; H, 3.75; N, 9.49; O, 21.67; S, 16.29. Found: C, 48.93; H, 3.71; N, 9.49. HRMS Calcd. for $C_{24}H_{22}N_4O_8S_3Na$ (M+Na) 613.0492 Found 613.0492.

General procedure for the synthesis of compounds 5a-c via iron mediated reduction of compounds 4a-c. To a dry 100 mL 3-neck round bottom flask equipped with a condenser was added 2.0mmol of compound **4** and 24 mmol of iron powder. To this was added 40 mL of degassed AcOH. The reaction was heated to 100 °C for 3 hours and then allowed to cool. A golden yellow color solid was collected by filtration and washed with water, saturated sodium bicarbonate, and water in this order. Purified by column chromatography.

4,7-bis(2,3-dihydrothieno[3,4-b][1,4]dioxin-5-yl)benzo[c][1,2,5]thiadiazole-5,6-diamine (5a). Column Chromatography (7:1 CH_2Cl_2:EtOAc, SiO_2) yield 87 % of a yellow solid. mp decomp. >260 °C. ^{1}H NMR (300 MHz, DMSO) δ 4.22 (s, 8H), 5.70 (s, 4H), 6.73 (s, 2H); ^{13}C

NMR (75 MHz, DMSO) δ 64.13, 64.32, 98.62, 99.65, 109.14, 138.96, 140.67, 141.48, 152.62. Elemental Anal. Calcd. for $C_{18}H_{14}N_4O_4S_3$: C, 48.42; H, 3.16; N, 12.55; O, 14.33; S, 21.54. Found: C, 48.52; H, 3.04; N, 12.12. HRMS Calcd. for $C_{18}H_{15}N_4O_4S_3$ (M+H) 447.0255 Found 447.0252

4,7-bis(3,4-dihydro-2H-thieno[3,4-b][1,4]dioxepin-6-yl)benzo[c][1,2,5]thiadiazole-5,6-diamine (5b). Column chromatography (5 % EtOAc/CH_2Cl_2, SiO_2) yield 72 % of a golden yellow solid. ^{1}H NMR (300 MHz, $CHCl_3$) δ 2.23 (p, 4H), 4.11 (t, 4 H), 4.18 (t, 4H), 4.27 (s, 4H), 6.81 (s, 2H). Elemental Anal. Calcd. for $C_{20}H_{18}N_4O_4S_3$: C, 50.62; H, 3.82; N, 11.81; O, 13.49; S, 20.27. Found: C, 50.38; H, 3.72; N, 11.42. HRMS Calcd. for $C_{20}H_{19}N_4O_4S_3$ (M+H) 475.0563 Found 475.0605.

4,7-bis(3,3-dimethyl-3,4-dihydro-2H-thieno[3,4-b][1,4]dioxepin-6-yl)benzo[c][1,2,5]thiadiazole-5,6-diamine (5c). Column chromatography (CH_2Cl_2, SiO_2) yield 91 % of a golden yellow solid. ^{1}H NMR (300 MHz, $CHCl_3$) δ 1.03 (s, 12H), 3.77 (s, 4 H), 3.82 (s, 4H), 4.29 (s, 4H), 6.76 (s, 2H). Elemental Anal. Calcd. for $C_{24}H_{26}N_4O_4S_3$: C, 54.32; H, 4.94; N, 10.56; O, 12.06; S, 18.31. Found: C, 54.09; H, 4.88; N, 10.34. HRMS Calcd. for $C_{24}H_{27}N_4O_4S_3$ (M+H) 531.1189 Found 531.1254.

General procedure for the synthesis of BXDOT-benzobis(thiadiazole) monomers 6a-c. To a flame dried 25 mL 3-neck round bottom flask was added 1.2 mmol of compound **5**, 7 mL of anhydrous pyridine, 2.6 mmol of N-thionylaniline, and 2.2 mmol of TMS-Cl. The solution was heated to 80 °C overnight. The reaction was allowed to cool, poured into water, and collected by filtration. Purified by column chromatography.

4,8-bis(2,3-dihydrothieno[3,4-b][1,4]dioxin-5-yl)benzo[1,2-c;4,5-c′]bis[1,2,5]thiadiazole (6a). Column chromatography (CH_2Cl_2, SiO_2) yield 84 % of a dark

purple solid. decomposition > 292 °C. ^{1}H NMR (300 MHz, DMSO) δ 4.22-4.29 (m, 8H), 7.05 (s, 2H). Elemental Anal. Calcd. for $C_{18}H_{10}N_4O_4S_4$: C, 45.56; H, 2.12; N, 11.81; O, 13.49; S, 27.03. Found: C, 45.52; H, 1.96; N, 11.62. HRMS Calcd. for $C_{18}H_{10}N_4O_4S_4$ (M+) 473.9585 Found 473.9604

4,8-bis(3,4-dihydro-2H-thieno[3,4-b][1,4]dioxepin-6-yl)benzo[1,2-c;4,5-c′]bis[1,2,5]thiadiazole (6b). Column chromatography (CH_2Cl_2, SiO_2) yield 85 % of a dark purple solid. ^{1}H NMR (300 MHz, $CDCl_3$) δ 2.28 (p, 4H), 4.24 (t, 4H), 4.29 (t, 4H), 6.98 (s, 2H). Elemental Anal. Calcd. for $C_{20}H_{14}N_4O_4S_4$: C, 47.79; H, 2.81; N, 11.15; O, 12.73; S, 25.52. Found: C, 47.80; H, 2.71; N, 10.76. HRMS Calcd. for $C_{20}H_{15}N_4O_4S_4$ (M+H) 502.9976 Found 502.9920.

4,8-bis(3,3-dimethyl-3,4-dihydro-2H-thieno[3,4-b][1,4]dioxepin-6-yl)benzo[1,2-c;4,5-c′]bis[1,2,5]thiadiazole (6c). Column chromatography (CH_2Cl_2, SiO_2) yield 71 % of a dark purple solid. ^{1}H NMR (300 MHz, $CDCl_3$) δ 1.06 (s, 12H), 3.89 (s, 4H), 3.97 (s, 4H), 6.93 (s, 2H); ^{13}C NMR (75 MHz, $CDCl_3$) δ 21.80, 39.34, 80.28, 80.60, 109.34, 114.21, 115.82, 149.49, 150.69, 152.99. Elemental Anal. Calcd. for $C_{24}H_{22}N_4O_4S_4$: C, 51.59; H, 3.97; N, 10.03; O, 11.45; S, 22.96. Found: C, 51.64; H, 3.91; N, 9.71. HRMS Calcd. for $C_{24}H_{23}N_4O_4S_4$ (M+H) 559.0597 Found 559.0598.

General procedure for the synthesis of BXDOT-dialkylthiadiazoloquinoxalines (7a-c and 8a-c). 0.47 mmol of compound **5** was placed in a 100 mL round bottom flask followed by 35 mL of acetic acid. Then 0.94 mmol of either 2,3-butane dione or 7,8-tetradecanedione was added and the soln was stirred for 2-12 h. The reaction was then poured into 40 mL of 5 % NaOH and extracted with dichloromethane. The organic layer was then washed with saturated

$NaHCO_3$,water, and dried over $MgSO_4$. Removal of solvent under reduced pressure followed by column chromatography gave the desired compounds.

4,9-bis(2,3-dihydrothieno[3,4-b][1,4]dioxin-5-yl)-6,7-dimethyl-[1,2,5]thiadiazolo[3,4-g]quinoxaline (7a). Column chromatography (CH_2Cl_2, SiO_2) yield 99 % of a dark red solid. ^1H NMR (300 MHz, $CDCl_3$) δ 2.74 (s, 6H), 4.22-4.25 (m, 4H), 4.30-4.32 (m, 4H), 6.72 (s, 2H); ^{13}C NMR (75 MHz, $CDCl_3$) δ 24.04, 64.72, 102.76, 110.15, 121.43, 137.93, 141.09, 141.67, 152.55, 155.15. Elemental Anal. Calcd. for $C_{22}H_{16}N_4O_4S_4$: C, 53.21; H, 3.25; N, 11.28; O, 12.89; S, 19.37. Found: C, 53.38; H, 3.28; N, 11.12. HRMS Calcd. for $C_{22}H_{17}N_4O_4S_4$ (M+H) 497.04064 Found 497.03902.

4,9-bis(3,4-dihydro-2H-thieno[3,4-b][1,4]dioxepin-6-yl)-6,7-dimethyl-[1,2,5]thiadiazolo[3,4-g]quinoxaline (7b). Column chromatography (CH_2Cl_2, SiO_2) yield 83 % of a dark red solid. ^1H NMR (300 MHz, $CDCl_3$) δ 2.23 (p, 4H), 2.73 (s, 6H), 4.20-4.25 (m, 8H), 6.92 (s, 2H); ^{13}C NMR (75 MHz, $CDCl_3$) δ 23.94, 34.31, 71.12, 71.64, 108.91, 116.09, 121.96, 138.21, 149.40, 150.58, 152.82, 155.17. Elemental Anal. Calcd. for $C_{24}H_{20}N_4O_4S_3$: C, 54.94; H, 3.84; N, 10.68; O, 12.20; S, 18.34. Found: C, 55.19; H, 3.82; N, 10.68. HRMS Calcd. for $C_{24}H_{21}N_4O_4S_3$ (M+H) 525.0725 Found 525.0673.

4,9-bis(3,3-dimethyl-3,4-dihydro-2H-thieno[3,4-b][1,4]dioxepin-6-yl)-6,7-dimethyl-[1,2,5]thiadiazolo[3,4-g]quinoxaline (7c). Column chromatography (CH_2Cl_2, SiO_2) yield 70 % of a dark red solid. ^1H NMR (300 MHz, $CDCl_3$) δ 1.03 (s, 12H), 2.73 (s, 6H), 3.89 (m, 8H), 6.88 (s, 2H); ^{13}C NMR (75 MHz, $CDCl_3$) δ 21.88, 23.92, 39.30, 80.10, 80.43, 108.27, 115.35, 121.85, 138.11, 149.08, 150.15, 152.74, 155.11. Elemental Anal. Calcd. for $C_{28}H_{28}N_4O_4S_3$: C, 57.91; H, 4.86; N, 9.65; O, 11.02; S, 16.56. Found: C, 58.43; H, 5.00; N, 9.29. HRMS Calcd. for $C_{28}H_{29}N_4O_4S_3$ (M+H) 581.1351 Found 581.1354.

4,9-bis(2,3-dihydrothieno[3,4-b][1,4]dioxin-5-yl)-6,7-dihexyl-[1,2,5]thiadiazolo[3,4-g]quinoxaline (8a). Column chromatography (CH_2Cl_2, SiO_2) yield 66 % of a dark purple solid. ^{1}H NMR (300 MHz, $CDCl_3$) δ 0.91 (t, 6H), 1.32-1.48 (m,12H), 1.92 (p, 4H), 3.00 (t, 4H), 4.21-4.24 (m, 4H), 4.30-4.33 (m, 4H), 6.72 (s, 2H); ^{13}C NMR (75 MHz, $CDCl_3$) δ 14.32, 22.87, 27.15, 29.44, 32.07, 35.54, 64.75, 64.81 102.61, 110.38, 121.38, 137.74, 140.84, 141.55, 152.57, 158.04. Elemental Anal. Calcd. for $C_{32}H_{36}N_4O_4S_3$: C, 60.35; H, 5.70; N, 8.80; O, 10.05; S, 15.10. Found: C, 60.33; H, 5.63; N, 8.77. HRMS Calcd. for $C_{32}H_{37}N_4O_4S_3$ (M+H) 637.19714 Found 637.19873.

4,9-bis(3,4-dihydro-2H-thieno[3,4-b][1,4]dioxepin-6-yl)-6,7-dihexyl-[1,2,5]thiadiazolo[3,4-g]quinoxaline (8b). Column chromatography (CH_2Cl_2, SiO_2) yield 71 % of a dark purple solid. ^{1}H NMR (300 MHz, $CDCl_3$) δ 0.90 (t, 6H), 1.30-1.42 (m,12H), 1.87 (p, 4H), 2.27 (p, 4H), 2.98 (t, 4H), 4.22 (m, 8H), 6.90 (s, 2H); ^{13}C NMR (75 MHz, $CDCl_3$) δ 14.29, 22.77, 27.06, 29.32, 31.92, 34.23, 35.46, 71.06, 71.59 108.81, 116.18, 121.84, 138.02, 149.10, 150.34, 152.60, 158.14. Elemental Anal. Calcd. for $C_{34}H_{40}N_4O_4S_3$: C, 61.42; H, 6.06; N, 8.43; O, 9.63; S, 14.47. Found: C, 61.30; H, 6.06; N, 8.35. HRMS Calcd. for $C_{34}H_{41}N_4O_4S_3$ (M+H) 665.2290 Found 665.2258.

4,9-bis(3,3-dimethyl-3,4-dihydro-2H-thieno[3,4-b][1,4]dioxepin-6-yl)-6,7-dihexyl-[1,2,5]thiadiazolo[3,4-g]quinoxaline (8c). Column chromatography (CH_2Cl_2, SiO_2) yield 33 % of a dark purple solid. ^{1}H NMR (300 MHz, $CDCl_3$) δ 0.90 (t, 6H), 1.03 (s, 12H), 1.25-1.43 (m, 12H), 1.88 (p, 4H), 2.98 (t, 4H), 3.88 (s, 8H), 6.86 (s, 2H); ^{13}C NMR (75 MHz, $CDCl_3$) δ 14.31, 21.86, 22.84, 27.22, 29.43, 31.97, 35.60, 39.27, 80.12, 80.44, 108.17, 115.54, 121.78, 138.03, 148.83, 149.98.152.62, 158.18. Elemental Anal. Calcd. for $C_{38}H_{48}N_4O_4S_3$: C, 63.30; H, 6.71; N,

7.77; O, 8.88; S, 13.34. Found: C, 63.13; H, 6.79; N, 7.68. HRMS Calcd. for $C_{38}H_{49}N_4O_4S_3$ (M+H) 721.2916 Found 721.2928.

CHAPTER 5
DTP BASED SOLUBLE DONOR-ACCEPTOR POLYMERS

Introduction

As discussed in Chapter 1, the DA approach towards low band gap polymers has proven to be an effective strategy towards controlling the band gap and thus the electronic properties of conjugated materials. However, the importance of planarity in the conjugated back bone cannot be forgotten. As was demonstrated in Chapter 4, the use of stronger donors such as EDOT and ProDOT relative to thiophene in these DAD monomers and polymers did not necessarily give lower band gap polymers. This was explained by the high degree of torsion between the donor and the acceptor. The λ_{max} for BEDOT-BBT (643nm) is blue shifted about 60 nm compared to BTh-BBT (702 nm). A high torsion angle was also seen in the TQ derivatives. While the TQ and BBT acceptors have generated low band gap materials for use in electroluminescence[5,118,159,160] and photovoltaic applications,[13,16,17,28,50,161] the most promising donor molecule so far has been thiophene, due to its synthetic flexibility and its ability to form a highly planar structure with the acceptor.

In keeping with this strategy, an ideal donor would be stronger than thiophene, have the planarity of thiophene, and improved synthetic flexibility towards solubility. Fused donors such as fluorene and carbazole have been used with similar acceptors, and while they give solubilities of ~10 mg/mL, they are not as strong of a donor as thiophene.[5,12,103,162] Two candidates that can provide solubility, planarity, and be stronger donors are cyclopentadithiophene[163-165] and dithienopyrrole (DTP).[166-168] While some work has been done using cyclopentadithiophene as a donor in DA oligomers/polymers,[117,169-171] little work has been done using DTP as a donor in DA oligomers/polymers.[17,26,166]

This work entails the polymerization of a strong soluble donor, 2,6-bis(tributylstannyl)-N-(3,4,5-tris(dodecyloxy)phenyl)-dithieno[3,2-b:2',3'-*d*]pyrrole,[53,172] polymerized with five different dibromo acceptors: Br_2BThBTD, Br_2BTD, Br_2BTh-TQHx_2, Br_2TQHx_2, Br_2BThBBT. The targeted polymers can be seen in Figure 5-1. A comparison of the acceptor strength on the optical and electronic properties were investigated along with a focus on the connectivity of the acceptor cores, whether it is the DTP donor connected directly to the acceptor or with a thiophene spacer. These polymers were characterized by NMR, GPC, UV-VIS, elemental analysis, electrochemistry, and spectroelectrochemistry.

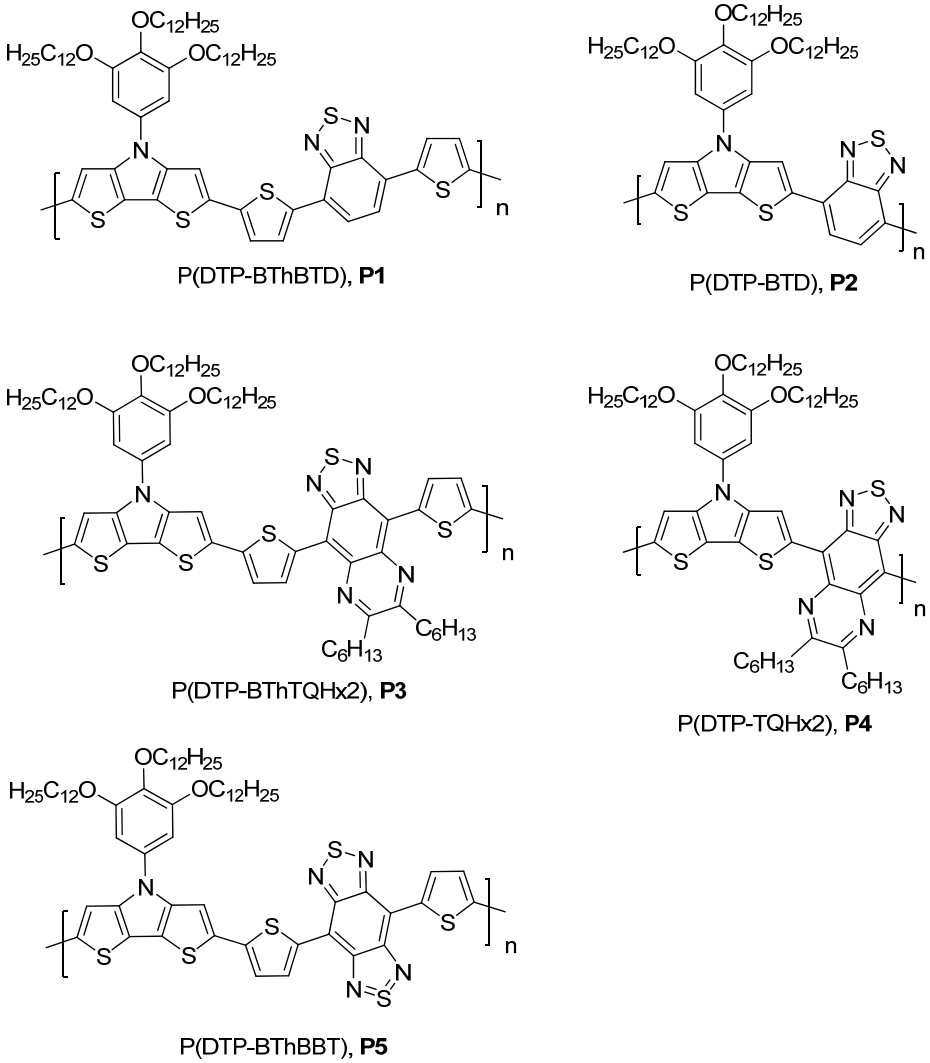

Figure 5-1. Targeted DTP based DA polymers.

Monomer/Polymer Synthesis and Characterization

The following donor, dibromo acceptors, and intermediates: 2,6-bis(tributylstannyl)-N-(3,4,5-tris(dodecyloxy)phenyl)-dithieno[3,2-b:2',3'-*d*]pyrrole,[53] 4,7-dibromobenzo[c][1,2,5]thiadiazole (Br_2BTD),[149] 4,7-bis(5-bromothiophen-2-yl)benzo[c][1,2,5]thiadiazole ($Br_2BThBTD$),[103] 4,7-bis(5-bromothiophen-2-yl)-2$\lambda^4\delta^2$-benzo[1,2-c;4,5-c′]bis[1,2,5]thiadiazole ($Br_2BThBBT$),[173] 6,7-dihexyl-4,9-di(thiophen-2yl)-[1,2,5]thiadiazolo[3,4-*g*]quinoxaline ($BThTQHx_2$)[111] and 4,7-dibromobenzo[c][1,2,5]thiadiazole-5,6-diamine[174] were prepared according to literature procedures. 4,9-bis(5-bromothiophen-2-yl)-6,7-dihexyl-[1,2,5]thiadiazolo[3,4-g]quinoxaline ($Br_2BThTQHx_2$), and 4,9-dibromo-6,7-dihexyl-[1,2,5]thiadiazolo[3,4-g]quinoxaline (Br_2TQHx_2), were prepared via bromination in DMF and condensation in acetic acid respectively (Figure 5-2).

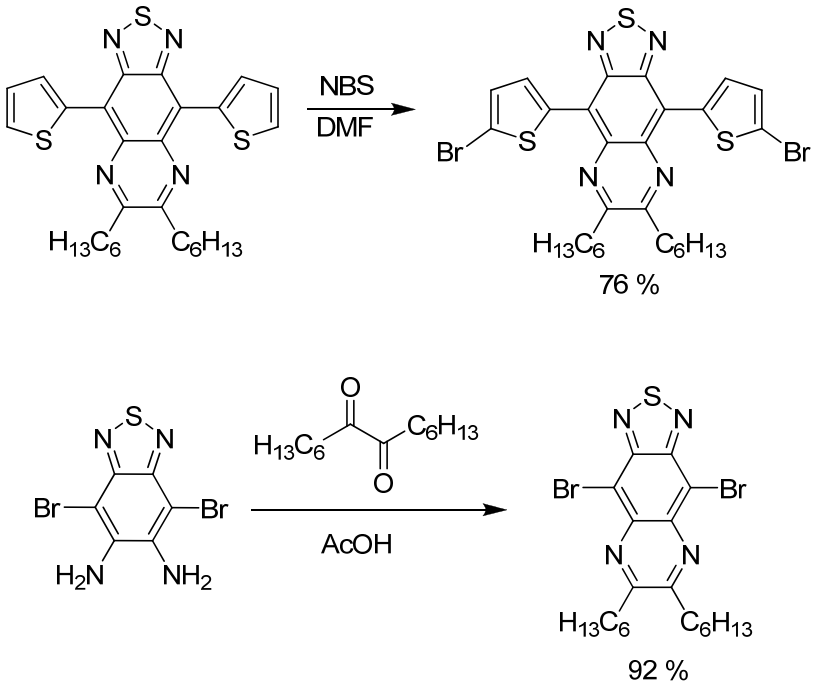

Figure 5-2. Synthesis of 4,9-bis(5-bromothiophen-2-yl)-6,7-dihexyl-[1,2,5]thiadiazolo[3,4-g]quinoxaline and 4,9-dibromo-6,7-dihexyl-[1,2,5]thiadiazolo[3,4-g]quinoxaline.

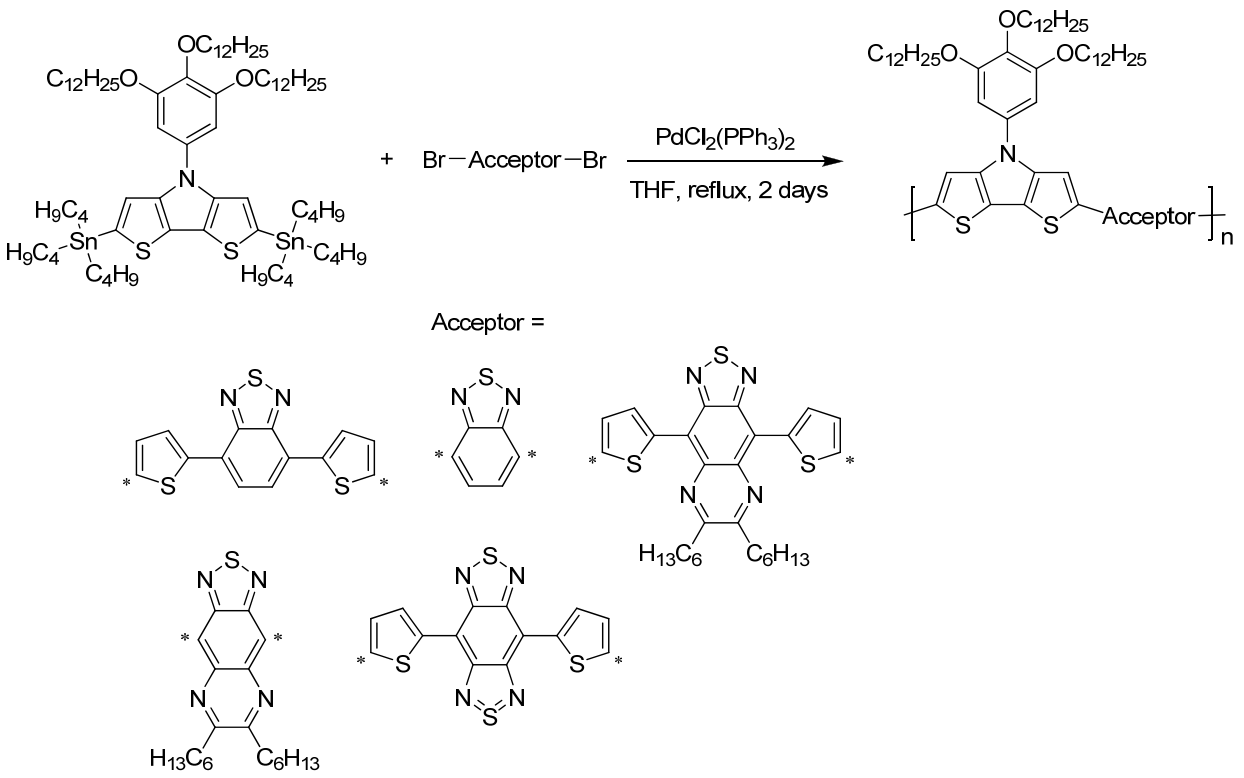

Figure 5-3. General synthesis of DTP based DA polymers via Stille Polymerization. * = –Br.

The advantage of the DTP donor is the ability to functionalize the pyrrole nitrogen. In this case, a trisdodecyloxyphenyl substituent was incorporated to maximize solubility. Polymers were made via Stille polymerization due to its mild reaction conditions, toleration of functional groups, and high yields.[110] A general polymerization can be seen in Figure 5-3. Usually the donor and the catalyst were placed in a dry 3-neck round bottom flask and subjected to 5 vacuum/argon backfill cycles. Then dry THF was added and the solution was degassed for ~1 h. This extra degassing was done to make sure all of the oxygen was removed since the donor is an oil and could still have oxygen trapped in it. Finally the acceptor was added and the solution was heated to reflux for ~2 days. After cooling, the solution was concentrated, precipitated into methanol, and collected by filtration. The crude polymer was then placed in a thimble and purified by Soxhlet extraction with methanol, acetone, hexane, and chloroform in that order with each one running ~1day. The volume of the chloroform fraction was then reduced, precipitated

into methanol, and collected by filtration yielding a black solid. It should be noted that, while the order of addition was not important for making P(DTP-BThBTD), it was very important for making P(DTP-BThBBT). When the donor and acceptor were combined in the same flask with THF and degassed, the reaction turned dark blue in color before any addition of catalyst. Upon subsequent addition of catalyst and polymerization, no polymer was isolated. Thus for the stronger TQ and BBT based polymers, the acceptor was always added last. The yield of the polymerization ranged from 83-95 % (Table 5-1) with the exception of P(DTP-BThTQHx$_2$) (46 %).

Polymer molecular weights were determined by GPC relative to polystyrene standards with THF as the mobile phase. Molecular weights ranged from 9,600 g/mol (satisfactory) for P(DTP-BThTQHx$_2$) up to 106,000 g/mol (excellent) for P(DTP-BThBTD) (Table 5-1). Examination of the GPC chromatograms show nice monomodal distributions for P(DTP-BThBTD), P(DTP-BTD), and P(DTP-TQHx$_2$) with low PDIs ($\sim \leq 2$). However, P(DTP-BThTQHx$_2$) and P(DTP-BThBBT) have bimodal distributions and high polydispersities (>3), indicating the presence of oligomers. One of the main contributing factors that could have resulted in low molecular weights is stoichiometric imbalance. Since all of the polymerizations were carried out using Pd(II)Cl$_2$(PPh$_3$)$_2$, it is known that to go to the active Pd(0) species, the Pd(II) species must get reduced by the stannyl compound to form the active Pd(0) species, which results in homo coupled product.[114] Thus it is necessary to adjust the amount of the stannyl monomer relative to the amount of catalyst being used in order to obtain higher molecular weights. There is also the issue of weighing out an exact amount of monomer when it is a viscous oil. The best way to approach this is to obtain the weight of the empty reaction flask, then add the monomer via pipette or by solution followed by evaporation of the solvent. Finally,

weigh the flask again and base all calculations for catalyst and the other monomer off the weight of the oil in the reaction flask. Another source of error is incomplete dryness of the oil, which would again result in a stoichiometric imbalance and reduce molecular weight.

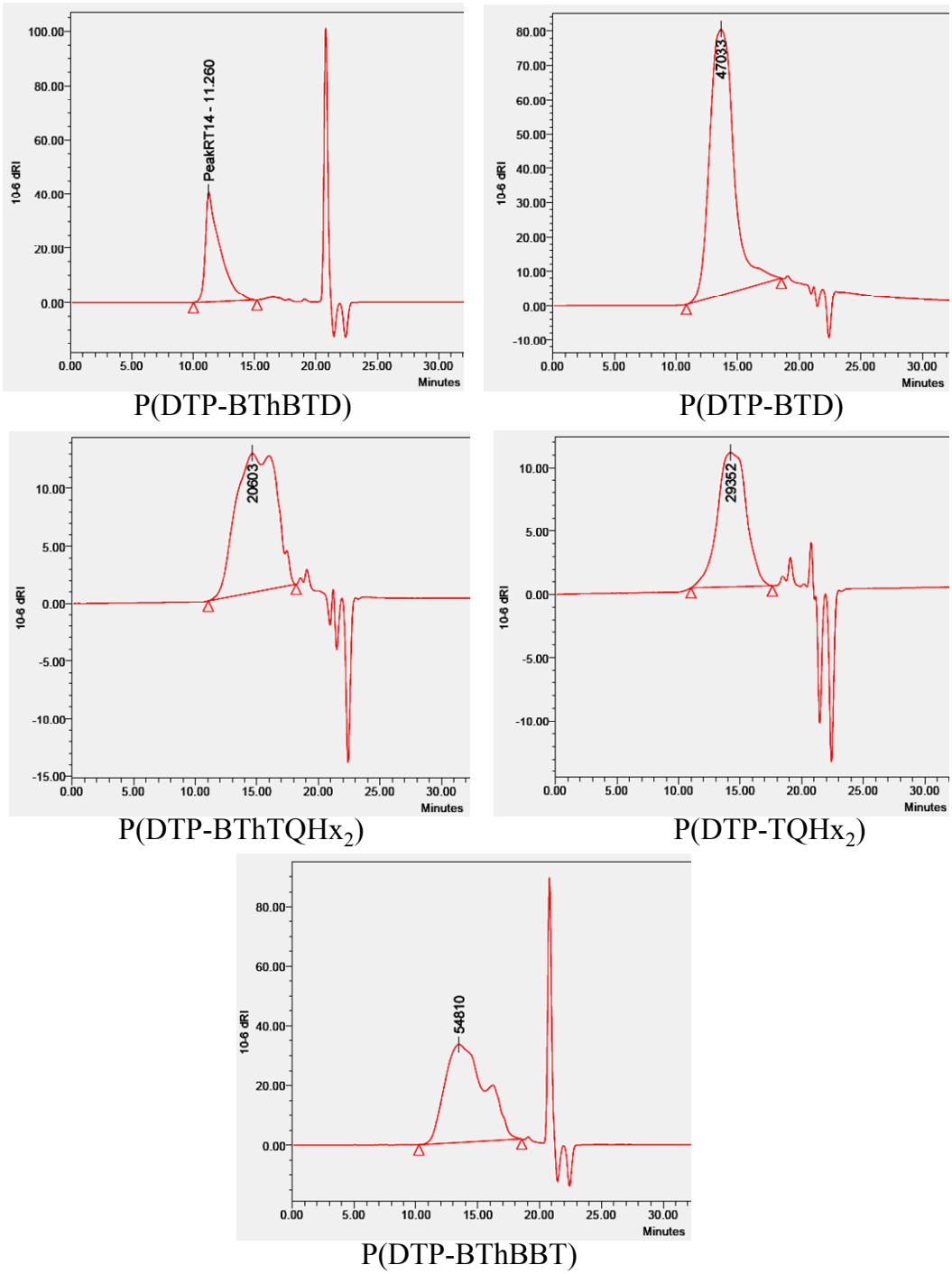

Figure 5-4. GPC chromatograms of P(DTP-acceptor) polymers.

Table 5-1. GPC estimated molecular weights (THF as mobile phase, relative to polystyrene standards) and yields of the Stille polymerization.

Polymer	M_n (g/mol)	PDI	DP	% Yield
P(DTP-BThBTD)	106,000	1.4	96	95
P(DTP-BTD)	24,000	2.2	25	95
P(DTP-BThTQHx$_2$)	9,600	2.9	7	46
P(DTP-TQHx$_2$)	19,000	2.0	16	83
P(DTP-BThBBT)	14,000	3.6	12	89

All polymers are soluble in chloroform, THF and toluene. Polymers were spray-cast from either chloroform or toluene solutions (3-4 mg/mL) onto ITO coated glass and dried under vacuum overnight. The neutral polymers were then analyzed by UV-VIS-NIR spectroscopy (Figure 5-5) and photographed (Figure 5-6). The neutral polymers all show a characteristic two band absorption, which is attributed to an ICT band that occurs at long wavelengths (low energy) and a π-π^* transition at the shorter wavelengths (higher energy) as has been discussed in the previous chapters. P(DTP-BThBTD) has a λ_{max} of 673 nm, a higher energy shoulder peak at 464 nm, and an optical band gap of 1.45 eV. Because the λ_{max} absorbs strongly through the whole visible spectrum, but tails off towards the higher energy peak with a slight dip at 500 nm, the polymer appears to be a dark greenish/blue in color. P(DTP-BTD) has a λ_{max} of 699 nm (low energy shoulder at ~1000 nm), a higher energy peak at 427 nm, and an optical band gap of 0.98 eV (the nature of this shoulder peak, possible aggregation, and the band gap will be discussed later in the chapter, but the band gap of 0.98 eV is doubtful). Due to the deeper trough just beyond 500 nm, and the ICT band and higher energy peak intensities almost being equivalent, yields an emerald green neutral polymer. P(DTP-BThTQHx$_2$) has a λ_{max} of 975 nm, an almost equally intense higher energy peak at 512 nm, and an optical band gap of 0.95 eV. Having this lower band gap means the ICT band is almost completely out of the visible spectrum leaving the higher energy peak absorption in the green part of the spectrum at 512 nm. This results in a light pink colored film. P(DTP-TQHx) has an ICT band at 1252 nm along with a less intense higher

energy peak at 476 nm. The profile of the absorption in the visible is quite similar to P(DTP-BThTQHx$_2$), but nearly as intense, resulting in a golden brown neutral polymer. The last polymer in the family, P(DTP-BThBBT) has a λ_{max} of 1219 nm and a higher energy peak with a slightly higher intensity at 533 nm. This higher energy peak absorbs strongly in the green and yellow portions of the spectrum, resulting in a light purple colored film.

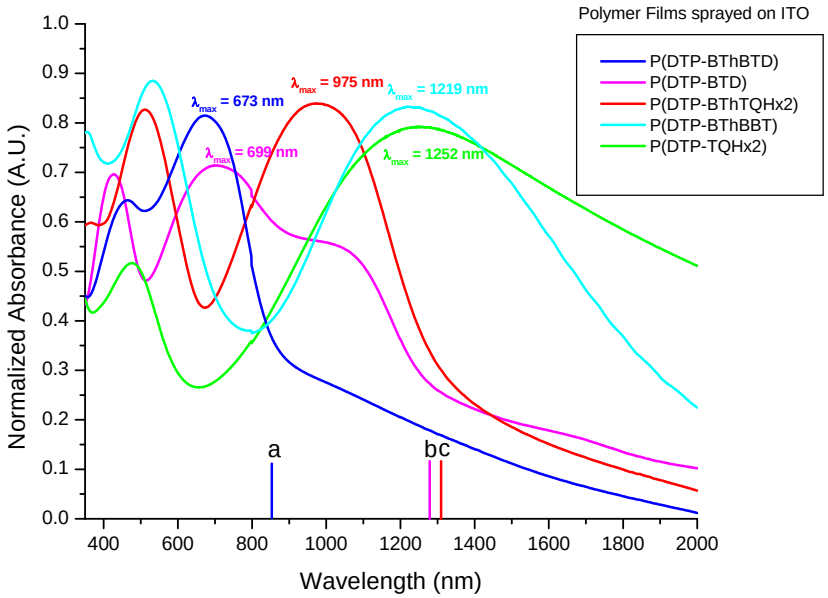

Figure 5-5. UV-VIS-NIR of neutral polymers spray cast onto ITO. (a) P(DTP-BThBTD) E_g = 1.45 eV, (b) P(DTP-BTD) E_g = 0.98 eV, (c) (PDTP-BThTQHx$_2$) E_g = 0.95 eV.

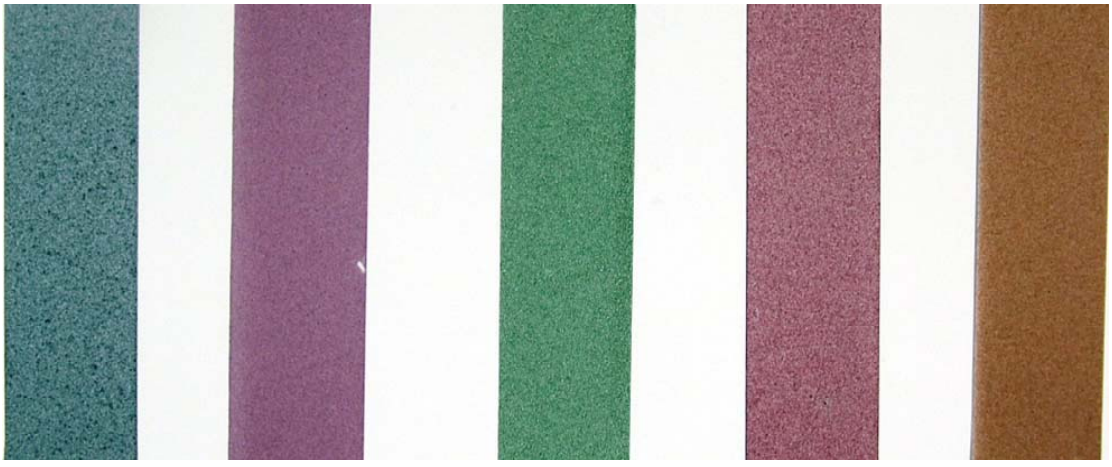

Figure 5-6. Pictures of spray cast neutral polymers on ITO. From left to right: P(DTP-BThBTD), P(BThBBT), P(DTP-BTD), P(DTP-BThTQHx2), and P(DTP-TQHx2).

There are a few trends to be observed. In staying in the bisthienyl (BTh) family of polymers, we see that in going from the weakest acceptor P(DTP-BThBTD) to the intermediate acceptor P(DTP-BThTQHx$_2$) there is a red shift in the λ_{max} by 302 nm from 673 nm to 975 nm respectively. Then, by moving on to the strongest acceptor in the family, P(DTP-BThBBT) there is a 244 nm red shift in λ_{max} relative to the intermediated acceptor P(DTP-BThTQHx$_2$) from 975 nm to 1219 nm. This red shifting of the λ_{max} suggests an increasing amount of ICT in going from BTD to TQ to BBT. This follows the trend of increased acceptor strength (due to increased amounts of electron accepting imine nitrogens) as discussed in chapter 1. The optical band gap also decreases by 0.5 eV in going from P(DTP-BThBTD) (1.45 eV) to P(DTP-BThTQHx$_2$) (0.95 eV).

Comparing the connectivity of the same core acceptor to the donor, we see that in going from P(DTP-BThTQHx2), which has a λ_{max} of 975 nm and a thiophene spacer between the DTP donor and the TQ acceptor, P(DTP-TQHx2), has a λ_{max} of 1252 nm and no thiophene spacer. Removal of the thiophene spacer has resulted in a 277 nm red shift in the λ_{max}. This demonstrates an increase in ICT between the donor and the acceptor relative to the addition of a thiophene spacer, which blue shifts the λ_{max} and the band gap. These effects have been seen before and are attributed to a decrease in the amount of ICT.[70,105,154]

For the two lowest band gap (long wavelength absorbing) polymers studied at present, P(DTP-BThBBT) and P(DTP-TQHx$_2$), it is hard to determine an optical band gap using ITO since these polymer begin to absorb well beyond the useful range of ITO. This is because ITO has a strong absorbance beyond 1600 nm, which makes baseline absorption hard to quantify for determining an onset of absorption.[53,156] By switching to single walled carbon nanotube (SWCNTs) electrodes, which are highly transparent into the IR,[124] we can overcome the

deficiencies of ITO for a more accurate determination of the optical band gap. To probe the optical band optical band gap even further, reflectance measurements on gold were performed which allows for improved characterization of the baseline deeper into the mid-IR. For these measurements, the polymers were spray-cast onto SWCNT or gold and analyzed. P(DTP-BThBBT) has a λ_{max} of 1208 nm and an estimated band gap of 0.63 eV while P(DTP-TQHx$_2$) has a λ_{max} of 1243 nm, but still has significant absorption beyond the range of the spectrophotometer, thus only a rough estimate of ~ 0.5 eV can be made for the band gap. Reflectance analysis for P(DTP-BThBBT) on gold estimates a band gap of ~ 0.5 eV. These band gaps are the lowest values for a soluble polymer to date.

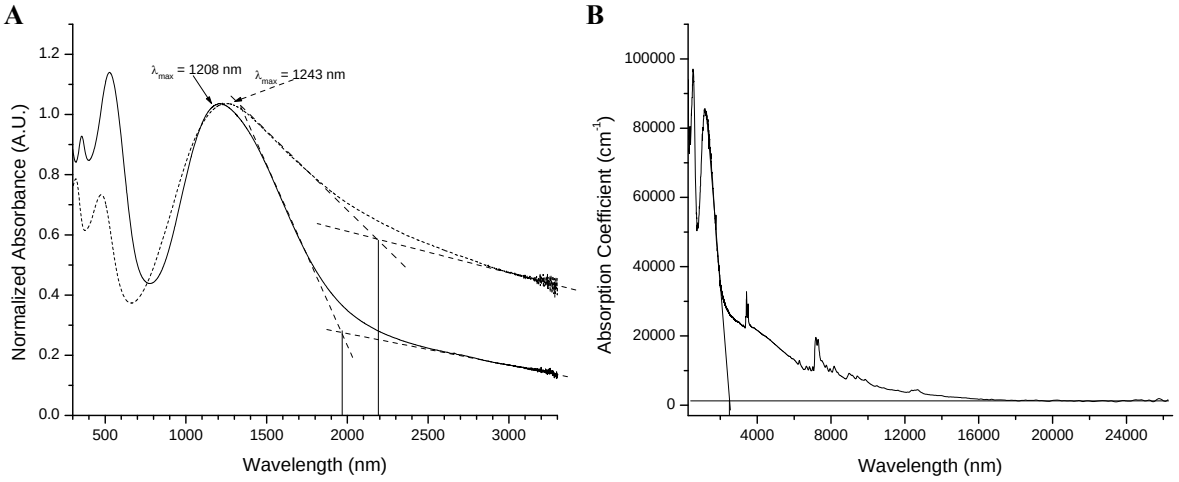

Figure 5-7. UV-VIS-NIR analysis of P(DTP-BThBBT) and P(DTP-TQHx$_2$) on SWCNTs and reflectance of P(DTP-BThBBT) on gold. A) UV-VIS-NIR of P(DTP-BThBBT) (solid) and P(DTP-TQHx$_2$) (dash) on SWCNTs. B) Reflectance spectrum of P(DTP-BThBBT) on gold.

It is important to note that throughout all of the UV-VIS-NIR spectra for this family of polymers (Figures 5-5, 5-6, and 5-7), there is a scattering effect on the base line absorption. Instead of the baseline being flat and having an absorbance at or near zero until the onset of absorption, we see a baseline that increases slowly up until the onset of absorption. It was not until doing the reflectance measurement on gold that we see a true baseline. The reason for this

is unknown, but might have to do with the resulting film morphology from spray casting. The films look speckled and rough to the eye, which might be the cause of the scattering. Further investigation is needed to look into this, such as a comparison of the spray-cast films to films made by drop casting or spin-coating.

In looking at the comparison of P(DTP-BThBTD) to P(DTP-BTD) the λ_{max} red shifts only 26 nm, from 673nm to 699 nm. In order to make a comparison of the band gaps between the two polymers, it has to be determined if the shoulder peak at 1000 nm is due to aggregation. UV-VIS-NIR of a P(DTP-BTD)/toluene polymer solution was measured over a broad range from 10 °C up to 90 °C. At 10 °C the λ_{max} is at 683 nm with the shoulder peaking at 1051 nm. Upon increasing the temperature, we see an initial decrease in the intensity of the λ_{max} followed by an increase and a blue shifting to 669 nm at 90 °C. More importantly, the shoulder peaking at 1051 nm is steadily decreasing and blue shifting over the whole temperature range, indicating aggregation. However, the shoulder does not completely disappear even at 90 °C. In order to look at this further, the solution was subjected to three consecutive 1:2 dilutions and a UV-VIS at each concentration was measured at 90 °C (Figure 5-9). Even at very dilute concentrations, it can be seen that the shoulder peak does not go away, indicating that the polymer is still aggregated and not molecularly dissolved.

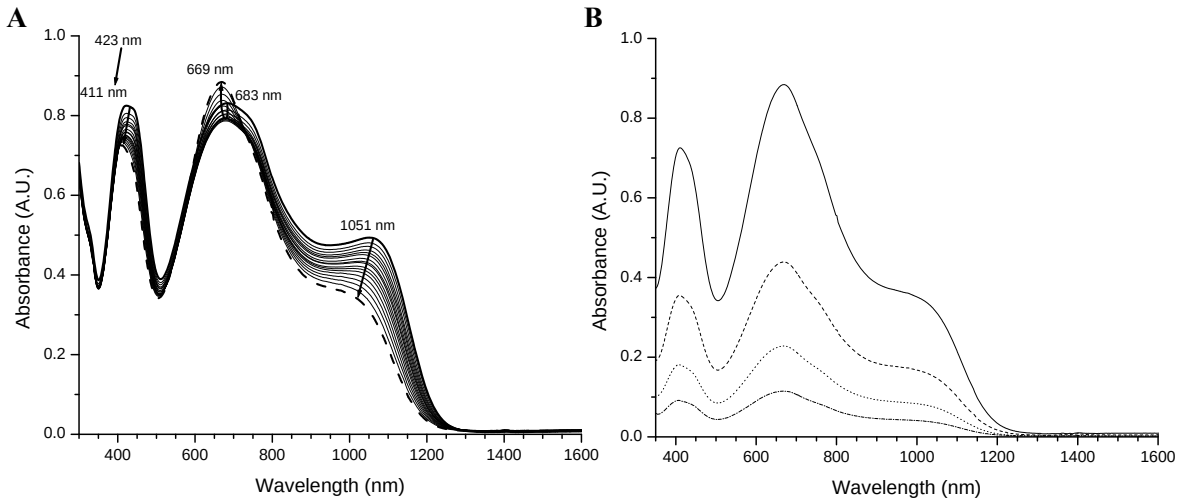

Figure 5-8. Solution thermochromism and concentration dependence UV-VIS-NIR analysis of P(DTP-BTD) in toluene. A) Thermochromism of a 5.32 x 10^{-5} M P(DTP-BTD)/toluene solution from 10 °C to 90 ºC in 5 °C increments (solid line = 10 ºC, dashed bold line = 90 ºC). B) Concentration dependence of UV-VIS-NIR spectra for a P(DTP-BTD)/toluene solution at 90 ºC (solid line = 5.32 x 10^{-5} M, dashed line = 2.66 x 10^{-5} M, dotted line = 1.33 x 10^{-5} M, and dash dot line = 6.65 x 10^{-6} M).

Electrochemical and Spectroelectrochemical Characterization

Polymer Electrochemistry

We have just talked about the very noticeable changes in the optical data for the polymers in moving from the weaker BTD, to the intermediate TQ, to the strongest BBT based acceptors. We have also noticed significant changes relative to having a thiophene spacer present or not. It is important to understand how the optical trends seen here initially will relate to the redox properties of the polymers. The polymers were analyzed by cyclic voltammetry (CV) and differential pulse voltammetry (DPV) to determine the electrochemical band gap, and the position of the HOMO/LUMO levels. Polymers were characterized as drop cast films on a platinum button working electrode in a three electrode cell with a platinum flag counter electrode and a Ag/Ag^{+} reference electrode (calibrated to Fc/Fc^{+}). All potentials reported are adjusted relative to SCE to be consistent with the literature values and the rest of this dissertation. Polymers were drop cast from either toluene or chloroform solutions onto platinum button

working electrodes. All polymers were scanned by CV until a reproducible CV was obtained (*ca.* 20-30 times). The onsets for oxidation and reduction were taken as the tangent of oxidation or reduction relative to the baseline. All experiments were carried out in 0.1 M tetrabutylammonium perchlorate/propylene carbonate (TBAP/PC) electrolyte solutions inside an argon filled dry box.

In order to better understand these systems, CV and DPV analysis of P(DTP-BThBTD) and P(DTP-BTD) can be seen in Figure 5-9. To avoid trapped charges and stability issues associated with full CV scans, separate films were used for oxidation and reduction. P(DTP-BThBTD) (Figure 5-9 A) shows a single reduction with an onset of ~ -1.3 V, however, no peak reduction potential could be obtained. The onset for oxidation is observed at 0.6 V, and increases until about 0.8 V, where upon further oxidation gives a very flat current response making it hard to determine the $E_{1/2}$. This can be attributed to the capacitive charging of the polymer film in its conducting state. If the film was not conducting, there should be a drop in the current response at potentials past the $E_{1/2}$ due to a site limited redox conductivity mechanism. This type of behavior has been studied by past group members, however, in-situ conductivity was performed to substantiate this.[38,67,68] The difference between the onset of oxidation and reduction corresponds to an electrochemical band gap of 1.9 eV, which is substantially higher than the optical band gap of 1.45 eV. A complete summary of all the onsets and HOMO/LUMO values for all of the polymers can be found in table 5-2. It can be seen that the current density observed for oxidation is almost 100 times more than is observed for reduction. This is probably due to the dense nature of the drop cast film, making it hard for the supporting electrolyte (i.e. the TBA^+) to flow in and out of the polymer film during reduction. This is a trend that can be seen throughout the CV and DPV analysis in the remainder of this chapter, however, for the non

BTD based polymers (Figures 5-10 and 5-11), the difference in currents between oxidation and reduction is only by a factor of ten.

When looking at the CV for P(DTP-BTD) (Figure 5-9 B), we see a very similar CV to that of P(DTP-BThBTD). The onset for reduction occurs at -1.25 V with no discernable peak reduction potential. Meanwhile, the oxidation produced a slightly sharper CV, where a peak oxidation at 1.04 V and an $E_{1/2}$ of 0.92 V could be observed. The onset for oxidation occurs at 0.55 V, yielding an electrochemical band gap of 1.8 eV, which is only 0.1 eV smaller relative to P(DTP-BThBTD).

DPV, which is a more sensitive technique than CV and gives more accurate onsets and sharper peaks, was attempted to resolve some of the peak potentials and increase the accuracy of the onsets. DPV analysis of P(DTP-BThBTD) (Figure 5-9 C) shows a reduction peak with an E_p at -1.47 V and an $E_{1/2}$ of -1.34 V. The reduction is quasi-reversible with adequate charge compensation on the reverse scan. This demonstrates the usefulness of DPV (increased sensitivity) relative to CV. Note the reduction onset occurs at -1.17 V and shows the typical faradaic response with no capacitive behavior. Meanwhile the oxidation is broad process and shows both faradaic and capacitive behavior, with an onset of oxidation at 0.46 V. This corresponds to a band gap of 1.65 eV, which is a lot closer to the optical band gap of 1.45 eV relative to CV. DPV analysis of P(DTP-BTD) (Figure 5-9 D) shows a very similar reduction, with an E_p at -1.45 V and an identical $E_{1/2}$ at -1.34 V. The reduction peak shows the typical faradaic response with an onset at -1.17 V. For oxidation, we see both faradaic and capacitive behavior with an onset of 0.37 V. This corresponds to an electrochemical gap of 1.54 eV. Based on the electrochemical data and the solution thermochromism, it is likely that the true band gap of P(DTP-BTD) is somewhere a lot closer to that of P(DTP-BThBTD).

Moving to the TQ family, CV analysis of P(DTP-BThTQHx$_2$) (Figure 5-10 A) shows an oxidation with an $E_{1/2}$ at 0.7 V and an onset of oxidation at 0.39 V. Again there is little current loss after the E_p, indicating capacitive behavior. The reduction CV shows two quasi-reversible reductions at an $E_{1/2}$ of -0.88 V and -1.28 V with a drop in current after the E_p, indicating a localized state. The onset for the first reduction is at -0.84 V, which is almost a 400 mV increase in reduction potential by switching from the BTD based polymers to BThTQHx$_2$ and can be attributed to the increased acceptor strength. The electrochemical band gap by CV is determined to be about 1.43 eV. This is still significantly higher than the optical band gap of ~ 0.95 eV.

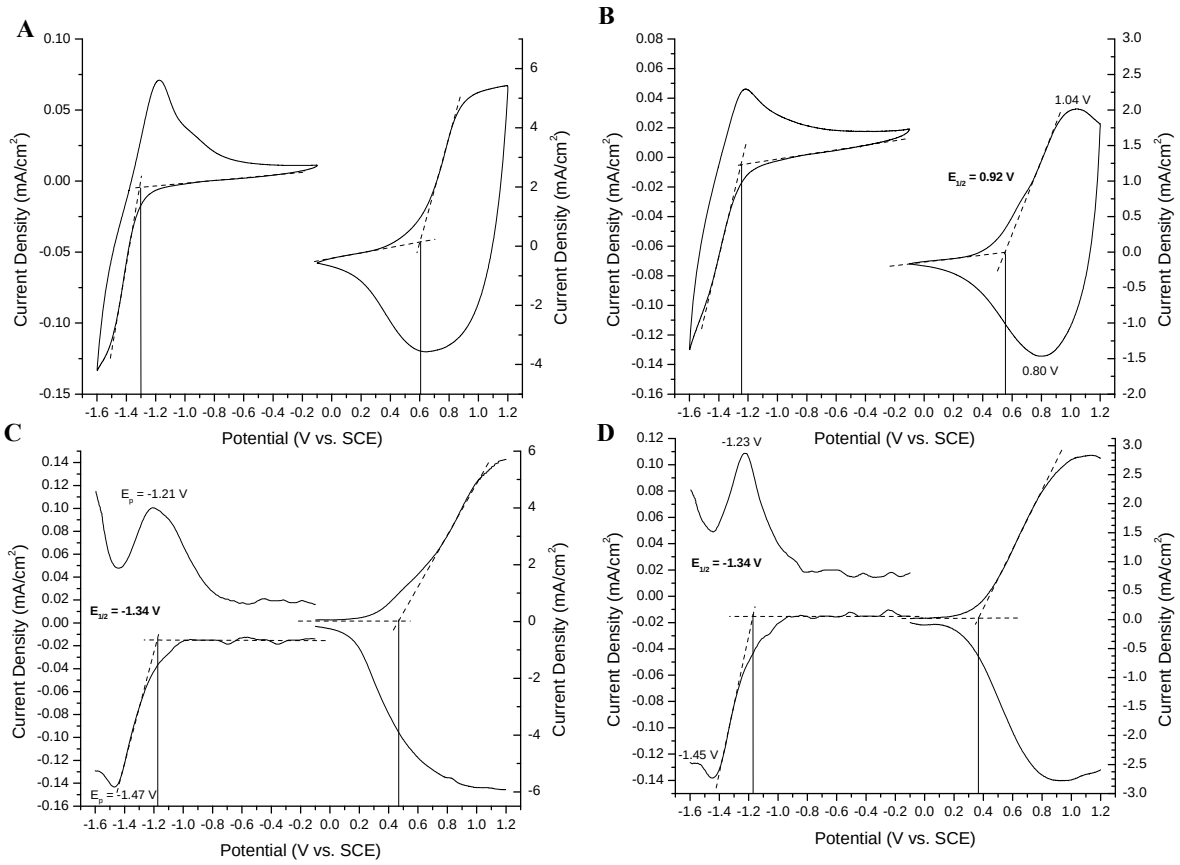

Figure 5-9. CV (scan rate = 25 mV/s) and DPV (step size of 2 mV and step time of 0.1 seconds) of P(DTP-BThBTD) and P(DTP-BTD) on a Pt button working electrode in 0.1 M TBAP-PC electrolyte solution. A) CV of P(DTP-BThBTD). B) CV of P(DTP-BTD). C) DPV of P(DTP-BThBTD). D) DPV of P(DTP-BTD).

Analysis of P(DTP-TQHx$_2$) by CV (Figure 10 B) shows some very interesting behavior. Only the first reduction is seen by CV. There are no recognizable peaks associated with the second reduction. This is unexpected. Perhaps the film is too dense to allow for the movement of the electrolyte in for the second reduction. Or maybe it might be a stability issue. Since the peaks are not well defined, only the onset could be attained, which is -0.70 V for reduction. The oxidation P(DTP-TQHx$_2$) shows an onset at 0.44 V, an $E_{1/2}$ at 0.79 V, and an E_p at 0.98 V. Upon further oxidizing potentials there is little current loss indicating some capacitive behavior. The electrochemical band gap is estimated to be 1.16 eV. Again, this is much higher than the optical band gap.

DPV analysis of P(DTP-BThTQHx$_2$) (Figure 10 C) shows two quasi-reversible reductions at $E_{1/2}$ = -0.86 and -1.30 V, with a large decrease in current after going to potentials increasingly cathodic of the $E_{1/2}$ implicating a localized charge state. The oxidation of the polymer shows some capacitive behavior beyond the $E_{1/2}$. The onset for reduction is located at -0.7 V, meanwhile the onset of oxidation occurs at 0.39 V, giving an electrochemical band gap of 1.09 eV. This value is fairly close to optical band gap of 0.95 eV.

Application of cathodic potentials by DPV to P(DTP-TQHx$_2$) (Figure 10 D) shows a quasi-reversible reduction at $E_{1/2}$ = -0.84 V with an onset at -0.65 V. This is in fairly good agreement to the bisthienyl derivative, however, unlike P(DTP-BThTQHx$_2$), the onset of oxidation is seen at 0.28 V, yielding an electrochemical band gap of 0.93 eV, which is much higher than the estimated 0.5 eV optical band gap.

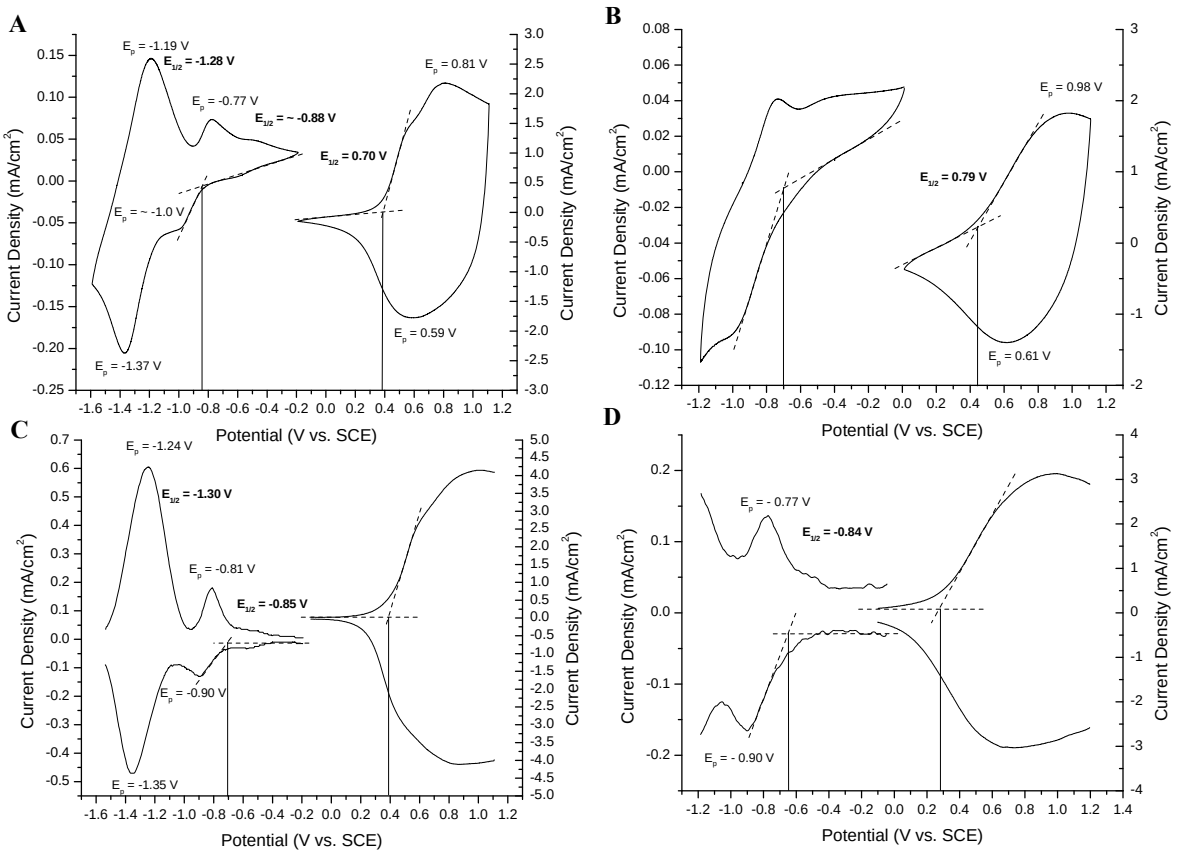

Figure 5-10. CV (scan rate = 50 mV/s) and DPV (step size of 2 mV and step time of 0.1 seconds) of P(DTP-BThTQHx$_2$) and P(DTP-TQHx$_2$) on a Pt button working electrode in 0.1 M TBAP-PC electrolyte solution. A) CV of P(DTP-BThTQHx$_2$). B) CV of P(DTP-TQHx$_2$). C) DPV of P(DTP-BThTQHx$_2$). D) DPV of P(DTP-TQHx$_2$).

Finally, P(DTP-BThBBT) was analyzed by CV and DVP. CV analysis (Figure 5-11 A) shows two quasi-reversible reductions at $E_{1/2}$ = -0.69 V and -1.08 V, with an onset for the first reduction at -0.51 V. The onset for oxidation was at 0.45 V with the oxidation having a capacitive nature beyond the E_p. DPV analysis (Figure 5-11 B) also shows two quasi-reversible reductions, at $E_{1/2}$ of -0.57 V and -1.08 V. The onset for the first reduction occurs at -0.39 V while the onset for oxidation occurs at 0.26 V, giving an electrochemical band gap of 0.65 eV. This estimate is very close to the optical band gap of 0.5 to 0.6 eV.

The general trend shown in going from the weaker BTD based acceptors to the stronger TQ and BBT based acceptors is the decrease in the HOMO/LUMO gap by a significant lowering

of the LUMO value relative to the HOMO level. When comparing the polymers, the electrochemical data estimates a larger band gap than is determined optically.

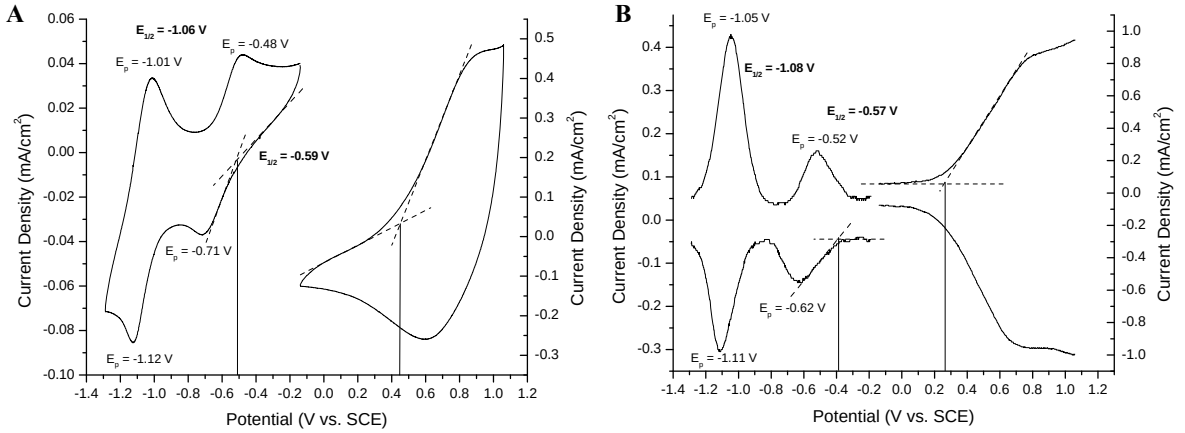

Figure 5-11. CV (scan rate = 50 mV/s) and DPV (step size of 2 mV and step time of 0.1 seconds) of P(DTP-BThBBT) on a Pt button working electrode in 0.1 M TBAP-PC electrolyte solution. A) CV of P(DTP-BThBBT). B) DPV of P(DTP-BThBBT).

Table 5-2. Summary of electrochemical data for P(DTP-Acceptors) investigated. All onset values are Volts vs. SCE. All HOMO/LUMO values were calculated by $E_{(VAC)} = E_{(SCE)} + 4.7$.[37] (* = aggregate).

Acceptor	E_{ox} (CV) onset	HOMO (CV) eV	E_{red} (CV) onset	LUMO (CV) eV	E_{ox} (DPV) onset	HOMO (DPV) eV	E_{red} (DPV) onset	LUMO (DPV) eV	E_g (optical)
BThBTD	0.6	5.3	-1.3	3.40	0.46	5.16	-1.17	3.53	1.45
BTD	0.55	5.25	-1.25	3.45	0.37	5.07	-1.17	3.53	0.98*
BThTQHx$_2$	0.39	5.09	-0.84	3.86	0.39	5.09	-0.70	4.00	0.95
TQHx$_2$	0.44	5.14	-0.70	4.00	0.28	4.98	-0.65	4.05	~ 0.5
BThBBT	0.45	5.15	-0.51	4.19	0.26	4.96	-0.39	4.31	0.5-0.6

Polymer Spectroelectrochemistry

The technique of spectroelectrochemistry was used to probe the electro-optical properties of this family of polymers. Polymer films were spray cast from chloroform or toluene solutions on to ITO coated glass working electrodes. The polymer films were then placed in a cuvette with a platinum wire counter electrode and a silver wire pseudo reference electrode (calibrated to

the Fc/Fc^+ redox couple and converted relative to SCE) and switched by repetitive potential scanning from a neutral potential to the desired charged state in a 0.1 M TBAP/PC solution until a reproducible CV was seen before spectroelectrochemical measurements were performed. The polymers were analyzed in both oxidation and reduction with reductive spectroelectrochemistry performed in an argon filled glove box using a Stellarnet photodiode array detector.

Oxidative spectroelectrochemistry was performed on P(DTP-BThBTD) (Figure 5-12 A). As discussed in Chapters 3 and 4, the long wavelength absorption in these donor-acceptor polymers is due to intramolecular charge transfer (CT), while the high energy peak is considered to be the π-π* transition (π-transition). For neutral P(DTP-BThBTD), we see a strong CT band at 660 nm that tails off through the visible region down to the π-transition band (shoulder) at 473 nm, which then falls off abruptly. This leaves the green and blue portions of the spectrum partially open resulting in a dark greenish/blue neutral film. The optical band gap is determined by the onset of absorption in the neutral polymer, which for P(DTP-BThBTD) occurs at ~ 870 nm, or 1.4 eV. Upon oxidation, the bleaching of both neutral transitions starts to occur around 0.5 V, which coincides nicely with the CV oxidation data. As the polymer is oxidized, polaron and bipolaron charge carriers are formed, resulting in an intermediate peak around 800 nm along with a low energy peak at a wavelength beyond 1600 nm. Upon full oxidation there is an intense charge carrier band 1600 nm, which is indicative of the polymer being in a more conducting state. The band then tails off as it passes into and all the way through the visible region, resulting in a more transmissive grey blue film.

Upon reduction of P(DTP-BThBTD) (Figure 5-12 B), a decrease in the CT band at applied potentials of -1.2 to -1.3 V is observed, which agrees well with the electrochemical data for reduction. At intermediate reduction levels there is the bleaching of the CT band and the

development of a broad absorption across the NIR and two new absorption bands at 500 nm and 800 nm, which upon further reduction disappear with the formation of a small band at 620 nm and an intense band in the NIR around 1300 nm. It has been demonstrated in the past with in the Reynolds group (PBEDOT-PyrPyr-Ph_2 in 0.1 M TBAP-ACN/DCM) that the formation of charge carriers bands in the NIR upon reduction were indeed n-type doping. This was confirmed with in-situ conductivity measurements.[67,68] In the reduced state we see a light purple colored film, that is indicative of n-type doping due to the strong charge carrier band formation in the NIR, however in-situ conductivity would have to be measured to confirm these suspicions.

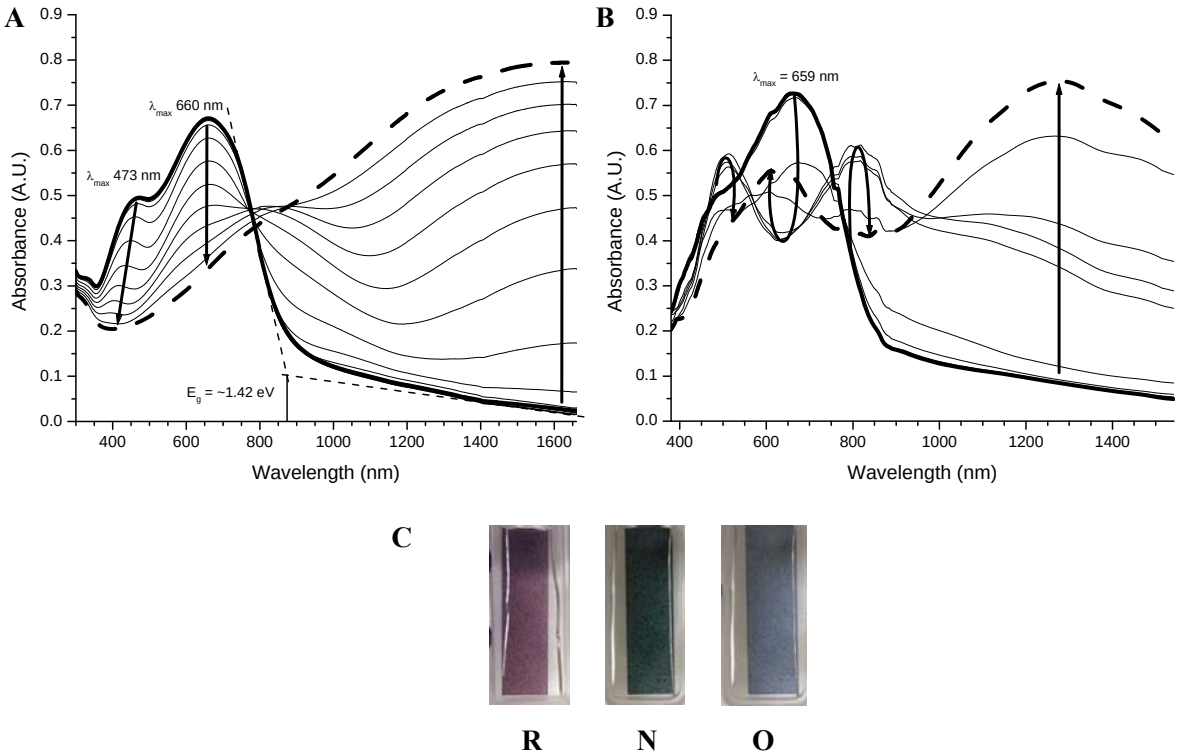

Figure 5-12. Spectroelectochemistry of P(DTP-BThBTD) in 0.1 M TBAP/PC and the associated colored states. A) Oxidative switching of a film from -0.16 V (bold) to 1.24 V (dashed) vs. SCE in 100 mV increments. B) Reductive switching of a film from -0.92 V (bold) to -1.72 V (dashed) vs. SCE in 100 mV increments. C) Pictures in the reduced (R), neutral (N) and oxidized (O) states.

Sticking with the same acceptor, but removing the thiophene spacer, oxidative spectroelectrochemistry was performed on P(DTP-BTD) (Figure 5-13 A). In the neutral polymer

the CT band is located at 676 nm (with a shoulder peak at 1020 nm attributed to aggregation), while the π transition band is at 427 nm and of equal intensity. The nice trough over the 500 nm region in the neutral state results in a deep emerald green neutral polymer. In comparison to P(DTP-BThBTD), the π-transition band in P(DTP-BTD) is blue shifted 46 nm and is now of equal intensity to the CT band, while the CT band is only slightly red shifted, but broadened by the aggregation peak. Upon oxidation there is a disappearance of the shoulder at 1020 nm with a slight red shifting of the CT band. Upon full oxidation there the charge carrier peaks can be seen at ~ 800 nm and ~1600 nm, while the π-transition band is bleached, resulting in a slightly more transparent grey/green film.

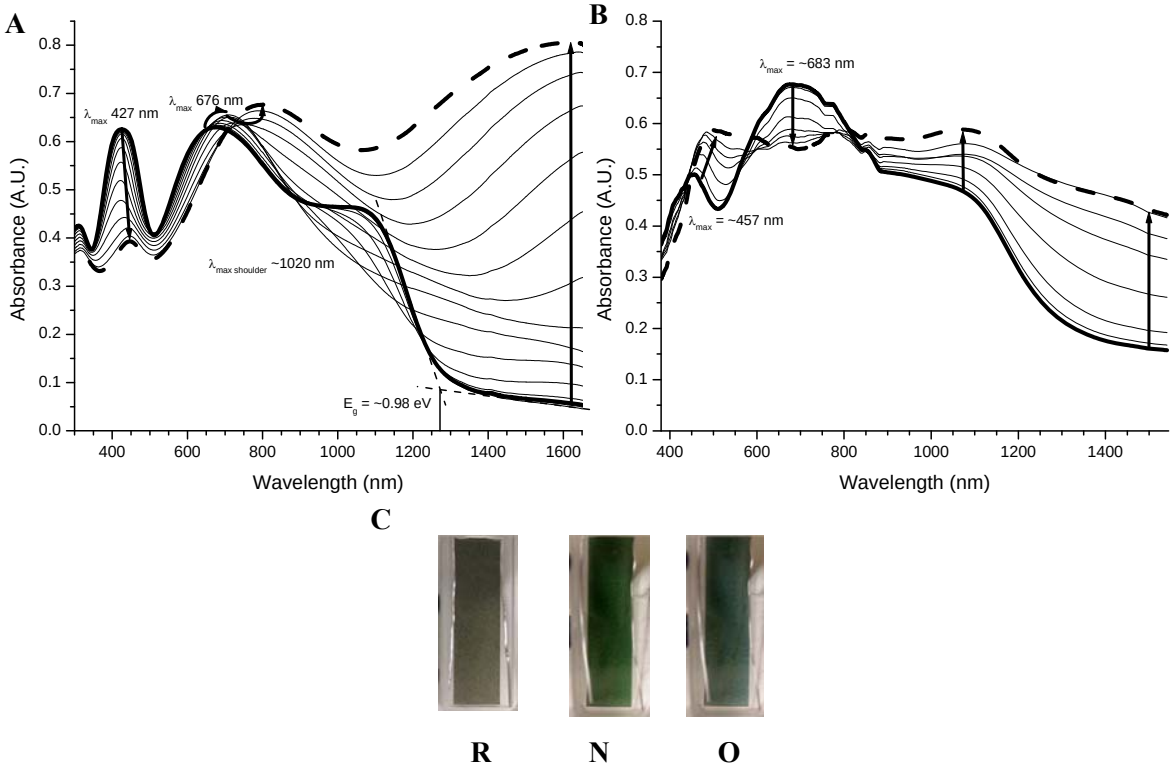

Figure 5-13. Spectroelectochemistry of P(DTP-BTD) in 0.1 M TBAP/PC and the associated colored states. A) Oxidative switching of a film from -0.31 V (bold) to 1.09 V (dashed) vs. SCE in 100 mV increments. B) Reductive switching of a film from -1.16 V (bold) to -1.86 V (dashed) vs. SCE in 100 mV increments. C) Pictures in the reduced (R), neutral (N) and oxidized (O) states.

Upon reduction of P(DTP-BTD) (Figure 5-13 B), a slight decrease in the CT band is observed, while concurrently the π-transition band and the aggregate peak are increasing. There is also the development of a broad charge carrier absorption across the NIR, peaking around 1070 nm, but the intensity is not nearly as strong as it was in P(DTP-BThBTD). This results in a relatively flat absorption across the visible region down to about 500 nm, where the absorption falls off. This yields a dark greenish grey polymer in the reduced state.

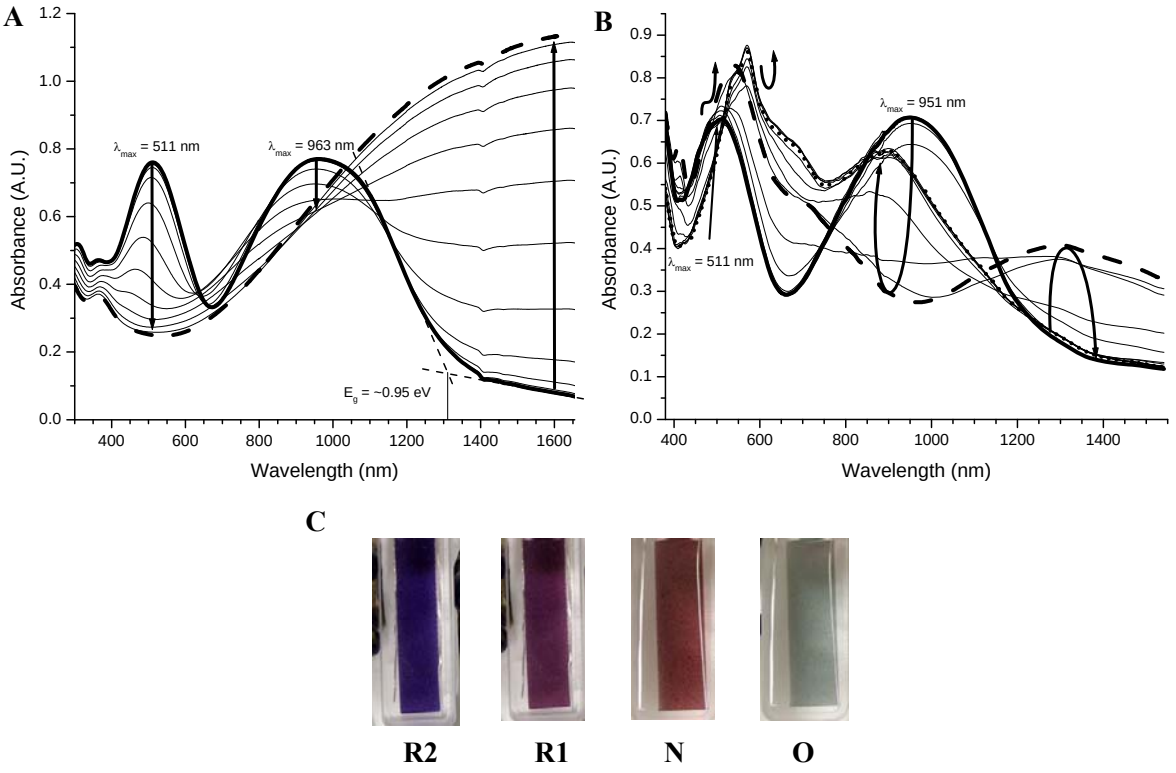

Figure 5-14. Spectroelectochemistry of P(DTP-BThTQHx$_2$) in 0.1 M TBAP/PC and the associated colored states. A) Oxidative switching of a film from -0.33 V (bold) to 1.07 V (dashed) vs. SCE in 100 mV increments. B) Reductive switching of a film from -0.54 V (bold) to -0.85 V (dashed) to -1.94 V (Dotted) vs. SCE in 100 mV increments. C) Pictures in the 2nd reduced (R2), 1st reduced (R1), neutral (N) and oxidized (O) states.

In switching to the stronger TQ based acceptor, the CT band has red shifted about 303 nm relative to P(DTP-BThBTD), while the π-transition band has red shifted 38 nm. Both bands (511 nm and 963 nm) are approximately the same intensity, with the gap between them centered

at 670 nm. This results in a light maroon colored neutral film. Upon oxidation of P(DTP-BThTQHx$_2$) (Figure 5-14 A), spectral changes start to occur at about +0.4 V, which corresponds well to the onset of oxidation from the electrochemistry data. As the polymer becomes oxidized the CT band and the π-transition band bleach completely, with formation of an intense charge carrier band that tails off through the near IR, with minimal absorption through the visible region. This results in a highly transparent, light grey colored film in the p-doped state.

Application of reducing potentials to P(DTP-BThTQHx$_2$) (Figure 5-14 B) through the first reduced state, results in a bleaching of the CT band with a concurrent red shift and increase in absorbance of the π-transition band (540 nm). There is also the formation of a possible charge carrier absorption band at 1300 nm, however, it is not that intense, indicating a more localized state. The resulting increased π-transition band declines very quickly through the blue and violet part of the spectrum while it tails off more slowly through the visible part of the spectrum into the NIR. This results in a bright deep purple colored film. Upon reaching the second reduction, the NIR band has completely bleached while the high energy band has red shifted and increased in intensity (570 nm). The formation of a new band at 900 nm was also observed. This results in a brilliant indigo colored film. With the lack of any intense bands in the NIR, it is likely that these reduced states are highly localized on the acceptor.

Examination of P(DTP-TQHx$_2$) allows one to probe the effect of removing the thiophene spacer. For Neutral P(DTP-TQHx$_2$), we see a 34 nm blue shift in the π-transition band (477 nm) along with a 276 nm red shift in the CT band (1239 nm) relative to P(DTP-BThTQHx$_2$) (Figure 5-15 A). The large shift in the CT band and increased intensity relative to the π-transition band can be attributed to the increased donor-acceptor interactions due to the removal of the thiophene spacer as discussed in the beginning of this chapter. With the π-transition band being the only

major absorption in the visible part of the spectrum, this leaves a gap from the yellow through the red parts in the visible spectrum, resulting in a golden brown neutral polymer. Upon oxidation there is a bleaching of the π-transition band and an increase in absorption in the NIR due to charge carrier formation. The new charge carrier band also tails back into the red portion of the visible spectrum, resulting a light olive green oxidized state.

Upon reduction (Figure 5-15 B) there is a large increase and red shift in the π-transition band out to 520 nm. Meanwhile there is a decrease in the CT band with the formation of a new, less intense band just past 1550 nm. This results in a dark brown colored film in the reduced state.

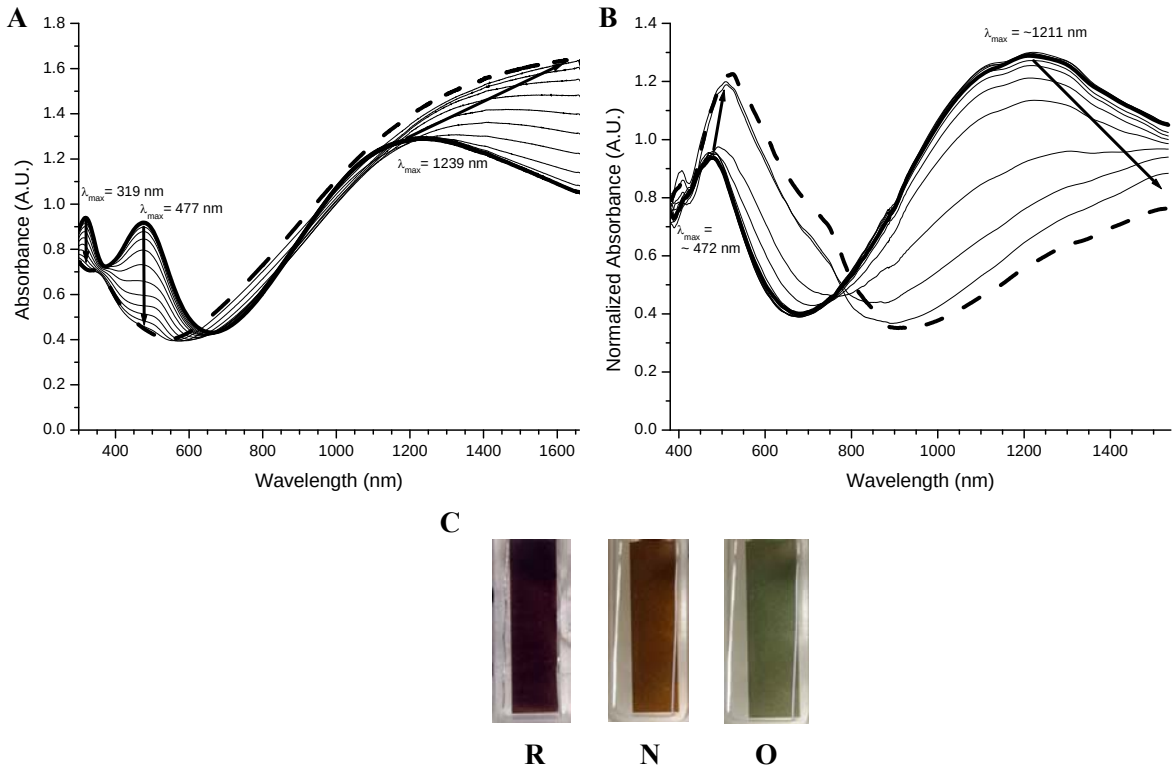

Figure 5-15. Spectroelectochemistry of P(DTP-TQHx$_2$) in 0.1 M TBAP/PC and the associated colored states. A) Oxidative switching of a film from -0.25 V (bold) to 1.15 V (dashed) vs. SCE in 100 mV increments. B) Reductive switching of a film from -0.21 V (bold) to -1.31 V vs. SCE in 100 mV increments. C) Pictures in the reduced (R), neutral (N) and oxidized (O) states.

To complete the series of the variable acceptor DA polymers, P(DTP-BThBBT), containing the strongest acceptor in the family, was analyzed. In the neutral polymer, the only major absorption is from the π-transition at 529 nm, which is 18 nm red shifted relative to the π-transition in P(DTP-BThTQHx$_2$). The CT band is sifted well into the NIR at 1231 nm, which is 276 nm beyond that for P(DTP-BThTQHx$_2$). A strong red shift in the CT band results from the use of the much stronger BBT based acceptor. The visible absorption of the π-transition band in neutral P(DTP-BThBBT) at 529 nm results in a purple/maroon colored film (Figure 5-16). Upon application of oxidizing potentials (Figure 5-16 A), there is a bleaching of the π-transition along with the concurrent formation of a highly intense charge carrier band in the NIR peaking around 1400 nm. As this intense band grows in, it starts to broaden and expand into the visible portion of spectrum with the tail reaching a minimum in the blue portion of the spectrum. This results in more transmissive grey blue film in the oxidized state.

Upon application of cathodic potentials to the polymer through the first reduction (Figure 5-16 B, dashed bold line), we see a red shift (11 nm) an increase in intensity of the π-transition out to 540 nm along with the development of a slight shoulder peak around 700 nm. While this is happening, the CT band is starting to bleach and there is the formation of a smaller less intense band at ~ 1450 nm. While this could be a true n-doped state, the lack of intensity of the new band suggests it might be more of a localized state. With the π-transition absorbing most of the visible portion of the spectrum, tailing off in both the purple and the red portions of the spectrum, the polymer becomes bright purple in color. In moving on to the second reduction, the peak that was developing at 700 nm has now red shifted out to ~ 775 nm and is now just as intense as the π-transition. This increase occurred at the expense of the complete bleaching of

the low energy absorption that formed during the first reduction, and results in a brighter blue/purple film.

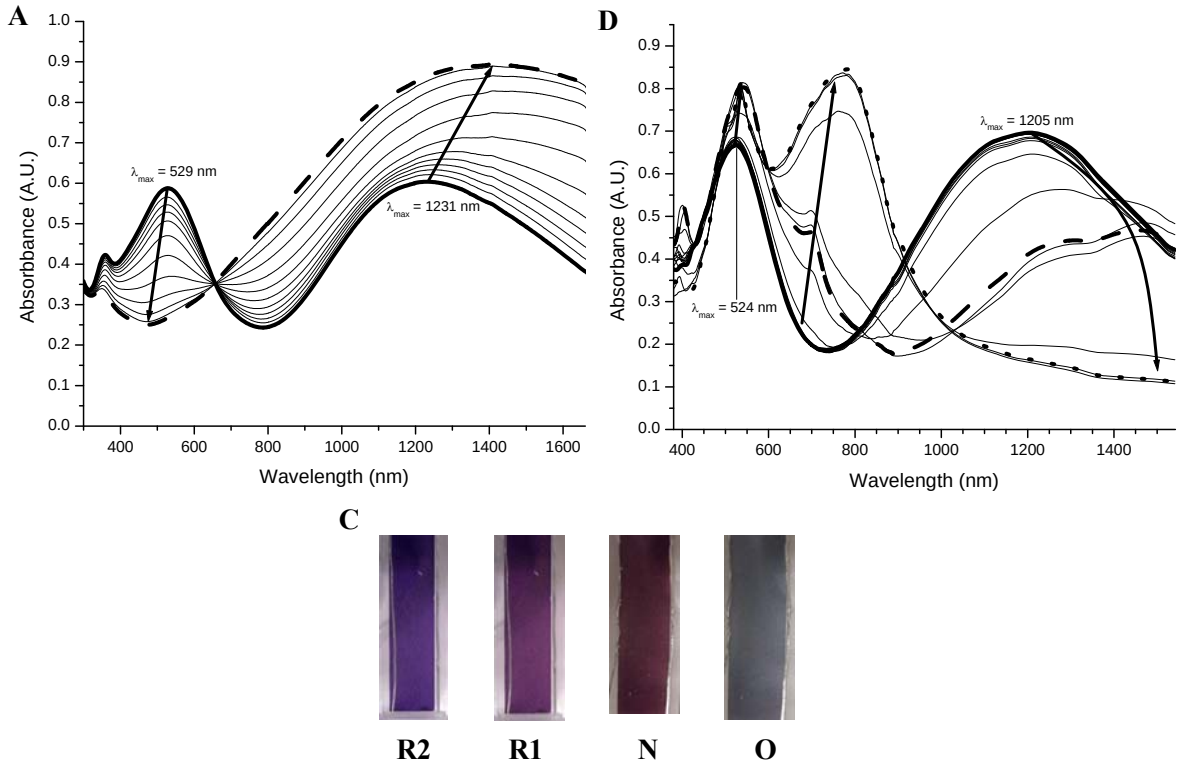

Figure 5-16. Spectroelectochemistry of P(DTP-BThBBT) in 0.1 M TBAP/PC and the associated colored states. A) Oxidative switching of a film from -0.13 V (bold) to 0.97 V (dash) vs. SCE in 100 mV increments. B) Reductive switching of a film from 0.05 V (bold) to -1.13 V (dashed) to -1.45 V (dotted) vs. SCE in 100 mV increments. C) Pictures in the 2nd reduced (R2), 1st reduced (R1), neutral (N) and oxidized (O) states.

Conclusions

When looking at all of the polymers in this family, a general trend upon oxidation is that the polymers go from a nicely colored neutral state to a more transparent oxidized state. When looking at the polymers with the thiophene spacer, the trend is to a more transparent grey to grey blue color while the others go to a green to blue/green. We also see that the two bisthienyl polymers capable of two reductions both go to rich purple colors upon the first reduction and then to deeply purple/blue colors upon the second reduction. This opens up the opportunity for making new copolymers containing two or more of these acceptors to control the color. Perhaps

an easier option is to make electrochromic devices with various blends of these polymers to ultimately control the final colors.

Depending on the desired properties for a certain material, we have demonstrated that these acceptors can tune the CT band absorption over ~ 600 nm window from 650 nm to 1250 nm. The interesting note here is the removal of the thiophene spacer from P(DTP-BThTQHx$_2$) resulted in a ~275 nm red shift in the CT band. The next course of action for continuing towards lower gap systems would be to make P(DTP-BBT). In terms of fine control over the absorption spectra and the band gap, the addition of more thiophene spacers could be used to make minor adjustments.

We have also demonstrated the use of the Stille methodology for making soluble donor-acceptor polymers with the ability to reach very high molecular weights in excess of 100 K number average molecular weight (P(DTP-BThBTD)). When the polymers are oxidized, they all show charge carrier band formation into the NIR or farther with increased intensity indicating delocalized bands. Upon reduction, we see a different story. For P(DTP-BThBTD) we see an intense charge carrier band in the NIR upon reduction, indicating delocalized bands indicative of n-type doping. This is the only polymer in the family that shows a more intense band upon reduction relative to the neutral spectrum. All of the other polymers show possible charge carrier band formation in the NIR upon first reduction, however, the intensity is much weaker than the neutral spectrum indicating that these bands are probably more localized on the acceptors. For the P(DTP-BThTQHx$_2$) and P(DTP-BThBBT), upon reaching the second reduction, there are no charge carrier bands seen in the NIR with only peaks in the visible region, indicating the charges are localized on the acceptors. These polymers are not a truly n-type doped system in this state.

Experimental

4,9-dibromo-6,7-dihexyl-[1,2,5]thiadiazolo[3,4-*g*]quinoxaline: 4,7-dibromobenzo[c][1,2,5]thiadiazole-5,6-diamine[174] (0.257 g, 0.793 mmol) was added to a flame dried 100 mL round bottom flask followed by 30 mL of degassed acetic acid. Next tetradecane-7,8-dione[139] was added and the solution was stirred overnight under argon in the dark. Then water (~ 50 mL) was added and the solution was extracted with dichloromethane. The organic layer was then washed with water, sodium bicarbonate, and water followed by drying over magnesium sulfate. The solvent was removed under reduced pressure and the crude solid was purified by column chromatography (3:2 hexanes:dichloromethane) yielding 0.375 g (92 %) of an orange solid. ^{1}H NMR (300 MHz, $CDCl_3$) δ 0.93 (t, 6H), 1.25-1.55 (m, 12H), 1.99 (p, 4H), 3.10 (t, 4H); ^{13}C NMR (75 MHz, $CDCl_3$) δ 14.18, 22.75, 26.64, 29.20, 31.89, 35.14, 35.23, 113.26, 137.78, 151.37, 160.28. HRMS Calcd. for $C_{20}H_{26}Br_2N_4S$ (M^+) 512.0245 Found 512.0190; Anal. Calcd. for $C_{20}H_{26}Br_2N_4S$: C, 46.71; H, 5.10; Br, 31.07; N, 10.89; S, 6.23. Found: C, 47.05; H, 5.15; N, 10.61.

4,9-bis(5-bromothiophen-2-yl-)-6,7-dihexyl-[1,2,5]thiadiazolo[3,4-*g*]quinoxaline: 6,7-di-hexyl-4,9-di(thiophen-2yl)-[1,2,5]thiadiazolo[3,4-*g*]quinoxaline (1.09 g, 2.09 mmol) is dissolved in 170 ml DMF and NBS (783 mg, 4.39 mmol) are added in the absence of light. The solution is stirred for 10 h, then methanol is added and the precipitate is filtered off, washed with cold methanol and dried, to obtain 1.08 g (76 %) of a blue solid. Mp: 140 °C -143 °C; Anal. Calcd. for $C_{28}H_{30}Br_2N_4S_3$: C 49.56, H 4.46, N 8.26 found C 49.64, H 4.44, N 8.23; HRMS (ESI TOF) *m/z* Calcd. for $C_{28}H_{30}Br_2N_4S_3$: 676.0049 (M^+) found 675.9999 (M^+); ^{1}H NMR ($C_2D_2Cl_4$): δ 8.82 (d, 2H), 7.23 (d, 2H), 3.01 (t, 4H), 2.02 (t, 4H), 1.60-1.36 (m, 12H) 0.97 (t, 6H); ^{13}C NMR

($C_2D_2Cl_4$): δ 159.27, 152.37, 139.11, 136.09, 134.63, 131.13, 121.93, 121.45, 36.99, 33.31, 30.80, 29.59, 24.09, 15.66.

***N*-(3,4,5-Tri(*n*-dodecyloxy)phenyl)-2,6-dithieno[3,2-*b*:2',3'-*d*]pyrrole (synthesized by Daniel Sweat and Susan Odom):** To an oven-dried 100 mL round-bottomed flask cooled under nitrogen was added dry deoxygenated toluene (4 mL), 3,3'-dibromo-2,2'-bithiophene (0.21 g, 0.65 mmol), and 3,4,5-tri(*n*-dodecyloxyphenyl)aniline (0.45 g, 0.70 mmol). A solution of Pd_2dba_3 (0.030 g, 0.0## mmol) and P^tBu_3 (0.3 mL, 10% solution in hexane) in dry deoxygenated toluene (2 mL) was added to the reaction mixture, followed by sodium *tert*-butoxide (0.175 g, 1.82 mmol). The reaction flask was assembled in a microwave reactor with a reflux condenser, and was heated at 90 Watts for 6 minutes (T_{max} = 57 ºC), then for 19 minutes at 95 Watts (T_{max} = 82 ºC), which was followed by an additional round of heating at 100 Watts for 20 minutes (T_{max} = 110 ºC). The reaction mixture was run through a short pad of silica gel, eluting with hexanes / dichloromethane (9:1, then 4:1), and after concentration by rotary evaporation, the product was further purified by column chromatography on silica gel using hexanes / dichloromethane (9:1 gradually increasing the ration to 1:1). After concentration by rotary evaporation, a pale yellow oil was obtained, which was precipitated from acetone to give the title compound as an off-white powder (0.38 g, 59%). ^{1}H NMR (500 MHz, CD_2Cl_2) δ 7.20 (d, J = 5.0 Hz, 2H), 7.18 (d, J = 5.0 Hz, 2H), 6.76 (s, 2H), 3.98 (m, 6H), 1.84 (quintet, J = 7.0 Hz, 4H), 1.75 (quintet, J = 7.0 Hz, 2H), 1.49 (m, 6H), 1.28 (m, 24H), 0.89 (m, 9H). ^{13}C NMR (75 MHz, CD_2Cl_2) δ 154.1, 144.4, 136.5, 135.4, 123.7, 116.7, 112.6, 101.7, 73.9, 69.6, 32.5, 32.1, 30.9, 30.3, 30.2 (2 peaks, 0.6 ppm apart), 29.9 (2 peaks, 0.04 ppm apart), 26.7, 26.6, 23.2 (2 peaks, 0.05 ppm apart), 14.4, 9 peaks missing in alkyl region, presumably due to overlap. EI-MS (*m/z*): 807.6. Anal. calcd. for $C_{50}H_{81}NS_2O_3$: C, 74.29; H, 10.10; N, 1.73. Found: C, 74.51; H, 10.19; N, 1.80.

2,6-bis(tributylstannyl)-N-(3,4,5-tris(dodecyloxy)phenyl)-dithieno[3,2-b:2',3'-*d*]pyrrole (Xuan): A deoxygenated solution of N-(3,4,5-tris(dodecyloxy)phenyl)-dithieno[3,2-*b*:2',3'-*d*]pyrrole(0.34 g, 0.42 mmol) in THF (200 mL) was cooled to –78 ^{o}C, ^{t}BuLi (1.5 mL, 2.4 mmol, 1.7 M in heptane) solution was added, and the reaction allowed to warm to room temperature and stirred for 1 h, before cooling to –78 ^{o}C again; $^{n}Bu_3SnCl$ (0.25 mL, 0.8 mmol) was then added and the reaction allowed to warm to room temperature and stir for 3 h. The reaction was quenched with addition of water and extracted with dichloromethane; the extracts dried over $MgSO_4$, concentrated under reduced pressure and stirred with NEt_3 (50 mL) for 2 h. After removal of the volatiles the residue was purified by column chromatography (SiO_2, pretreated with NEt_3, eluting with hexanes), after which a pale yellow oil (0.75 g, 66 %) was obtained.^{1}H NMR (400 MHz, CD_2Cl_2, δ): 7.18 (t, J = 7 Hz, 2H), 6.76(s, 2H), 4.10-3.98 (m, 6H), 1.90-1.80(m, 6H), 1.70-1.12 (m, 80 H), 0.91 (t, J = 7.2 Hz, 27H). ^{13}C-NMR (400 MHz, $CDCl_3$, δ): 153.5, 146.7, 135.7 *(two peaks separated by ca. 5.0 Hz)*, 135.5, 122.1, 119.2, 101.5, 73.7, 69.1, 32.0*(two peaks separated by ca. 2.3 Hz)*, 30.5, 29.9, 29.8 *(two peaks separated by ca. 5.3 Hz)*, 29.5*(two peaks separated by ca. 2.3 Hz)*, 29.2, 29.1, 29.0, 27.4, 26.3*(two peaks separated by ca. 2.3 Hz)*, 22.8, 14.3, 13.8, 11.1(4 C missing probably due to overlaps). MS (MALDI): *m/z* 1385.8 (calcd for $C_{74}H_{133}NO_3S_2Sn_2$, 1386.4). Elemental Analysis: (Calculated) C: 64.11; H: 9.67: N: 1.01; Found C: 64.16; H: 9.54: N: 0.98.

P(DTP-BThBTD)$_n$: To a 100 mL 3-neck round bottom flask were added 4,7-bis(5-bromothiophen-2-yl)-[2,1,3]-benzothiadiazole (0.35 g, 0.76 mmol), 2,6-bis(tributylstannyl)-N-(3,4,5-tris(dodecyloxy)phenyl)-dithieno[3,2-b:2',3'-*d*]pyrrole (1.11 g, 0.80 mmol) and dry THF (100 mL), vacuum pump filled for 5-6 times, and degassed with Argon for 30 min. $PdCl_2(PPh_3)_2$(0.027 g, 0.04 mmol) was added, and the solution was stirred at 60-70 °C for 2

days. The solution was dropped in ca 500 mL methanol, and the solid was filtered. The crude product was purified by Soxhlet washings with methanol, acetone and hexanes each for 1 day, and extraction with chloroform for 1 day. After the second precipitation, a black solid (0.80 g, 95%) was obtained. ^{1}H NMR (300 MHz, THF-d^8): δ 8.20-7.80 (br, 4H), 7.51-7.02 (br, 4H), 6.83(br, 2H), 4.11 (br, 6H), 1.94–1.21 (br, 60 H), 0.91 (br, 9H). M_n =106,000, M_w = 147,000, PDI = 1.4. Elemental Analysis: (Calculated) C: 69.46; H: 7.92; N: 3.80; Found C: 69.72; H: 7.77; N: 3.69. TGA (N_2) T_d = 368 ºC.

P(DTP-BTD)$_n$: To a 100 mL 3-neck round bottom flask were added 2,6-bis(tributylstannyl)-N-(3,4,5-tris(dodecyloxy)phenyl)-dithieno[3,2-*b*:2',3'-*d*]pyrrole (0.32 g, 0.23 mmol), $PdCl_2(PPh_3)_2$(0.008 g, 0.01 mmol) and dry THF (30 mL), vacuum pump filled for 5 times, and degassed with Argon for 60 min. 4,7-dibromobenzo[c][1,2,5]thiadiazole (0.06 g, 0.22 mmol) was added, and the solution was stirred at 60-70 °C for 2 days. The solution was dropped in ca 500 mL methanol, and the solid was filtered. The crude product was purified by Soxhlet washings with methanol, acetone and hexanes each for 1 day, and extraction with chloroform for 1 day. After the second precipitation, a black solid (0.20 g, ca 95 %) was obtained. M_n =24,000, M_w = 53,000, PDI = 2.2. Elemental Analysis: (Calculated) C: 71.37; H: 8.88; N: 4.46; Found C: 70.28; H: 8.44; N: 4.27. TGA (N_2) T_d = 352 ºC.

P(DTP-BThTQHx$_2$)$_n$: To a 100 mL 3-neck round bottom flask were added 2,6-bis(tributylstannyl)-N-(3,4,5-tris(dodecyloxy)phenyl)-dithieno[3,2-*b*:2',3'-*d*]pyrrole (0.56 g, 0.40 mmol), $PdCl_2(PPh_3)_2$(0.014 g, 0.02 mmol) and dry THF (50 mL), vacuum pump filled for 5 times, and degassed with Argon for 60 min. 4,9-Bis(5-bromothiophen-2-yl)-6,7-dihexyl-[1,2,5]thiadiazolo[3,4-*g*]quinoxaline (0.26 g, 0.39 mmol) was added, and the solution was stirred at 60-70 °C for 2 days. The solution was dropped in ca 700 mL methanol, and the solid was

filtered. The crude product was purified by Soxhlet washings with methanol, acetone and hexanes each for 1 day, and extraction with chloroform for 1 day. After the second precipitation, a black solid (0.23 g, ca 50%) was obtained. M_n =9,600, M_w = 28,000, PDI = 2.9. Elemental Analysis: (Calculated) C: 70.59; H: 8.43; N: 5.28; Found C: 70.63; H: 8.30; N: 4.90. TGA (N_2) T_d = 367 ºC.

P(DTP-TQHx$_2$)$_n$: To a 100 mL 3-neck round bottom flask were added 2,6-bis(tributylstannyl)-N-(3,4,5-tris(dodecyloxy)phenyl)-dithieno[3,2-*b*:2',3'-*d*]pyrrole (0.57 g, 0.40 mmol), $PdCl_2(PPh_3)_2$(0.014 g, 0.02 mmol) and dry THF (50 mL), vacuum pump filled for 5 times, and degassed with Argon for 60 min. 4,9-Dibromo-6,7-dihexyl-[1,2,5]thiadiazolo[3,4-*g*]quinoxaline (0.20 g, 0.39 mmol) was added, and the solution was stirred at 60-70 °C for 2 days. The solution was dropped in ca 600 mL methanol, and the solid was filtered. The crude product was purified by Soxhlet washings with methanol, acetone and hexanes each for 1 day, and extraction with chloroform for 1 day. After the second precipitation, a black solid was obtained. Mn =19,000, Mw = 38,000, PDI = 2.0**.** Elemental Analysis: (Calculated) C: 72.30; H: 9.27; N: 6.02; Found C: 71.93; H: 9.07; N: 5.42. TGA (N_2) T_d = 341 ºC.

P(DTP-BThBBT)$_n$: To a 100 mL 3-neck round bottom flask were added 2,6-bis(tributylstannyl)-N-(3,4,5-tris(dodecyloxy)phenyl)-dithieno[3,2-*b*:2',3'-*d*]pyrrole (0.66 g, 0.48 mmol), $PdCl_2(PPh_3)_2$(0.016 g, 0.02 mmol) and dry THF (50 mL), vacuum pump filled for 5 times, and degassed with Argon for 60 min. 4,7-bis(5-bromothiophen-2-yl)-2$\lambda^4\delta^2$-benzo[1,2-c;4,5-c′]bis[1,2,5]thiadiazole (0.23 g, 0.45 mmol) was added, and the solution was stirred at 60-70 °C for 2 days. The solution was dropped in ca 600 mL methanol, and the solid was filtered. The crude product was purified by Soxhlet washings with methanol, acetone and hexanes each for 1 day, and extraction with chloroform for 1 day. After the second precipitation, a black solid

(0.47 g, 88%) was obtained. ^{1}H NMR (300 MHz, THF-d^{8}): δ 9.02 (br, 2H), 7.55-5.78 (br, 6H), 4.15 (br, 6H), 1.94–1.21 (br, 60 H), 0.91 (br, 9H). M_n =14,000, M_w = 51,000, PDI = 3.6, Elemental Analysis: (Calculated) C: 65.99; H: 7.36; N: 6.01; Found C: 65.23; H: 7.30; N: 5.60. TGA (N_2) T_d = 331 ºC.

APPENDIX A
X-RAY CRYSTALLOGRAPHIC DATA

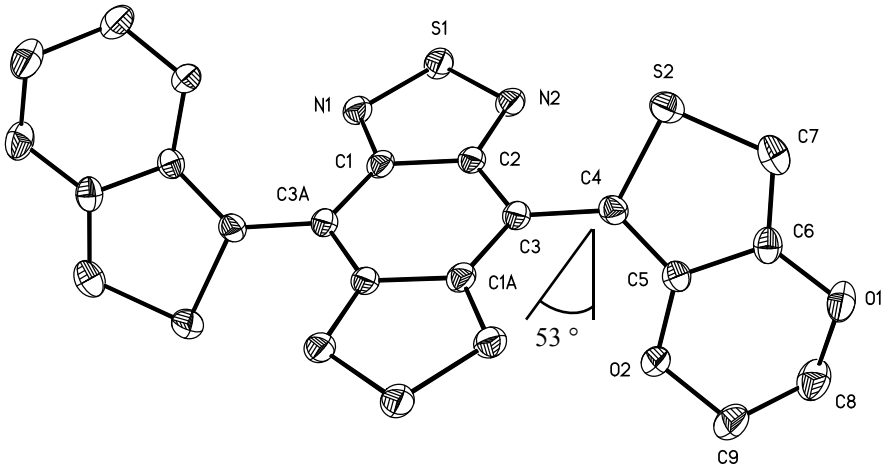

Figure A-1. Crystal Structure for compound **6a** (Chapter 4).

Table A-1. Crystal data and structure refinement for **6a** (Chapter 4).

Identification code	stec1	
Empirical formula	C18 H10 N4 O4 S4	
Formula weight	474.54	
Temperature	173(2) K	
Wavelength	0.71073 Å	
Crystal system	Triclinic	
Space group	P-1	
Unit cell dimensions	a = 6.2143(7) Å	α= 69.407(2)°.
	b = 10.8663(12) Å	β= 81.976(2)°.
	c = 14.9797(16) Å	γ = 75.468(2)°.
Volume	915.13(17) $Å^3$	
Z	2	
Density (calculated)	1.722 Mg/m^3	
Absorption coefficient	0.557 mm^{-1}	
F(000)	484	
Crystal size	0.17 x 0.06 x 0.04 mm^3	
Theta range for data collection	1.45 to 27.49°.	
Index ranges	-7≤h≤8, -8≤k≤14, -19≤l≤19	
Reflections collected	6248	

Independent reflections	4090 [R(int) = 0.0325]
Completeness to theta = 27.49°	97.7 %
Absorption correction	Integration
Max. and min. transmission	0.9794 and 0.9419
Refinement method	Full-matrix least-squares on F^2
Data / restraints / parameters	4090 / 0 / 270
Goodness-of-fit on F^2	1.031
Final R indices [I>2sigma(I)]	R1 = 0.0374, wR2 = 0.0923 [3205]
R indices (all data)	R1 = 0.0518, wR2 = 0.0980
Largest diff. peak and hole	0.422 and -0.311 e.Å^{-3}

$R1 = \Sigma(||F_o| - |F_c||) / \Sigma|F_o|$

$wR2 = [\Sigma[w(F_o^2 - F_c^2)^2] / \Sigma[w(F_o^2)^2]]^{1/2}$

$S = [\Sigma[w(F_o^2 - F_c^2)^2] / (n-p)]^{1/2}$

$w= 1/[\sigma^2(F_o^2)+(m*p)^2+n*p]$, $p = [\max(F_o^2,0)+ 2* F_c^2]/3$, m & n are constants.

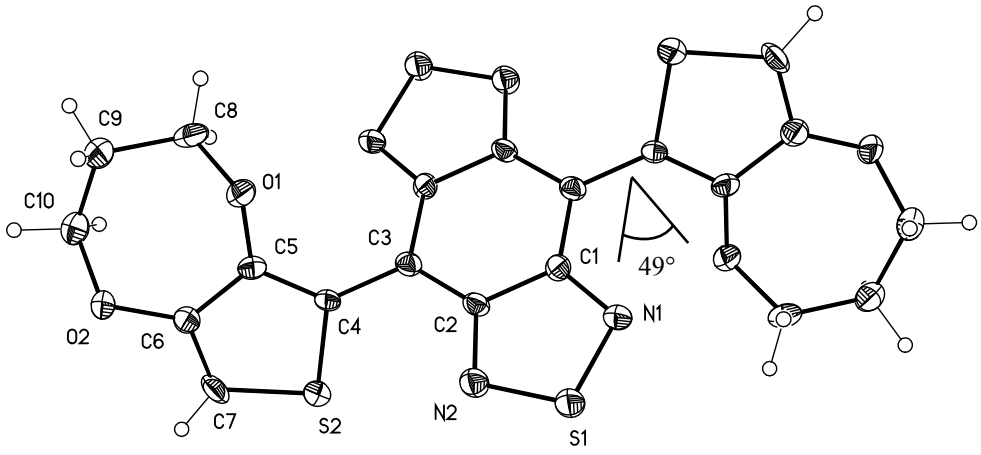

Figure A-2. Crystal Structure for compound **6b** (Chapter 4).

Table A-2. Crystal data and structure refinement for **6b** (Chapter 4).

Identification code	stec5	
Empirical formula	C20 H14 N4 O4 S4	
Formula weight	502.59	
Temperature	173(2) K	
Wavelength	0.71073 Å	
Crystal system	Monoclinic	
Space group	$P2_1/n$	
Unit cell dimensions	a = 12.4928(16) Å	α= 90°.
	b = 10.8585(14) Å	β= 98.658(3)°.
	c = 15.5644(19) Å	γ = 90°.
Volume	2087.3(5) $Å^3$	
Z	4	
Density (calculated)	1.599 Mg/m^3	
Absorption coefficient	0.493 mm^{-1}	
F(000)	1032	
Crystal size	0.18 x 0.04 x 0.02 mm^3	
Theta range for data collection	1.95 to 27.49°.	
Index ranges	-15≤h≤16, -14≤k≤14, -15≤l≤20	
Reflections collected	13942	
Independent reflections	4780 [R(int) = 0.1190]	
Completeness to theta = 27.49°	99.7 %	

Absorption correction	Integration
Max. and min. transmission	0.9902 and 0.9164
Refinement method	Full-matrix least-squares on F^2
Data / restraints / parameters	4780 / 0 / 289
Goodness-of-fit on F^2	0.885
Final R indices [I>2sigma(I)]	R1 = 0.0676, wR2 = 0.1526 [1990]
R indices (all data)	R1 = 0.1736, wR2 = 0.1777
Largest diff. peak and hole	1.181 and -0.371 e.$Å^{-3}$

$R1 = \Sigma(||F_o| - |F_c||) / \Sigma|F_o|$

$wR2 = [\Sigma[w(F_o^2 - F_c^2)^2] / \Sigma[w(F_o^2)^2]]^{1/2}$

$S = [\Sigma[w(F_o^2 - F_c^2)^2] / (n-p)]^{1/2}$

$w= 1/[\sigma^2(F_o^2)+(m*p)^2+n*p]$, $p = [\max(F_o^2,0)+ 2* F_c^2]/3$, m & n are constants.

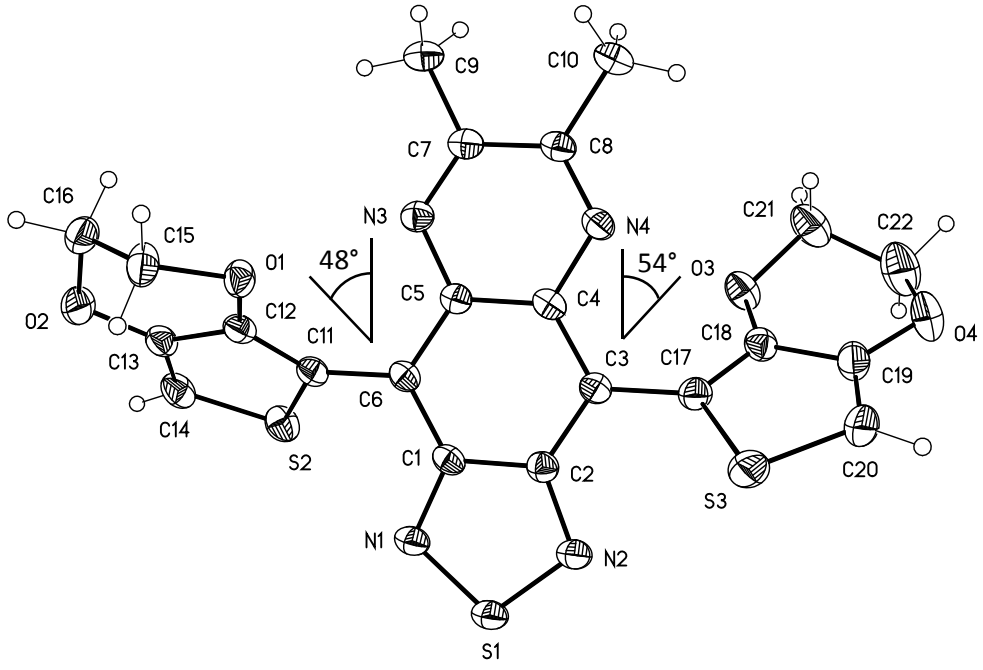

Figure A-3. Crystal Structure for compound **7a** (Chapter 4).

Table A-3. Crystal data and structure refinement for 7**a** (Chapter 4).

Identification code	stec3	
Empirical formula	C22 H16 N4 O4 S3	
Formula weight	496.57	
Temperature	173(2) K	
Wavelength	0.71073 Å	
Crystal system	Triclinic	
Space group	P-1	
Unit cell dimensions	a = 7.4627(8) Å	α= 101.290(2)°.
	b = 11.0846(12) Å	β= 98.186(2)°.
	c = 13.0708(14) Å	γ = 95.442(2)°.
Volume	1041.08(19) Å^3	
Z	2	
Density (calculated)	1.584 Mg/m^3	
Absorption coefficient	0.397 mm^{-1}	
F(000)	512	
Crystal size	0.18 x 0.11 x 0.04 mm^3	

Theta range for data collection	1.61 to 27.50°.
Index ranges	$-4 \leq h \leq 9$, $-14 \leq k \leq 14$, $-16 \leq l \leq 16$
Reflections collected	7161
Independent reflections	4673 [R(int) = 0.0294]
Completeness to theta = 27.50°	97.7 %
Absorption correction	Integration
Max. and min. transmission	0.9843 and 0.9319
Refinement method	Full-matrix least-squares on F^2
Data / restraints / parameters	4673 / 0 / 298
Goodness-of-fit on F^2	1.037
Final R indices [I>2sigma(I)]	R1 = 0.0407, wR2 = 0.0974 [3658]
R indices (all data)	R1 = 0.0564, wR2 = 0.1035
Largest diff. peak and hole	0.371 and -0.222 e.Å^{-3}

$R1 = \Sigma(||F_o| - |F_c||) / \Sigma|F_o|$

$wR2 = [\Sigma[w(F_o^2 - F_c^2)^2] / \Sigma[w(F_o^2)^2]]^{1/2}$

$S = [\Sigma[w(F_o^2 - F_c^2)^2] / (n-p)]^{1/2}$

$w= 1/[\sigma^2(F_o^2)+(m*p)^2+n*p]$, $p = [\max(F_o^2,0)+ 2* F_c^2]/3$, m & n are constants.

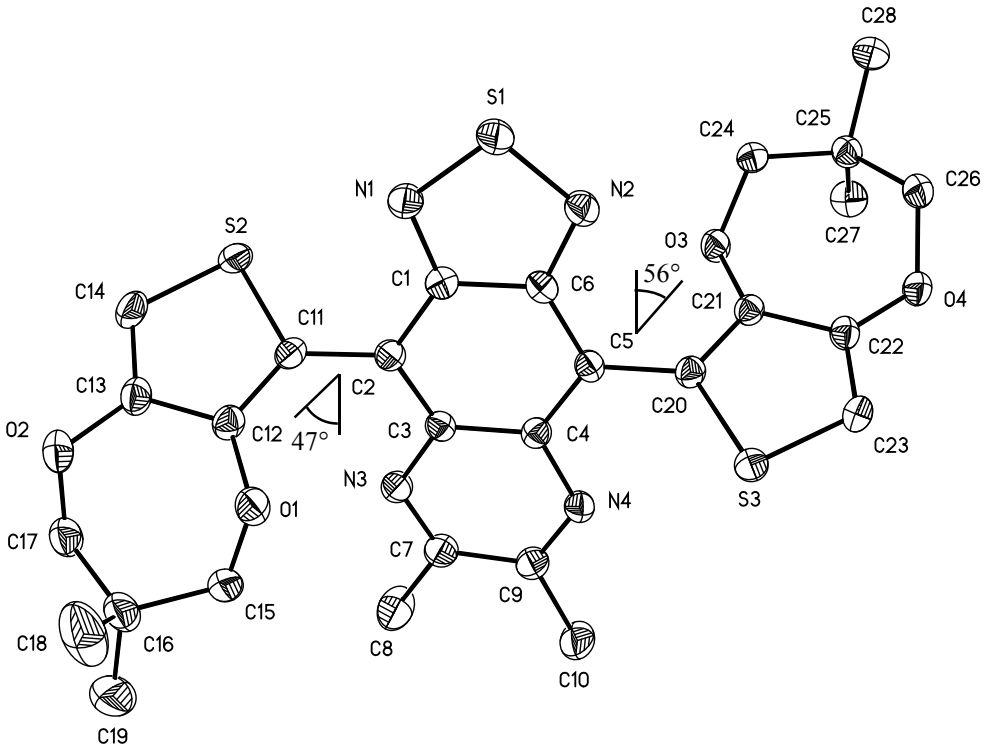

Figure A-4. Crystal Structure for compound **7c** (Chapter 4).

Table A-4. Crystal data and structure refinement for **7c** (Chapter 4).

Identification code	stec6	
Empirical formula	C28 H28 N4 O4 S3	
Formula weight	580.72	
Temperature	173(2) K	
Wavelength	0.71073 Å	
Crystal system	Monoclinic	
Space group	$P2_1/c$	
Unit cell dimensions	a = 9.3368(5) Å	α= 90°.
	b = 22.1015(12) Å	β= 108.654(1)°.
	c = 14.1452(7) Å	γ = 90°.
Volume	2765.6(3) $Å^3$	
Z	4	
Density (calculated)	1.395 Mg/m^3	
Absorption coefficient	0.310 mm^{-1}	

F(000)	1216
Crystal size	0.17 x 0.17 x 0.17 mm^3
Theta range for data collection	1.78 to 27.50°.
Index ranges	$-11 \leq h \leq 12$, $-28 \leq k \leq 28$, $-18 \leq l \leq 11$
Reflections collected	18666
Independent reflections	6335 [R(int) = 0.0319]
Completeness to theta = 27.50°	99.7 %
Absorption correction	Integration
Max. and min. transmission	0.9489 and 0.9489
Refinement method	Full-matrix least-squares on F^2
Data / restraints / parameters	6335 / 0 / 352
Goodness-of-fit on F^2	1.054
Final R indices [I>2sigma(I)]	R1 = 0.0400, wR2 = 0.1048 [4962]
R indices (all data)	R1 = 0.0543, wR2 = 0.1117
Largest diff. peak and hole	0.392 and -0.251 $e.Å^{-3}$

$R1 = \Sigma(||F_o| - |F_c||) / \Sigma|F_o|$

$wR2 = [\Sigma[w(F_o^2 - F_c^2)^2] / \Sigma[w(F_o^2)^2]]^{1/2}$

$S = [\Sigma[w(F_o^2 - F_c^2)^2] / (n-p)]^{1/2}$

$w= 1/[\sigma^2(F_o^2)+(m*p)^2+n*p]$, $p = [\max(F_o^2,0)+ 2* F_c^2]/3$, m & n are constants.

APPENDIX B

ELECTROCHEMICAL POLYMERIZATION OF MONOMERS FROM CHAPTER 4

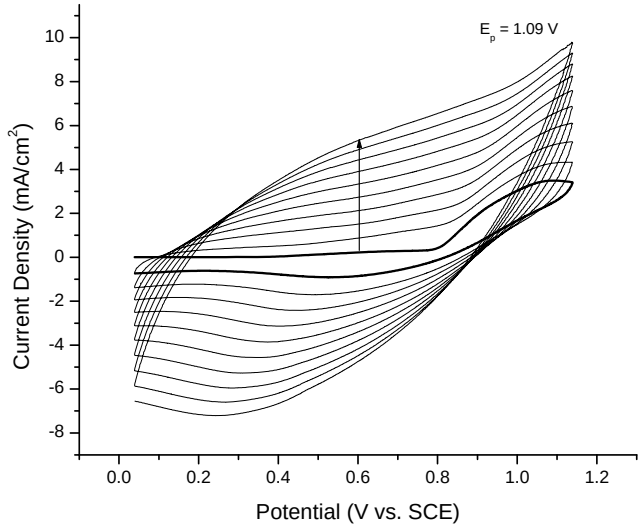

Figure B-1. Repetitive scan electropolymerization (50 mV/s, 10 cycles) from a 5 mM monomer 0.1 M TBAP/DCM solution of **6a** yielding **P6a**.

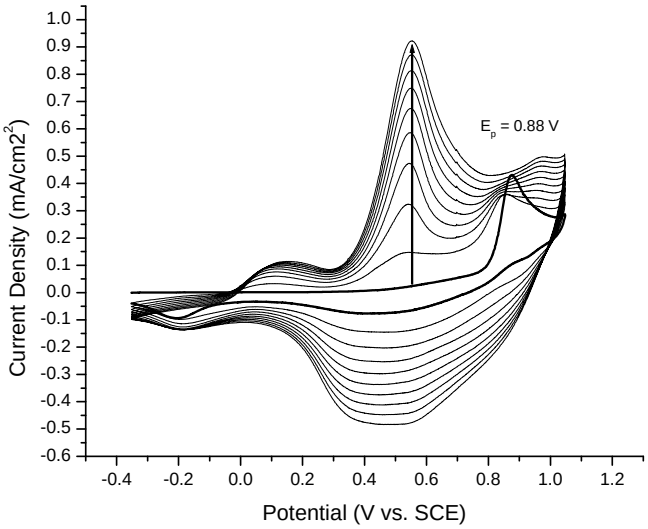

Figure B-2. Repetitive scan electropolymerization (50 mV/s, 10 cycles) from a 5 mM monomer 0.1 M TBAP/PC:DCM (9:1) solution of **7a** yielding **P7a**.

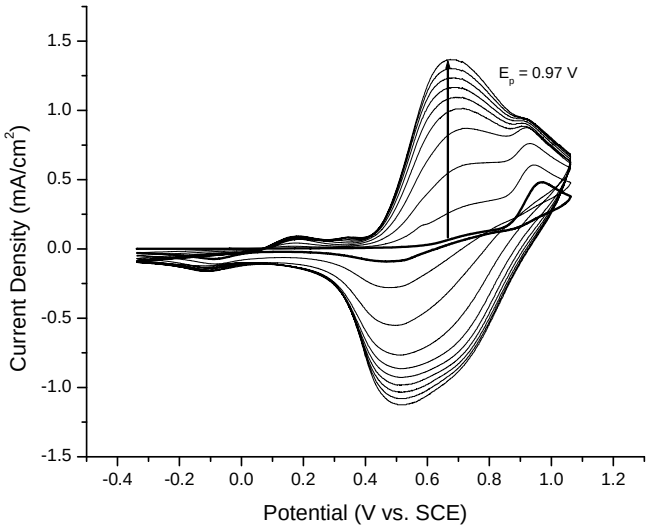

Figure B-3. Repetitive scan electropolymerization (50 mV/s, 10 cycles) from a 5 mM monomer 0.1 M TBAP/PC:DCM (9:1) solution of **8a** yielding **P8a**.

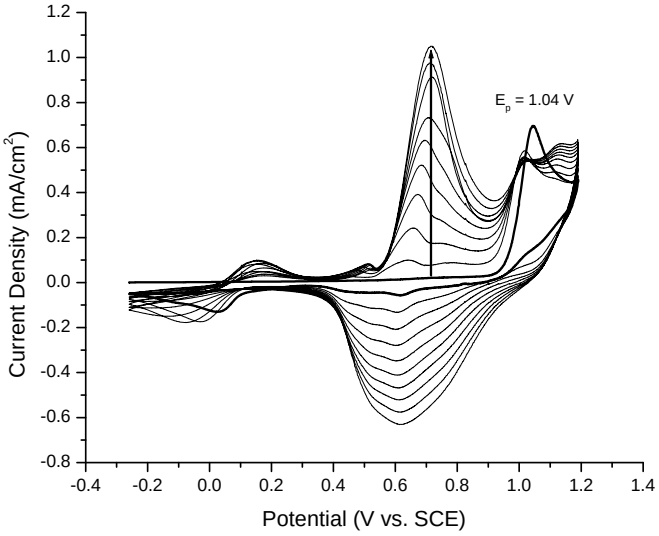

Figure B-4. Repetitive scan electropolymerization (50 mV/s, 10 cycles) from a 5 mM monomer 0.1 M TBAP/PC:DCM (9:1) solution of **7b** yielding **P7b**.

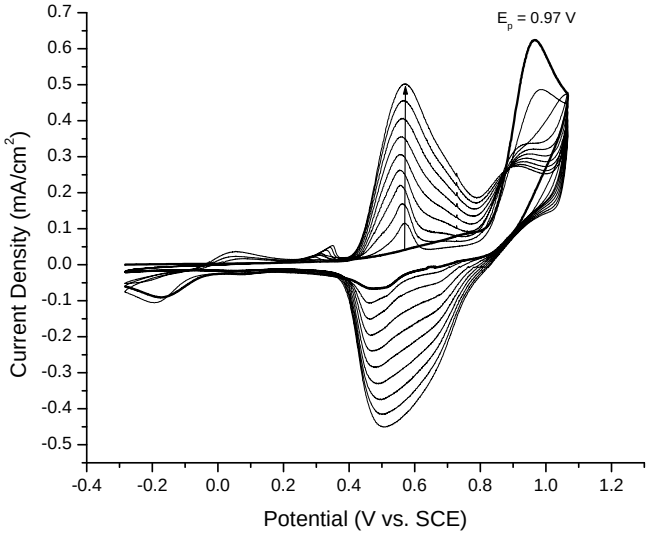

Figure B-5. Repetitive scan electropolymerization (50 mV/s, 10 cycles) from a 5 mM monomer 0.1 M TBAP/PC:DCM (9:1) solution of **8b** yielding **P8b**.

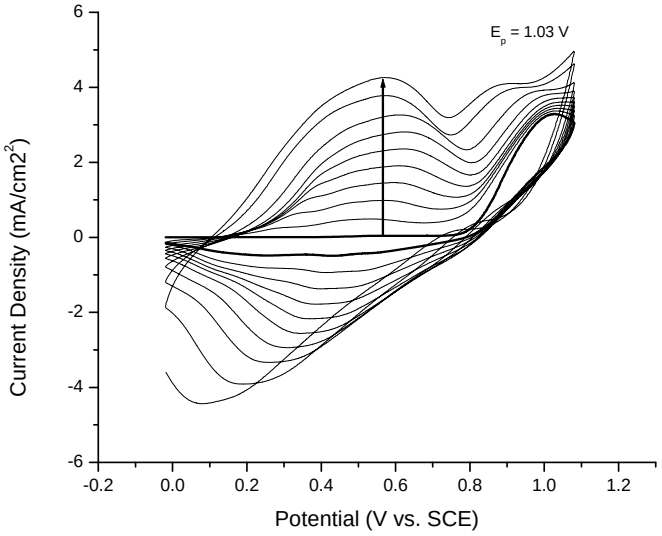

Figure B-6. Repetitive scan electropolymerization (50 mV/s, 10 cycles) from a 5 mM monomer 0.1 M TBAP/DCM solution of **6c** yielding **P6c**.

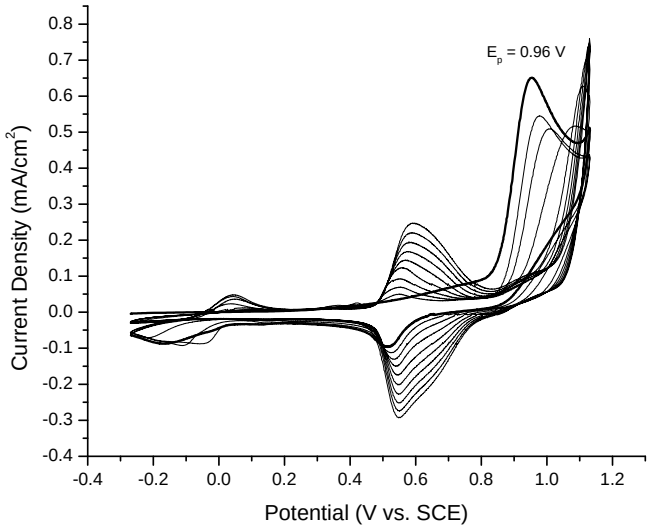

Figure B-7. Repetitive scan electropolymerization (50 mV/s, 10 cycles) from a 5 mM monomer 0.1 M TBAP/PC:DCM (9:1) solution of **7c** yielding **P7c**.

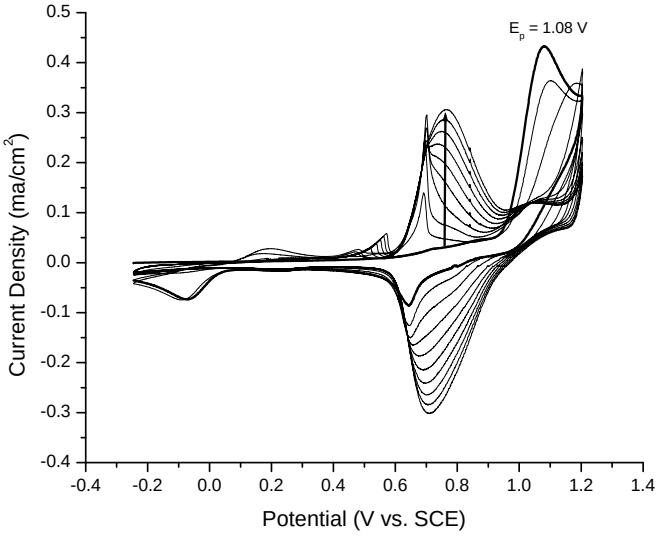

Figure B-8. Repetitive scan electropolymerization (50 mV/s, 10 cycles) from a 5 mM monomer 0.1 M TBAP/PC:DCM (9:1) solution of **8c** yielding **P8c**.

LIST OF REFERENCES

1. Shirakawa, H.; Louis, E. J.; MacDiarmid, A. G.; Chiang, C. K.; Heeger, A. J. *J. Chem. Soc., Chem. Commun.* **1977**, 578-80.

2. Chiang, C. K.; Fincher, C. R., Jr.; Park, Y. W.; Heeger, A. J.; Shirakawa, H.; Louis, E. J.; Gau, S. C.; MacDiarmid, A. G. *Phys. Rev. Lett.* **1977**, 39, 1098-101.

3. Kulkarni, A. P.; Kong, X.; Jenekhe, S. A. *Macromolecules* **2006**, 39, 8699-8711.

4. Blouin, N.; Leclerc, M. *Acc. Chem. Res.* **2008**, 41, 1110-1119.

5. Abay, G.; Erik, P.; Mats, R. A.; Olle, I. *Appl. Phys. Lett.* **2007**, 90, 113510.

6. Köhnen, A.; Riegel, N.; Kremer, J. H. W. M.; Lademann, H.; Müller, D. C.; Meerholz, K. *Adv. Mater.* **2009**, 21, 879-884.

7. Gunbas, G. E.; Camurlu, P.; Akhmedov, I. M.; Tanyeli, C.; Önal, A. M.; Toppare, L. *J. Electroan. Chem.* **2008**, 615, 75-83.

8. Walczak, R. M.; Reynolds, J. R. *Adv. Mater.* **2006**, 18, 1121-1131.

9. Beaujuge, P. M.; Ellinger, S.; Reynolds, J. R. *Adv. Mater.* **2008**, 20, 2772-2776.

10. Thompson, B. C.; Kim, Y. G.; McCarley, T. D.; Reynolds, J. R. *J. Am. Chem. Soc.* **2006**, 128, 12714-12725.

11. Groenendaal, L. B.; Zotti, G.; Aubert, P. H.; Waybright, S. M.; Reynolds, J. R. *Adv. Mater.* **2003**, 15, 855-879.

12. Blouin, N.; Michaud, A.; Gendron, D.; Wakim, S.; Blair, E.; Neagu-Plesu, R.; Belletete, M.; Durocher, G.; Tao, Y.; Leclerc, M. *J. Am. Chem. Soc.* **2008**, 130, 732-742.

13. Bundgaard, E.; Krebs, F. C. Sol. *Energy Mater. Sol. Cells* **2007**, 91, 1019-1025.

14. Colladet, K.; Fourier, S.; Cleij, T. J.; Lutsen, L.; Gelan, J.; Vanderzande, D.; HuongNguyen, L.; Neugebauer, H.; Sariciftci, S.; Aguirre, A.; Janssen, G.; Goovaerts, E. *Macromolecules* **2007**, 40, 65-72.

15. Yongfang Li, Y. Z. *Adv. Mater.* **2008**, 20, 2952-2958.

16. Zoombelt, A. P.; Fonrodona, M.; Wienk, M. M.; Sieval, A. B.; Hummelen, J. C.; Janssen, R. A. J. *Org. Lett.* **2009**, 11, 903-906.

17. Zhou, E.; Nakamura, M.; Nishizawa, T.; Zhang, Y.; Wei, Q.; Tajima, K.; Yang, C.; Hashimoto, K. *Macromolecules* **2008**, 41, 8302-8305.

18. Wienk, M. M.; Turbiez, M.; Gilot, J.; Janssen, R. A. J. *Adv. Mater.* **2008**, 20, 2556-2560.

19. Boudreault, P. L. T.; Michaud, A.; Leclerc, M. *Macromol. Rapid Commun.* **2007**, 28, 2176-2179.

20. Marchioni, F.; Yang, J.; Walker, W.; Wudl, F. *J. Phys. Chem. B* **2006**, 110, 22202-22206.

21. Carlberg, J. C.; Inganaes, O. *J. Electrochem. Soc.* **1997**, 144, L61-L64.

22. Zhang, J.; Kong, L. B.; Wang, B.; Luo, Y. C.; Kang, L. *Synth. Met.* **2009**, 159, 260-266.

23. Bhat, D. K.; Kumar, M. S. *J. Mater. Sci.* **2007**, 42, 8158-8162.

24. Stenger-Smith, J. D.; Webber, C. K.; Anderson, N.; Chafin, A. P.; Zong, K.; Reynolds, J. R. *J. Electrochem. Soc.* **2002**, 149, A973-A977.

25. Laforgue, A.; Simon, P.; Sarrazin, C.; Fauvarque, J. F. *J. Power Sources* **1999**, 80, 142-148.

26. Liu, J.; Zhang, R.; Sauve, G.; Kowalewski, T.; McCullough, R. D. *J. Am. Chem. Soc.* **2008**.

27. Wu, P. T.; Kim, F. S.; Champion, R. D.; Jenekhe, S. A. *Macromolecules* **2008**, 41, 7021-7028.

28. Steckler, T. T.; Zhang, X.; Hwang, J.; Honeyager, R.; Ohira, S.; Zhang, X. H.; Grant, A.; Ellinger, S.; Odom, S. A.; Sweat, D.; Tanner, D. B.; Rinzler, A. G.; Barlow, S.; Brédas, J. L.; Kippelen, B.; Marder, S. R.; Reynolds, J. R. *J. Am. Chem. Soc.* **2009**, 0.

29. Champion, R. D.; Cheng, K. F.; Pai, C. L.; Chen, W. C.; Jenekhe, S. A. *Macromol. Rapid Commun.* **2005**, 26, 1835-1840.

30. Yamamoto, T.; Yasuda, T.; Sakai, Y.; Aramaki, S. *Macromol. Rapid Commun.* **2005**, 26, 1214-1217.

31. Hoffmann, R. *Angew. Chem., Int. Ed.***1987**, 26, 846-878.

32. Salaneck, W. R.; Brédas, J. L. *Synth. Met.* **1994**, 67, 15-22.

33. Moliton, A.; Hiorns, R. C. *Polym. Int.* **2004**, 53, 1397-1412.

34. Fincher, C. R.; Chen, C. E.; Heeger, A. J.; MacDiarmid, A. G.; Hastings, J. B. *Phys. Rev. Lett.* **1982**, 48, 100.

35. Kaufman, J. H.; Kaufer, J. W.; Heeger, A. J.; Kaner, R.; MacDiarmid, A. G. *Phys. Rev. B* **1982**, 26, 2327.

36. Salzner, U. *Curr. Org. Chem.* **2004**, 8, 569-590.

37. Thompson, B. C. Variable band gap poly(3,4-alkylenedioxythiophene)-based polymers for photovoltaic and electrochromic applications. Ph.D. Thesis, University of Florida, Gainesville, FL, 2005.

38. Thomas, C. A.; Zong, K.; Abboud, K. A.; Steel, P. J.; Reynolds, J. R. *J. Am. Chem. Soc.* **2004**, 126, 16440-16450.

39. Thomas, C. A. Donor-acceptor methods for band gap reduction in conjugated polymers: the role of electron rich donor heterocycles. Ph.D. Thesis, University of Florida, Gainesville, FL, 2002.

40. Reeves, B. D. Processable disubstituted poly(propylenedioxythiophenes) Ph.D. Thesis, University of Florida, Gainesville, FL, 2005.

41. Boudreaux, D. S.; Chance, R. R.; Brédas, J. L.; Silbey, R. *Phys. Rev. B* **1983**, 28, 6927.

42. Thomann, H.; Dalton, L. R.; Tomkiewicz, Y.; Shiren, N. S.; Clarke, T. C. *Phys. Rev. Lett.* **1983**, 50, 533.

43. Brédas, J. L.; Street, G. B. *Acc. Chem. Res.* **1985**, 18, 309-315.

44. Brédas, J. L.; Thémans, B.; Fripiat, J. G.; André, J. M.; Chance, R. R. *Phys. Rev. B* **1984**, 29, 6761.

45. Brédas, J. L.; Scott, J. C.; Yakushi, K.; Street, G. B. *Phys. Rev. B* **1984**, 30, 1023.

46. Roncali, J. *Macromol. Rapid Commun.* **2007**, 28, 1761-1775.

47. Roncali, J. *Chem. Rev.* **1997**, 97, 173-206.

48. van Mullekom, H. A. M.; Vekemans, J. A. J. M.; Havinga, E. E.; Meijer, E. W. *Mater. Sci. Eng.* **2001**, 32, 1-40.

49. Kroon, R.; Lenes, M.; Hummelen, J. C.; Blom, P. W. M.; de Boer, B. *Polymer Reviews* **2008**, 48, 531-582.

50. Bundgaard, E.; Krebs, F. C. *Sol. Energy Mater. Sol. Cells* **2007**, 91, 954-985.

51. Ajayaghosh, A. *Acc. Chem. Res.* **2005**, 38, 449-459.

52. Rasmussen, S. C.; Pomerantz, M. *Handbook of Conducting Polymers (3rd Edition)* **2007**, 1, 12/1-12/42.

53. Steckler, T. T.; Zhang, X.; Hwang, J.; Honeyager, R.; Ohira, S.; Zhang, X. H.; Grant, A.; Ellinger, S.; Odom, S. A.; Sweat, D.; Tanner, D. B.; Rinzler, A. G.; Barlow, S.; Brédas, J. L.; Kippelen, B.; Marder, S. R.; Reynolds, J. R. *J. Am. Chem. Soc.* **2009**, 131, 2824-2826.

54. Rudge, A.; Davey, J.; Raistrick, I.; Gottesfeld, S.; Ferraris, J. P. *J. Power Sources* **1994**, 47, 89-107.

55. Irvin, J. A.; Irvin, D. J.; Stenger-Smith, J. D. *Handbook of Conducting Polymers (3rd Edition)* **2007**, 2, 9/1-9/29.

56. Arbizzani, C.; Mastragostino, M.; Soavi, F. *J. Power Sources* **2001**, 100, 164-170.

57. Kobayashi, M.; Colaneri, N.; Boysel, M.; Wudl, F.; Heeger, A. J. *J. Chem. Phys.* **1985**, 82, 5717.

58. Brédas, J. L.; Heeger, A. J.; Wudl, F. *J. Chem. Phys.* **1986**, 85, 4673-4678.

59. van Mullekom, H. A. M.; Vekemans, J. A. J. M.; Meijer, E. W. *Chem. Commun.* **1996**, 2163-2164.

60. Osaka, I.; McCullough, R. D. *Acc. Chem. Res.* **2008**, 41, 1202-1214.

61. McCullough, R. D. *Adv. Mater.* **1998**, 10, 93-116.

62. McCullough, R. D.; Tristram-Nagle, S.; Williams, S. P.; Lowe, R. D.; Jayaraman, M. *J. Am. Chem. Soc.* **1993**, 115, 4910-11.

63. Havinga, E. E.; ten Hoeve, W.; Wynberg, H. *Synth. Met.* **1993**, 55, 299-306.

64. Salzner, U.; Karalti, O.; Durdagi, S. *J. Mol. Model.* **2006**, 12, 687-701.

65. Salzner, U. J. *Phys. Chem. B* **2002**, 106, 9214-9220.

66. Salzner, U.; Kose, M. E. J. *Phys. Chem. B* **2002**, 106, 9221-9226.

67. DuBois, C. J.; Abboud, K. A.; Reynolds, J. R. *J. Phys. Chem. B* **2004**, 108, 8550-8557.

68. DuBois, C. J.; Reynolds, J. R. *Adv. Mater.* **2002**, 14, 1844-1846.

69. Zhang, Q. T.; Tour, J. M. *J. Am. Chem. Soc.* **1998**, 120, 5355-5362.

70. Beaujuge, P. M.; Ellinger, S.; Reynolds, J. R. *Nat Mater* **2008**, 7, 795-799.

71. Udum, Y. A.; Yildiz, E.; Gunbas, G.; Toppare, L. *J. Polym. Sci., Part A: Polym. chem.* **2008**, 46, 3723-3731.

72. Reddinger, J. L.; Reynolds, J. R. *Adv. Polym. Sci.* **1999**, 145, 57-122.

73. Reynolds, J. R.; Ruiz, J. P.; Child, A. D.; Nayak, K.; Marynick, D. S. *Macromolecules* **1991**, 24, 678-687.

74. Reynolds, J. R.; Child, A. D.; Ruiz, J. P.; Hong, S. Y.; Marynick, D. S. *Macromolecules* **1993**, 26, 2095-2103.

75. Irvin, J. A.; Reynolds, J. R. *Polymer* **1998**, 39, 2339-2347.

76. Sotzing, G. A.; Reynolds, J. R.; Steel, P. J. *Chem. Mater.* **1996**, 8, 882-889.

77. Niemi, V. M.; Knuuttila, P.; Österholm, J. E.; Korvola, J. *Polymer* **1992**, 33, 1559-1562.

78. Irvin, J. A. Low oxidation potential electroactive polymers. Ph.D. Thesis, University of Florida, Gainesville, FL, **1998**.

79. Loewe, R. S.; Khersonsky, S. M.; McCullough, R. D. *Adv. Mater.* **1999**, 11, 250-253.

80. Yamamoto, T.; Morita, A.; Miyazaki, Y.; Maruyama, T.; Wakayama, H.; Zhou, Z. H.; Nakamura, Y.; Kanbara, T.; Sasaki, S.; Kubota, K. *Macromolecules* **1992**, 25, 1214-1223.

81. Yamamoto, T.; Maruyama, T.; Zhou, Z. H.; Ito, T.; Fukuda, T.; Yoneda, Y.; Begum, F.; Ikeda, T.; Sasaki, S. *J. Am. Chem. Soc.* **1994**, 116, 4832-4845.

82. Yamamoto, T. *Macromol. Rapid Commun.* **2002**, 23, 583-606.

83. Anderson, J. C.; Namli, H.; Roberts, C. A. *Tetrahedron* **1997**, 53, 15123-15134.

84. Schlüter, A. D. *J. Polym. Sci., Part A: Polym. chem.* **2001**, 39, 1533-1556.

85. Miyakoshi, R.; Yokoyama, A.; Yokozawa, T. *J. Polym. Sci., Part A: Polym. chem.* **2008**, 46, 753-765.

86. Bai, L.; Wang, J. X. *Curr. Org. Chem.* **2005**, 9, 535-553.

87. Jayakannan, M.; van Dongen, J. L. J.; Janssen, R. A. J. *Macromolecules* **2001**, 34, 5386-5393.

88. Miyaura, N.; Suzuki, A. *Chem. Rev.***1995**, 95, 2457-2483.

89. Goodson, F. E.; Wallow, T. I.; Novak, B. M. *Macromolecules* **1998**, 31, 2047-2056.

90. Stille, J. K. *Pure Appl. Chem.* **1985**, 57, 1771-80.

91. Stille, J. K. *Angew. Chem., Int. Ed.***1986**, 25, 508-524.

92. Sheina, E. E.; Liu, J.; Iovu, M. C.; Laird, D. W.; McCullough, R. D. *Macromolecules* **2004**, 37, 3526-3528.

93. Iovu, M. C.; Sheina, E. E.; Gil, R. R.; McCullough, R. D. *Macromolecules* **2005**, 38, 8649-8656.

94. Yamamoto, T. *Synlett* **2003**, 2003, 0425-0450.

95. Rehahn, M.; Schlüter, A. D.; Wegner, G.; Feast, W. J. *Polymer* **1989**, 30, 1060-1062.

96. Marsitzky, D.; Brand, h.; Geerts, Y.; Klapper, M.; Müllen, K. *Macromol. Rapid Commun.* **1998**, 19, 385-389.

97. Jayakannan, M.; Lou, X.; van Dongen, J. L. J.; Janssen, R. A. J. *J. Polym. Sci., Part A: Polym. chem.* **2005**, 43, 1454-1462.

98. Wang, F.; Wilson, M. S.; Rauh, R. D.; Schottland, P.; Thompson, B. C.; Reynolds, J. R. *Macromolecules* **2000**, 33, 2083-2091.

99. Galand, E. M. Processable variable band gap conjugated polymers for optoelectronic devices. Ph.D. Thesis, University of Florida, Gainesville, FL, 2006.

100. Wienk, M. M.; Struijk, M. P.; Janssen, R. A. J. *Chem. Phys. Lett.* **2006**, 422, 488-491.

101. Karsten, B. P.; Viani, L.; Gierschner, J.; Cornil, J. r. m.; Janssen, R. A. J. *J. Phys. Chem. A* **2008**, 112, 10764-10773.

102. Cheng, K. F.; Chueh, C. C.; Lin, C. H.; Chen, W. C. *J. Polym. Sci., Part A: Polym. chem.* **2008**, 46, 6305-6316.

103. Admassie, S.; Inganas, O.; Mammo, W.; Perzon, E.; Andersson, M. R. *Synth. Met.* **2006**, 156, 614-623.

104. Zhu, Y.; Champion, R. D.; Jenekhe, S. A. *Macromolecules* **2006**, 39, 8712-8719.

105. Liu, C. L.; Tsai, J. H.; Lee, W. Y.; Chen, W. C.; Jenekhe, S. A. *Macromolecules* **2008**, 41, 6952-6959.

106. Letizia, J. A.; Salata, M. R.; Tribout, C. M.; Facchetti, A.; Ratner, M. A.; Marks, T. J. *J. Am. Chem. Soc.* **2008**, 130, 9679-9694.

107. He, Y.; Wang, X.; Zhang, J.; Li, Y. *Macromol. Rapid Commun.* **2009**, 30, 45-51.

108. Hou, J.; Park, M. H.; Zhang, S.; Yao, Y.; Chen, L. M.; Li, J. H.; Yang, Y. *Macromolecules* **2008**, 41, 6012-6018.

109. Chen, C. P.; Chan, S. H.; Chao, T. C.; Ting, C.; Ko, B. T. *J. Am. Chem. Soc.* **2008**, 130, 12828-12833.

110. Bao, Z.; Chan, W. K.; Yu, L. J. *Am. Chem. Soc.* **1995**, 117, 12426-35.

111. Kitamura, C.; Tanaka, S.; Yamashita, Y. *Chem. Mater.* **1996**, 8, 570-8.

112. Lee, B. L.; Yamamoto, T. *Macromolecules* **1999**, 32, 1375-1382.

113. Koeckelberghs, G.; DeCremer, L.; Persoons, A.; Verbiest, T. *Macromolecules* **2007**, 40, 4173-4181.

114. Moore, J. S. *Macromol. Rapid Commun.* **1992**, 13, 91-96.

115. Wiberg, K. B.; Lewis, T. P. *J. Am. Chem. Soc.* **1970**, 92, 7154-7160.

116. Ono, K.; Tanaka, S.; Yamashita, Y. *Angew. Chem., Int. Ed.* **1994**, 33, 1977-1979.

117. Moule; x; J., A.; Tsami, A.; xfc; nnagel, T. W.; Forster, M.; Kronenberg, N. M.; Scharber, M.; Koppe, M.; Morana, M.; Brabec, C. J.; Meerholz, K.; Scherf, U. *Chem. Mater.* **2008**, 20, 4045-4050.

118. Qian, G.; Dai, B.; Luo, M.; Yu, D.; Zhan, J.; Zhang, Z.; Ma, D.; Wang, Z. Y. *Chem. Mater.* **2008**, 20, 6208-6216.

119. Li, X.; Liu, A.; Xun, S.; Qiao, W.; Wan, X.; Wang, Z. Y. *Org. Lett.* **2008**, 10, 3785-3787.

120. Tanaka, S.; Yamashita, Y. *Synth. Met.* **1995**, 69, 599-600.

121. Pavlishchuk, V. V.; Addison, A. W. *Inorg. chim. Acta* **2000**, 298, 97-102.

122. Gaupp, C. L. Structure-property relationships of electrochromic 3,4-alkylenedioxyheterocycle-based polymers and copolymers. Ph.D. Thesis, University of Florida, Gainesville, FL, 2002.

123. Bard, A. J.; Faulkner, L. R. Electrochemical Methods: Fundamentals and Applications 2nd Ed.; Wiley: New York, 2001.

124. Wu, Z.; Chen, Z.; Du, X.; Logan, J. M.; Sippel, J.; Nikolou, M.; Kamaras, K.; Reynolds, J. R.; Tanner, D. B.; Hebard, A. F.; Rinzler, A. G. *Science* **2004**, 305, 1273-1276.

125. Demanze, F.; Yassar, A.; Garnier, F. *Macromolecules* **1996**, 29, 4267-4273.

126. Huang, H.; Pickup, P. G. *Chem. Mater.* **1998**, 10, 2212-2216.

127. Zhang, Q. T.; Tour, J. M. *J. Am. Chem. Soc.* **1997**, 119, 5065-5066.

128. Ajayaghosh, A. *Chem. Soc. Rev.* **2003**, 32, 181-191.

129. Sotzing, G. A.; Thomas, C. A.; Reynolds, J. R.; Steel, P. J. *Macromolecules* **1998**, 31, 3750-3752.

130. Yamashita, Y.; Ono, K.; Tomura, M.; Tanaka, S. *Tetrahedron* **1997**, 53, 10169-10178.

131. Ferraris, J. P.; Henderson, C.; Torres, D.; Meeker, D. *Synth. Met.* **1995**, 72, 147-152.

132. Jonforsen, M.; Johansson, T.; Inganas, O.; Andersson, M. R. *Macromolecules* **2002**, 35, 1638-1643.

133. Irvin, D. J.; DuBois, C. J., Jr.; Reynolds, J. R. *Chem. Commun.* **1999**, 2121-2122.

134. Kanbara, T.; Miyazaki, Y.; Yamamoto, T. *J. Polym. Sci., Part A: Polym. chem.* **1995**, 33, 999-1003.

135. Yamamoto, T.; Zhou, Z. h.; Kanbara, T.; Shimura, M.; Kizu, K.; Maruyama, T.; Nakamura, Y.; Fukuda, T.; Lee, B. L.; Ooba, N.; Tomaru, S.; Kurihara, T.; Kaino, T.; Kubota, K.; Sasaki, S. *J. Am. Chem. Soc.* **1996**, 118, 10389-10399.

136. Sotzing, G. A.; Reddinger, J. L.; Reynolds, J. R.; Steel, P. J. *Synth. Met.* **1997**, 84, 199-201.

137. Gurunathan, K.; Murugan, A. V.; Marimuthu, R.; Mulik, U. P.; Amalnerkar, D. P. *Mater. Chem. Phys.* **1999**, 61, 173-191.

138. Sonmez, G.; Meng, H.; Wudl, F. *Chem. Mater.* **2003**, 15, 4923-4929.

139. Srinivasan, N. S.; Lee, D. G. *J. Org. Chem.* **1979**, 44, 1574-1574.

140. Lee, D. G.; Chang, V. S. *J. Org. Chem.* **1979**, 44, 2726-30.

141. Lee, D. G.; Chang, V. S. *Synthesis* **1978**, 462-3.

142. DuBois, C. J. Donor-acceptor methods for band gap control in conjugated polymers. Ph.D. Thesis, University of Florida, Gainesville, FL, 2003.

143. Shukla, A. K.; Sampath, S.; Vijayamohanan, K. *Curr. Sci.* **2000**, 79, 1656-1661.

144. Arbizzani, C.; Mastragostino, M.; Soavi, F. J. *Power Sources* **2001**, 100, 164-170.

145. Mastragostino, M.; Arbizzani, C.; Soavi, F. J. *Power Sources* **2001**, 97-98, 812-815.

146. Jonforsen, M.; Johansson, T.; Spjuth, L.; Inganäs, O.; Andersson, M. R. *Synth. Met.* **2002**, 131, 53-59.

147. Ruiz Delgado, M. C.; Hernandez, V.; Lopez Navarrete, J. T.; Tanaka, S.; Yamashita, Y. *J. Phys. Chem. B* **2004**, 108, 2516-2526.

148. de Leeuw, D. M.; Simenon, M. M. J.; Brown, A. R.; Einerhand, R. E. F. *Synth. Met.* **1997**, 87, 53-59.

149. Pilgram, K.; Zupan, M.; Skiles, R. J. *Heterocycl. Chem.* **1970**, 7, 629-33.

150. Uno, T.; Takagi, K.; Tomoeda, M. *Chem. Pharm. Bull.* **1980**, 28, 1909-12.

151. Karikomi, M.; Kitamura, C.; Tanaka, S.; Yamashita, Y. *J. Am. Chem. Soc.* **1995**, 117, 6791-6792.

152. Borjas, R.; Buttry, D. A. *Chem. Mater.* **1991**, 3, 872-878.

153. Zotti, G.; Schiavon, G.; Zecchin, S. *Synth. Met.* **1995**, 72, 275-281.

154. Cheng, K. F.; Liu, C. L.; Chen, W. C. *J. Polym. Sci., Part A: Polym. chem.* **2007**, 45, 5872-5883.

155. Yamashita, Y.; Tomura, M. *J. Mater. Chem.* **1998**, 8, 1933-1944.

156. Steckler, T. T.; Abboud, K. A.; Craps, M.; Rinzler, A. G.; Reynolds, J. R. *Chem. Commun.* **2007**, 4904-4906.

157. Kumar, A.; Welsh, D. M.; Morvant, M. C.; Piroux, F.; Abboud, K. A.; Reynolds, J. R. *Chem. Mater.* **1998**, 10, 896-902.

158. Welsh, D. M.; Kumar, A.; Meijer, E. W.; Reynolds, J. R. *Adv. Mater.* **1999**, 11, 1379-1382.

159. Yang, Y.; Farley, R. T.; Steckler, T. T.; Eom, S. H.; Reynolds, J. R.; Schanze, K. S.; Xue, J. *Appl. Phys. Lett.* **2008**, 93, 163305.

160. Chen, M. X.; Perzon, E.; Robisson, N.; Jönsson, S. K. M.; Andersson, M. R.; Fahlman, M.; Berggren, M. *Synth. Met.* **2004**, 146, 233-236.

161. Sun, M.; Wang, L.; Zhu, X.; Du, B.; Liu, R.; Yang, W.; Cao, Y. *Sol. Energy Mater. Sol. Cells* **2007**, 91, 1681-1687.

162. Michinobu, T.; Okoshi, K.; Osako, H.; Kumazawa, H.; Shigehara, K. *Polymer* **2008**, 49, 192-199.

163. Zotti, G.; Schiavon, G.; Berlin, A.; Fontana, G.; Pagani, G. *Macromolecules* **1994**, 27, 1938-1942.

164. Jeffries, A. T.; Moore, K. C.; Ondeyka, D. M.; Springsteen, A. W.; MacDowell, D. W. H. *J. Org. Chem.* **1981**, 46, 2885-2889.

165. Asawapirom, U.; Scherf, U. *Macromol. Rapid Commun.* **2001**, 22, 746-749.

166. Pappenfus, T. M.; Hermanson, B. J.; Helland, T. J.; Lee, G. G. W.; Drew, S. M.; Mann, K. R.; McGee, K. A.; Rasmussen, S. C. *Org. Lett.* **2008**, 10, 1553-1556.

167. Ogawa, K.; Rasmussen, S. C. *Macromolecules* **2006**, 39, 1771-1778.

168. Ogawa, K.; Rasmussen, S. C. *J. Org. Chem.* **2003**, 68, 2921-2928.

169. Zhu, Z.; Waller, D.; Gaudiana, R.; Morana, M.; Muhlbacher, D.; Scharber, M.; Brabec, C. *Macromolecules* **2007**, 40, 1981-1986.

170. Soci, C.; Hwang, I. W.; Moses, D.; Zhu, Z.; Waller, D.; Gaudiana, R.; Brabec, C. J.; Heeger, A. J. *Adv. Funct. Mater.* **2007**, 17, 632-636.

171. Zhang, M.; Tsao, H. N.; Pisula, W.; Yang, C.; Mishra, A. K.; Mullen, K. *J. Am. Chem. Soc.* **2007**, 129, 3472-3473.

172. This molecule was provided by Xuan Zhang from Seth Marder's group at the Georgia Institute of Technology, as part of an ongoing joint collaboration.

173. Bundgaard, E.; Krebs, F. C. *Macromolecules* **2006**, 39, 2823-2831.

174. Yamashita, Y.; Ono, K.; Tomura, M.; Tanaka, S. *Tetrahedron* **1997**, 53, 10169-10178.

BIOGRAPHICAL SKETCH

Timothy T. Steckler is the son of Thomas and Lillian Steckler. He was born and raised in Brookfield, WI. He received his bachelor's of science degree in chemistry from Winona State University–Winona, MN. While at WSU, under the advisement of Dr. Thomas W. Nalli and Dr. Robert W. Koptizke, he was encouraged to continue on in his education. Tim then went to the University of Florida to work under the advisement of John R. Reynolds. There, he worked as a synthetic organic chemist of conjugated polymers. He received his Ph.D. from the University of Florida in the spring of 2009